Ionizing radiation as imaging tool for coal characterization and gasification research

by

Jakobus Willem Hoffman

20392567

Dissertation submitted in fulfillment of the requirements for the degree *Master of Engineering* at the Potchefstroom Campus of the North-West University

Supervisor: Prof. Q.P. Campbell

April 2012

Declaration

I, Jakobus Willem Hoffman hereby declare that the following dissertation with the title "**IONIZING RADIATION AS IMAGING TOOL FOR COAL CHARACTERIZATION AND GASIFICATION RESEARCH**", submitted in fulfilment of the requirements for the degree Master of Engineering (Chemical), is my own original work and has not been submitted previously by anyone at any institution. Whenever there was a need to quote, the original author was included in the attached reference list. All the individuals that assisted me during this study are mentioned in the acknowledgements.

Signed at Potchefstroom on ..... 2011.

_____

J.W. Hoffman

Acknowledgements

I would like to thank the following people for providing guidance and assistance during the course of this investigation:

- Prof. Q.P. Campbell (principal study leader)
- Mrs. K.M. Spies
- Mr. F.C. de Beer (assistant study leader)
- Mr. P. Keanly for technical assistance
- Mrs. M. du Toit for helping with experiments
- Mrs. J. Brits for also helping with experiments

I am grateful for all the help that the abovementioned people have given me.

Abstract

In this study, imaging with ionizing radiation was evaluated as a research technique in coal research. Part of the evaluation was to conduct a thorough literature survey as well as a preliminary investigation into coal pyrolysis and gasification with micro-focus X-ray tomography. The literature survey summarizes previous research experiences, primarily focussing on the possibility of utilizing a specific coal bed for carbon dioxide sequestration and methane production. This includes quantifying the fracture and cleat network and visualizing the orientation of this network. The cleat and fracture spacing and aperture are used to calculate certain parameters necessary to model gas flow. Other aspects include non-destructive characterization which consisted of determining the porosity and the minerals and macerals present and the respective mineral distribution. The literature survey also includes a section on the utilization of neutrons in coal research and a description of a neutron imaging facility in South Africa is presented.

Three coal samples from the Waterberg and Highveld regions of South Africa were used to investigate the process of pyrolysis through micro-focus X-ray tomography. The samples swelled significantly when 50% pyrolysis was achieved after which the samples became brittle. This verified the plastic nature of the coal, that is prevalent under these conditions. It was also possible to perform qualitative characterizations prior to and during the process. Regions of low and high density materials could also be visualized. The distribution of the minerals is indicative of the permeability of the organic matrix. Two coal samples of the Highveld regions were used to investigate gasification up to a level of 30%. It was possible to verify that the reaction progressed according to the mechanisms proposed by the un-reacted shrinking core model. The mineral matter and the high density coal macerals did not influence the reaction in any way.

Key words: coal, pyrolysis, gasification, characterization, micro-focus X-ray tomography

Uittreksel

Visualisering deur ioniserende straling was ondersoek as ‘n navorsingstegniek in steenkool navorsing. Hierdie ondersoek het bestaan uit ‘n volledige literatuurstudie asook ‘n voorlopige naspeuring van steenkool pirolise en vergassing. Die literatuurstudie het hoofsaaklik bestaan uit die resultate van vorige navorsingsprojekte wat oorwegend die be-oordeling van ‘n steenkoolbank as ‘n moontlike bron vir die produksie van metaan en die berging van koolstofdioksied behels het. Dit het meer spesifiek gehandel oor die kwantifisering, visualisering en orientasie van die kraak-netwerk. Die kraak verspreiding en openingsdikte word gebruik in die berekening van parameters wat benodig word om gasvloei te modeleer. Ander aspekte wat behandel was, sluit in nie-destruktiewe karakterisering wat bestaan het uit die berekening van die porositeit, en die teenwoordigheid asook die verspreiding van minerale en maserale. Die literatuurstudie sluit ‘n seksie in wat handel oor die toepassing van neutrone in steenkoolnavorsing en ‘n beskrywing van ‘n neutron beeldvormings fasiliteit in Suid-Afrika word gegee.

Drie steenkoolmonsters onderskeidelik van die Waterberg en van die Hoëveld gebiede van Suid-Afrika, was gebruik om die proses van pirolise te ondersoek met behulp van mikrofokus X-straal tomografie. Die monsters het beduidend geswel toe ‘n vlak van 50% bereik is, wat met gevolglike brosheid gepaardgegaan het. Dit het die verwagte plastiese natuur van die steenkool by hierdie kondisies bevestig. Dit was ook moontlik om ‘n kwalitatiewe karakterisering te doen voor en tydens die proses, asook om gebiede van lae en hoë digtheid te visualiseer. Die deurdringbaarheid van die organiese matriks kon afgelei word van die verspreiding van die minerale. Twee steenkoolmonsters van die Hoëveld gebied was gebruik om vergassing tot ‘n vlak van 30% te ondersoek. Dit was moontlik om te bevestig dat die reaksie verloop het soos uiteengesit in die reaksiemeganismes van die krimpende-kern model. Dit het nie voorgekom asof die minerale en die hoë digtheid steenkool maserale enige effek op die reaksie gehad het nie.

Sleutelwoorde: steenkool, pirolise, vergassing, karakterisering, mikrofokus X-straal tomografie

Table of Contents

List of figures

List of tables

List of abbreviations

Abbreviation	**Description**
CT	Computed Tomography
SANCRAT	South African National Centre for Radiography and Tomography
MIXRAD	Micro-focus X-ray Radiography and Tomography
SCM	Shrinking Core Model
RPM	Random Pore Model
CAT	Computed Axial Tomography
3D	Three Dimensional
2D	Two Dimensional
SEM	Scanning Electron Microscope
µCT	Micro-focus Computed Tomography
MA	Missing attenuation
FWHM	Full-width-half-maximum
PH	Peak height
CIA	Colour image analysis
SANRAD	South African Neutron Radiography and Tomography
PC	Personal computer
TGA	Thermo-gravimetric analyzer
Necsa	South African Nuclear Energy Corporation

List of symbols

Symbol	Description (Unit)
X	Conversion or fraction converted (-)
t	Time (s)
r_s	Intrinsic Reaction Rate - change in number of moles per unit volume ($mol/m^3.s$)
k	Rate constant - specific rate of reaction based on volume (mol/m^3)
τ	Time for complete conversion (s)
ρ	Density - Mass per unit volume (kg/m^3)
ρ_t	The density of any region of interest during gas uptake (kg/m^3)
ρ_d	The density of any region of interest prior to any gas uptake (kg/m^3)
d	Radius of unreacted particle (m)
b	Stoichiometric coefficient (-)
k_g	Mass transfer coefficient of the gas film – diffusion rate constant ($mol/m^2.Pa.s$)
C_g	Concentration of gas (mol/m^3)
C_w	Concentration of water (mol/m^3)
C_s	Concentration of solids (mol/m^3)
D	Effective diffusion coefficient in porous structures-diffusion rate constant (m^2/s)
k_s	Rate constant - specific rate of reaction based on reaction surface area (mol/m^2)
Ψ	Structural factor – constant incorporating effect of pores (-)
L	Total length of pore axis per unit volume (m^{-2})

Symbol	Description (Unit)
S	Total initial surface area per unit volume (m^{-1})
p	Symbol for Proton (-)
n	Symbol for Neutron (-)
e^-	Symbol for Electron (-)
v	Symbol for Neutrino (-)
V	Volume (m^3)
(μ/ρ)	Mass attenuation coefficient – ability of a substance to absorb or scatter electromagnetic radiation per unit mass (cm^2/g)
I	Exit ionizing radiation intensity (photons/cm^2)
I_0	Incident ionizing radiation intensity (photons/cm^2)
τ^*	Photoelectric absorption component of mass attenuation coefficient (cm^{-1})
σ_0	Coherent scattering component of mass attenuation coefficient (cm^{-1})
σ	Compton scattering component of mass attenuation coefficient (cm^{-1})
π	Pair production component of mass attenuation coefficient (cm^{-1})
CT_N	Mean CT response of material N – CT number of voxel with material N (-)
K	Constant equal to 1000 (-)
μ	Measured linear attenuation coefficient – Mass attenuation coefficient multiply by the density (cm^{-1})
μ_w	Linear attenuation coefficient of water (cm^{-1})
μ_s	Linear attenuation coefficient of solids (cm^{-1})
CT_{coal}	The CT response of coal that is evacuated of any gases (-)

Symbol	Description (Unit)
CT_{gas}	The CT response of nitrogen saturated porous regions (-)
φ	Average coal porosity – void fraction (-)
P	The pressure of any region of interest during any time of gas uptake (Pa)
Y	The linear attenuation coefficient value (cm^{-1})
X_p	The pixel value (number of pixels)
Δxp	The peak width (number of pixels)
X_p	Pixel position of peak minima (no of pixels)
A	Amplitude of sine function (-)
λ	Wavelength (m)
ω	Phase angle (radians)
E_r	Error for determining the optimized value for PH (-)
E	Energy of X-rays used in a particular CT scan (eV)
Z	Atomic number of object (-)
$m_{100\%}$	Mass of volatiles driven off at 100% pyrolysis (g)
$m_{50\%}$	Mass of volatiles driven off at 50% pyrolysis (g)
$m_{initial}$	Mass of coal particle prior to experimentation (g)
m_{final}	Mass of coal particle at the end of experiment (g)

1. General Introduction

Millions of years ago the energy from the sun could only be utilized during the day when photosynthesizing plants converted this energy into more useful forms. Since the Neolithic revolution human beings began exploiting this vast energy source during the day, and since the discovery of fossil fuels this exploitation turned into a non-stop twenty four hour operation due to the utilization of "stored" energy from the sun. Since then the energy industry grew exponentially together with the world population. Even today the primary fuel of the world is fossil fuels, with oil being the most prominent. There are however a few substantial drawbacks to using fossil fuels including the extremely limited reserves and pollution.

A few alternative energy sources to conventional fossil fuels exist including nuclear energy and renewable energy sources like bio fuels. These energy sources are however much more difficult to exploit in reality than fossil fuels (Jubert & Masudi, 2009). That is why a significant amount of research is conducted on extracting the most (and consequently limiting waste and pollution) from the limited reserves remaining. This study will focus on the evaluation of computed tomography (CT), a relatively new research technique in coal studies, to aid in obtaining a better understanding of coal and coal processes. Understanding more about coal enables the scientist and engineer to optimize current processes and equipment so as to limit pollution and maximize the amount of energy extracted from coal. Section 1.1 of this general introductory chapter depicts the background information and motivation as to why coal research is important. The objectives are listed in section 1.2, whilst the layout of this report is described in section 1.3.

1.1 Background and motivation

Fossil fuels are currently the primary energy source of the world and are exploited for electricity, transport and industrially important operations. Figure 1.1 indicates the contribution by the major energy sources in world energy requirements. Coal is a very attractive energy source since it is relatively cheap to exploit from the vast deposits found around the world, and the technology to process coal is trusted and mature enough for developing countries (Jubert & Masudi, 2009).

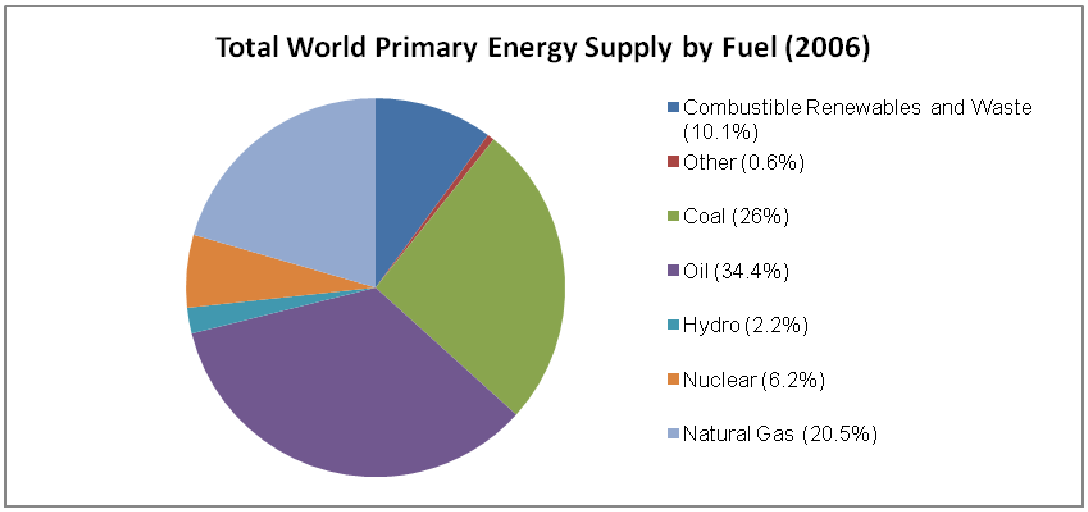

Figure 1.1: Total Energy Supply 2006 (WCI, 2009)

At current production levels the proven coal reserves in the world will last for 119 years, making coal the fossil fuel with the largest remaining reserves (WCI, 2009). Figure 1.2 depicts the proposed energy requirements for various periods of time. It is evident from this figure that the energy sector will face many difficulties in the future since the demand is directly proportional to the ever increasing world population.

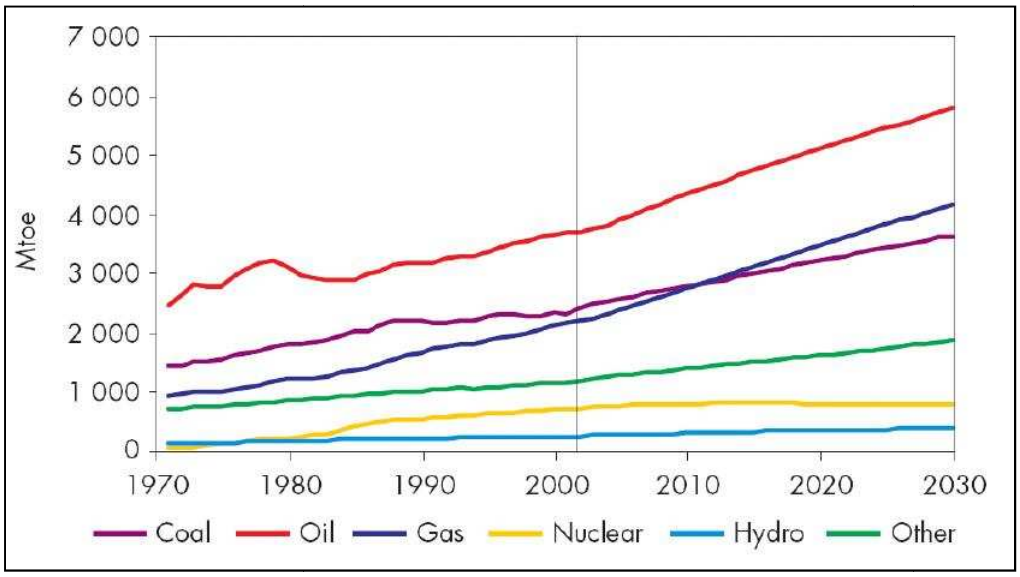

Figure 1.2: World primary energy demand by fuel (Gupta, 2006)

Coal is specifically important for developing countries, including South Africa, and can be seen as the primary form of energy and an economically important issue in these countries (Jubert & Masudi, 2009).

The amount of coal mined in South Africa tripled in the first few years of the 21st century (Fourie *et al*., 2006, Jubert & Masudi, 2009). Although most of the coal mined in South Africa is used domestically, a significant amount of coal is exported and forms an integral part of the economy. Around 70 million tons of coal is burned annually in power stations whilst 50 million tons is converted in the petrochemical sector of which Sasol is the most noteworthy (Fourie *et al*., 2006).

Most of South African coal is of low grade (it contains little volatile matter and significant amounts of non-reactive carbon and inhibiting mineral matter)(Chamber of Mines of South Africa, 2009). Low quality coals have the disadvantage of significant mineral matter and high sulphur contents which can add drastically to NO_x and SO_x emissions which in turn lead to all kinds of environmental- and health problems. The total amount of accessible coal in South Africa is about 55 billion tons, of which only 2% is anthracite and 1.6% of this anthracite is used in metallurgical processes (Chamber of Mines of South Africa, 2009).

At facilities such as Sasol, coal is processed (gasification) into syngas, which contain mostly carbon monoxide and hydrogen. Industrially important chemicals and gaseous fuels are produced from syngas as well as co-products from the gasification process (mostly oils, ammonia, tars, cresols, phenols and sulphur). Gasification is a tried and trusted technology in South Africa and the gasifiers established at Sasol have been optimized specifically for utilising low grade coal (Van Dyk *et al*., 2005).

Most previous gasification studies involved powders and small particles in which the mass lost during gasification was investigated (Everson *et al.,* 2005). The resulting mass loss curves represent the different phases of the overall gasification process, from which kinetic information can be obtained. Very little information is obtained from these experiments on how the internal structure of the coal influences and alters the outcome of the kinetic information. Coal bed methane is also the topic of major research currently undertaken worldwide, and depends largely on the internal structure of coal (cleats and fractures) (Karacan & Okandan, 2001; Verhelst *et al.*, 1996). The opposite of extraction is also true, since the addition of certain gases to un-mineable coal seams is equally important. Carbon dioxide sequestration is currently a buzz-word associated with climate change solutions and is considered a very important research topic (Denis *et al.,* 2009). Therefore, a strong need exists for studying the internal structure of coal to better understand processes (including gasification) and how to optimize the flow of gaseous materials within.

Previous research methods that investigated the internal structure of coal included thin section preparation, which is a tedious, labour intensive and time consuming destructive method. It is evident from the abovementioned paragraphs that coal is important in South Africa not only as the primary domestic fuel but also due to the crucial role it plays in the economy and international trade. Any knowledge obtained in the characteristics and beneficiation of coal and related science will lead to a more environmentally friendly and sustainable exploitation of this important and abundant natural resource.

The North-West University (Potchefstroom Campus) has a very active coal research group that strives to be leaders in clean coal technology. This study will add to that leadership in the sense that an alternative method to current coal studies will be investigated to better quantify behavioural diversity within samples. To do this would require performing a feasibility study which consists of determining the transitions that accompany coal transformations and are often challenging and difficult to obtain.

1.2 Objectives of this investigation

The purpose of this study can be divided into the following objectives:

- Perform a complete literature survey to evaluate CT as an alternative research technique in coal studies, with special emphasis on the limitations and capabilities of the technique.
- Determine which aspects of coal research were investigated with CT in past studies.
- A well optimized experimental apparatus will be required to produce the best possible experimental data. Therefore, a part of this project would consist of defining the optimum CT system specifically for coal research.
- Characterization of the MIXRAD facility will be necessary to determine what is possible in South Africa.
- Perform coal characterization in a non-destructive way.
- Investigate pyrolysis and the first stages of gasification with micro-focus X-ray CT.

1.3 Scope of the dissertation

- Chapter one is the introductory overview of the investigation and discusses the background and motivation as to why coal research and specifically this research is important. The objectives of the study are also listed in chapter one.
- Chapter two present a complete literature review. This include relevant information on how different physical and chemical characteristics of coal influences processes like gasification and on how the internal structure of coal influences physical processes like gas flow, with special emphasis on coal bed methane extraction. An overview of the CT process and effects of different technologies and ionizing radiations are provided. The last paragraphs of chapter two highlight a few lessons that were learned in CT studies in the geosciences.
- A number of CT applications in coal research will be discussed from chapter three to chapter five. Chapter three describes in detail how the CT technique was used to investigate carbon dioxide sequestration and methane production from coal beds. Chapter four describes how quantitative information can be obtained from cleats and fractures that can be used to model fluid flow in coal. This can also play an important role in coal bed methane production and carbon dioxide sequestration. Chapter five is one of the most important chapters and describes how coal can be characterized non-destructively with CT.
- An overview of the experimental method used in this study is given in chapter six. This includes detail discussions on the materials and characterization methods that are commonly used. The main focus of this chapter is the experimental setup of the CT equipment that is used to obtain the experimental data. The equipment is optimized for general research as to eliminate the most common artifacts associated with digital tomography, and therefore includes discussions on image reconstruction and advanced analysis.
- Chapter seven presents the results of a preliminary coal investigation where the coal has been characterized non-destructively, and the structural changes during pyrolysis and gasification were followed. This chapter presents the results for six coal samples of which two have undergone gasification up to a level of 30%. All of the samples were scanned at 0%, 50% and 100% pyrolysis and the swelling was quantified.
- Chapter eight presents the conclusions made and includes a few recommendations for future investigations.

2. Literature Review

Before starting a research investigation it is necessary to have an idea of what the outcomes should be. The outcomes of the research are a function of the characteristics of the objects under investigation, as well as the capabilities and limitations of the equipment used and the related experimental method(s). This knowledge is only obtainable through a thorough literature review. In this chapter the literature review for this investigation starts with a discussion on coal which includes sections on its physical and chemical characteristics and their influence in different beneficiation processes. The second part of this chapter provides information on gasification and how different coal properties affect this process. This chapter concludes with discussions on ionizing radiation as an imaging tool with emphasis on X-ray imaging and the utilization of the technique in general research and an in-depth discussion of the different technologies available and previous research conducted.

2.1 Chemical and physical properties of coal

Knowledge of coal properties is crucial in predicting and optimizing certain coal processing equipment behaviour and performance. From the following paragraphs it will be demonstrated that the need for techniques to obtain more information on the composition of coal is indeed very important. The CT technique that forms the basis of this investigation will permit the researcher to study most of these properties in a non-destructive fashion.

2.1.1 Coal macerals

Coal is a heterogeneous substance that comprises mainly of carbon, hydrogen, nitrogen, sulphur, oxygen and other chemical species and thus includes both organic (groups of macerals) and inorganic material. The organic constituents and more specifically the fixed carbon content of a coal, can serve as a correlation for reactivity, especially for high-rank coals.

The maceral composition plays a significant role in determining coal type and rank and subsequently its quality and reactivity (Crelling *et al.,* 1992). Maceral density typically varies from 1.2 to 1.7 g/cm^3 (Verhelst *et al.,* 1996) with inertinite having the highest density and liptinite having the lowest density (Stach *et al.,* 1982). The process in which coal is prepared for gasification is called devolatilization (separation of tars and volatiles) and is also substantially influenced by maceral groups.

Vitrinite

Coal rank can be seen as a measure of the degree of the maturity of the coal and subsequently the progression in the coalification process (Falcon & Falcon, 1987). There are many ways to determine the rank including determining optical and chemical parameters. Vitrinite reflectance is typically an optical parameter that indicates the rank and is the preferred method of choice in South Africa. Coal rank ranges from lignite to bituminous and anthracite, as indicated in figure 2.1 (Stutzer & Noè, 1940:240). Much research has been conducted to find a relationship between the rank of coal and the reactivity, and unfortunately no clear trend could be agreed upon (Cloke & Lester, 1994; Ye *et al.*, 1998). Rank is thus in general only a classification tool to determine the maturity and likely behaviour of different coals.

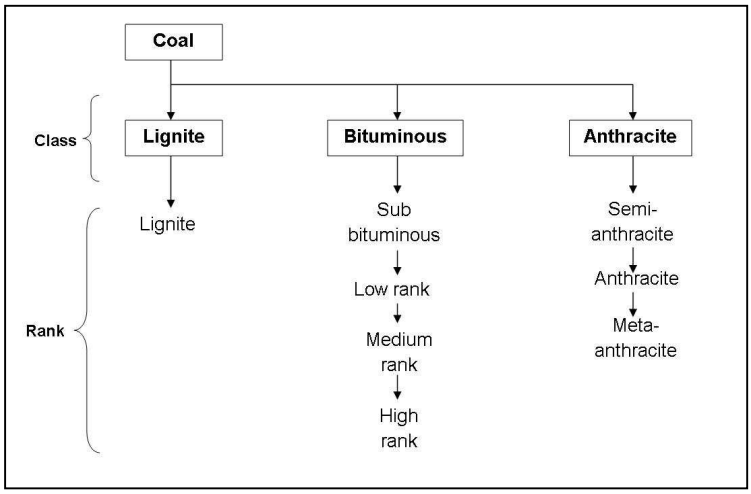

Figure 2.1: Petrographic classification of coal by rank and type (Stutzer & Noè, 1940:240)

Vitrinite reflectance can also serve as an indication of fixed carbon content, since there is a correlation between these two properties (Berkowitz, 1985). There is a strong relationship between vitrinite content and the calorific value and porosity of resulting chars. Cloke & Lester (1994) reported that the chars ranged, depending on the rank, from hollow multi chambered to hollow single chambered.

This demonstrates that the vitrinite content has an effect on the changes in the internal structure of coal during certain processes. Vitrinite content is also closely related to the microporous surface area as will be seen in section 2.1.3.

Liptinite

Cloke & Lester (1994) reported that liptinite is the maceral group with the highest hydrogen and volatile content and thus will also play a considerable role in the formation of chars (refer to section 2.2). Liptinite contains more volatile matter than vitrinite, resulting in incredibly small combustion times and thus would not add drastically to the reactivity of the char in processes like gasification.

Inertinite

Inertinite has the highest carbon to hydrogen ratio of all the macerals, with very little volatiles and hydrogen. Inertinite variation is also closely related to changes in rank. At sufficiently high-rank, the inertinite results in extremely dense chars that are considered to be non-reactive (Cloke & Lester, 1994).

Microlithotypes

It is relatively rare for macerals to occur completely alone in nature, but they occur much rather in the form of associations with more than one maceral. These associations are termed microlithotypes and the most common include the monomaceral, bimaceral and trimaceral microlithotypes (Stach *et al*., 1982:141). The chemical properties of the monomaceral microlithotypes are closely related to the individual macerals that constitute them.

Bimacerals include clarite (vitrinite and liptinite), vitrinertite (vitrinite and inertinite) and durite (inertinite and liptinite), whilst trimacerals are deemed trimacerite (Stach *et al*., 1982:141). Macerals do not only form associations with other macerals but also with mineral matter - these associations are called carbominerites and are also divided into different groups depending on the specific minerals involved (Stach *et al*., 1982:151).

2.1.2 Mineral constituents

The mineral matter in coal is defined as all the inorganic constituents in the coal matrix (Falcon & Falcon, 1987). Mineral matter and its respective distribution in coal are of significant importance since it can have inhibiting or catalytic effects in different reactions. Clay minerals, which are the most abundant (60 - 80%), and alkali and alkali-earth metals, can have a catalytic effect on steam gasification (Hüttinger & Nattermann, 1994; Stach *et al*., 1982:158). These types of minerals will result in enlarged surface areas and consequently more reactive sites. For instance, pyrite acts as a catalyst in pyrolysis and combustion processes (Chen *et al.*, 2000). Other important minerals include carbonate minerals, sulphides, oxides and heavy minerals like zircon (Stach *et al*., 1982:158).

Certain minerals within coal can however have a negative effect during certain reaction systems as it lowers the reactivity of the coal. This happens when certain temperatures during these processes are exceeded; some of the mineral constituents melt and block the active reaction sites (Bai *et al*., 2008). Mineral constituents, specifically the dense minerals included in the coal matrix, can in effect increase the heat capacity of the coal particles, and thus consequently lower the reactivity (Wigley *et al.*, 1997). To solve this problem would require the coal to be demineralised which can in effect also lower the reactivity, as discussed in the previous paragraph. It is therefore necessary to evaluate the mineral matter involved and determine the effect it has on reactivity, and decide how to demineralise accordingly (Bai *et al.,* 2008).

Mineral matter content can also serve as a guide to determine reactivity in low-rank coals. The reactivity of low-rank coals does not correlate well with the fixed carbon content reactivity predictions, and is predominantly influenced by the catalytic effect of certain mineral constituents. This, however, is not the case for high-rank coals, as the reactivity is closely related to the carbon content in the coal (Hüttinger & Nattermann, 1994).

2.1.3 Physical Properties

There are many reasons why coals have distinct reactivities. The chemical reasons were discussed in the previous sections of this chapter, whilst the physical properties are discussed in this section.

The amount and distribution of the active sites in which reactions like steam gasification can occur, can explain some of the variation in reactivity reported in literature. The amount and nature of the active sites depend on the crystallite orientation and the impurities contained on the surface (Laine *et al.*, 1963). These impurities can occur as the result of contamination in the mining and processing activities (Liu *et al.*, 2005). Laine *et al.* (1963) concluded that the crystallite structure is reoriented upon heating to yield a surface that consists predominantly of the basal planes of the crystallites. Upon oxidation it is observed that the attack on the surface occurred mainly at the intersections of the surfaces of the basal planes.

Oxidation resulted in the particles being penetrated and the basal plane edges being exposed, and consequently results in a higher reactivity. Laine *et al.* (1963) stated that the reason as to why edge carbon atoms are more reactive than basal plane carbon atoms, are because of geometric and impurity considerations. The edge carbon atoms are more likely to form bonds with chemisorbed oxygen, a step required for production of gaseous carbon oxides. It has been discussed in a previous section how inorganic materials, a constituent of impurities, can catalyze reactions, resulting in higher reactivities.

Senneca *et al.* (1998) conducted research on South African and German coals to investigate this effect and concluded that untreated South African coal has an unordered physical structure and contains a significant amount of calcium in the crystalline phase. When the coal samples were heated between 900 and 1400 ℃, the structure ordered in terms of layering and size. The investigators also found that at this temperature there is a formation of low crystallinity phases around the calcium. This thermo-deactivation of inertinite rich South African coal resulted in lower reactivity.

Three types of pores are generally classified by using X-ray diffraction measurements and the amount in which they occur is dependent on the rank and origin (Gan *et al.,* 1972). Low-rank coals primarily contain macropores whilst 80% of the total pore volume of coking coals consists of transitional and micropores. High-rank coals (anthracite) primarily have a microporous structure and consequently a large reaction surface area. Chi & Perlmutter (1989) concluded that the pores are mainly responsible for intra-particle mass transfer of reaction and product materials and the macroporous surface area is negligible when compared to the microporous surface area. Even though the micropores entail the largest surface area, it is not clear where exactly reactions like gasification occur. Hurt *et al.* (1991) concluded that gasification would rather occur in the macroporous regions since these regions contain more active sites.

Kühl *et al.* (1992) studied the alterations in the porous structure of coal when undergoing steam gasification and found that the macroporous structure change very little as the reaction progresses, whilst the microporous structure expands significantly. Micropores are considered to have widths of less than 5 nm whilst macropores have widths of larger than 50 nm (Koopal, 2001). It is known that pores are produced during the initial stages in which volatiles are driven off. It is interesting to note that the microporous structure evolves and the volume increases due to the loss of carbon even after the volatiles have been driven off, whilst the macroporous structure forms only during the initial stages of charring. Porosity is generally quantified by using the more conventional destructive methods, including mercury porosimetry, gas adsorption (specifically CO_2) and microscopic observation (Yao *et al.,* 2009).

Carbon monoxide adsorption is generally used to determine micro-porosity and micropore distributions because this technique enables access to the smallest pores at moderate temperatures (Clarkson & Bustin, 1999). It is observed from carbon monoxide adsorption that a high vitrinite content coal has a greater micropore surface area than a low vitrinite content coal of the same rank. Nitrogen adsorption confirmed this observation and revealed that low vitrinite content coal has a greater amount of intermediate and macropores. Mercury porosimetry indicated that coal has a multimodal pore volume distribution but all the previously mentioned techniques of porosity determination confirmed that the micropore volume is the primary gas absorber (Clarkson & Bustin, 1999).

Cleats and fractures are key attributes to the macroscopic physical structure of coal and coal beds and play crucial roles in determining and modeling flow parameters. Flow direction in coal beds are determined by the cleat and fracture structure and is controlled by Darcy permeability. Important parameters in cleat and fracture classification and quantification include size, spacing, connectedness, aperture, minerals present and orientation (Mazumder *et al.,* 2006). Past research that has been performed included cutting the samples and utilizing advanced image analysis to determine these properties. This however influences the transport kinetics due to an alteration of the physical structure (Mazumder *et al.,* 2006).

Cleats and fractures are usually classified according to their orthogonal plane system resulting in two major classes i.e. the face and butt cleats. Cleat and fracture spacing are in the order of millimetres to centimetres and a quantitative density analysis can therefore only be accurate if cleat and fracture data is incorporated.

Mazumder *et al.* (2006) stated that cleat spacing is closely related to coal rank and mineral content and decreases from lignite to medium-volatile bituminous coal whilst there is a tendency to increase through the anthracite range. Coals with low mineral contents had smaller spacing between consecutive cleats and fractures than coals with high mineral content (Mazumder *et al.,* 2006).

2.2 Gasification

Gasification is a complex process in which coal is converted into a more useful form. The gasification process consists mainly of two distinct phases; devolatilization or pyrolysis and carbon conversion.

It has been stated earlier that pyrolysis is a complex process in which the plastic nature of coal is altered to produce a solid material consisting mainly of carbon and minerals. This solid material, which undergoes the actual gasification reactions (see below), is called char and the pyrolysis process is also referred to as charring. Chermin & Van Krevelen (1956) divided the pyrolysis process into three distinct stages i.e. a depolymerisation stage, a devolatilization stage and finally a high temperature gas extraction stage. In the first stage or polymerization stage, an unstable metaphase with a plastic and elastic nature is formed. During this stage the individual coal particles coalesce and start to behave like a single entity with distinct properties.

The second stage initiates when the coal particles are heated even further and primarily involves driving off tars and non-aromatic groups like phenols. The escaping gas has difficulty passing through the coal particles (due to their plastic nature). In this second process the coal could significantly swell; a phenomenon that is more severe in coal with high liptinite content. At this point there are still some gases present in the coal structure and they are removed in the third stage. This typically includes methane and hydrogen gases that require sufficiently high temperatures to be driven off.

As the methane and hydrogen are driven off (the third stage), the density of the coal sample generally decreases, which results in a coal sample with lower mass. It is interesting to note that there are many theories as to how coal form a metaphase with a plastic nature. The theory described above is the most generally accepted one and is called the metaplast theory (Chermin & Van Krevelen, 1956).

Pyrolysis is an important step since the swelling and cracking during charring forms integral parts of the porosity and reaction surfaces exhibited by the coal samples. Thus, pyrolysis plays an important role in coal reactivity. There is consensus amongst coal researchers that the reactivity of a char decrease with increasing amount (percentage) of fixed carbon (Cloke & Lester, 1994; Crelling *et al.*, 1992).

Gasification occurs simultaneous with pyrolysis in a commercial gasifier at temperatures of approximately 1000 ℃ and pressures of approximately 30 bar (Van Dyk *et al.,* 2005). Most of the reactions involved are heterogeneous solid-gas reactions that occur parallel to each other. Commercial gasifiers are optimized to maximize energy consumption and therefore exothermic reactions provide the energy necessary for the endothermic reactions. The primary gasification reactions include reactions in which the syngas constituents, carbon monoxide and hydrogen, are produced. The water-gas-shift reaction is of significance in steam gasification since it can decrease the amount of syngas that is produced. Van Dyk *et al.* (2005) reported that the water-gas-shift reaction takes place at almost chemical equilibrium conditions in commercial gasifiers as to maximize product formation.

2.2.1 Conditions influencing the gasification reactions

Reaction rate kinetics is sensitive to the fluctuation of certain conditions including temperature, pressure, gas and coal composition as well as particle size. Each of these conditions is being described in the following paragraphs with emphasis on how fluctuations have an influence on the gasification reaction.

Temperature

Most chemical reactions are sensitive to changes in temperature, including gasification of coal. The result of an increase in reaction temperature is usually an increase in reaction rate (Zhang *et al.,* 2006). There is however a maximum temperature that, beyond which the reaction rate does not change significantly, primarily due to two factors, namely the deactivation of carbon and the melting temperature of included minerals. The problems associated with the latter were already discussed in section 2.1.2. Mineral-fusion temperatures are important when considering absolute temperatures.

High mineral-fusion temperature coals exhibit a relative independence on increasing temperature, with the reactivity remaining relatively constant as the temperature increased, whilst low mineral-fusion temperature coals exhibited a strong decline in reactivity beyond a certain maximum temperature. This can be attributed to the formation of ash on the reactive sites, decreasing the active surface area for low mineral-fusion temperatures (Liu *et al*., 2006).

Temperature influences the reaction rate kinetics in three regimes, each with its own distinct mechanism of control i.e. intrinsic chemical reaction, pore diffusion and ash layer diffusion (Walker *et al*., 1959). The first regime occurs at lower temperatures and the controlling mechanism is predominantly intrinsic chemical reaction. The reaction rate is relatively slow in this regime since the reaction gases diffused into the porous particles rather than reacting at the active surface areas. The reaction gases can diffuse faster into the solid matrix than they can be consumed and the reaction occurs uniformly throughout the particle (Walker *et al*., 1959).

At higher intermediate temperatures the second regime is apparent. In this regime the reactant gases are diffusing into the solid matrix at a rate at which they are consumed at a reactive interface so that they leave an unreacted core. Diffusion through the product layer surrounding the unreacted core is the mechanism that controls the rate of reaction and it is fast compared to the intrinsic chemical reaction controlled regime (Walker *et al*., 1959). At really high temperatures the reaction rate is so fast that the reaction gases do not enter the solid matrix but rather react at the reaction surfaces. This is regime three, and the rate controlling mechanism is the diffusion into the ash layer (Walker *et al*., 1959).

Pressure

Wall *et al.* (2001) studied the influence of alternating reactant pressure on gasification reactions and concluded that the reaction rate increases as the reactant gas pressure increases. This can be attributed to an increase in the swelling of coal particles as the reactant pressure is increased from atmospheric to 10 atm. This was observed especially with vitrinite rich particles, where an increase in reactant pressure resulted in a more porous vitrinite structure. It should be noted that the intrinsic reaction rate (discussed in section 2.2.2) is less dependent on pressure and remain approximately the same as the pressure increases.

Reactant/product gas and coal compositions

Steam concentrations do not have a significant role on the reaction rate at low conversions whilst the opposite is true when conversions exceed 30% (Lu & Do, 1994; Everson et *al.*, 2005). The product gases, hydrogen and carbon monoxide, have an inhibiting effect on the reaction rate and this is especially true at low temperatures (Weeda *et al.,* 1993). The effect of coal composition was discussed in detail in section 2.1.

Particle size

Particles originating from the same parent coal can have distinct and different reactivities (Jones *et al.,* 1985). This effect can be attributed to the physical processing of the coal i.e. grinding and milling. Due to the heterogeneous structure of coal, milling and crushing can lead to particles breaking at weaker areas, which will probably be rich in less dense macerals like inertinite. The product would be bigger particles rich in harder materials like vitrinite and smaller particles rich in materials like inertinite.

Wells and Smoot (1985) concluded that the rate of reaction is independent of particle size at low temperature whilst there is a definite dependence when the temperature is appropriately high. Reaction is also very independent of the particle size if the size range is small enough. Hanson *et al.* (2002) found that reaction rate is independent of particle size if the particle diameters are between 0.5 and 2.7 mm.

2.2.2 Modelling gasification reactions

Various researchers have indicated that gasification can be modelled by the following equation (Everson *et al*., 2005; Lu & Do, 1992).

$$\frac{dX}{dt} = r_s f(X) \qquad \textbf{Equation 2.1}$$

According to this equation the overall reaction rate depends on the intrinsic reaction rate (r_s) and the structure of the coal particle ($f(X)$ is a structure factor). The structural factor can be modelled by using structural models such as the random pore and shrinking core models, whilst the intrinsic reaction rate can be developed by using the Langmuir-Hinshelwood equations (Everson *et al*., 2005).

Non-structural models can also be used to model steam gasification and are generally simpler to use, but does not include certain parameters and are sometimes inadequate.

Gasification reaction rate particle models

The following paragraphs describe the different models that are frequently utilized to model gasification.

The volumetric or homogeneous model

The volumetric model considers the effect of structural changes as insignificant by reducing the heterogeneous reactions to homogeneous reactions and has the following assumptions (Zhang *et al*., 2008).

- The reactant gas reacts on all possible active sites
- The active sites are uniformly distributed on the outside and inside surfaces of the particle

The volumetric model is represented by the following equation (Zhang *et al.,* 2008).

$$\frac{dX}{dt} = k(1 - X) \qquad \textbf{Equation 2.2}$$

The shrinking core model (SCM)

A very popular non-structural model to consider is the SCM which assumes that the particle size remains constant throughout the reaction (Everson et *al.*, 2005). At the beginning of the reaction all the active sites are concentrated at the outer particle surface so that the chemical reaction occurs exclusively on the outer surface. As the reaction proceeds, the reaction zone moves inward leaving behind an ash layer which offers resistance to the transport of reaction and product gases. In this way the core of unreacted coal is always decreasing in size until the reaction completes (Levenspiel, 1999:569). There are three rate controlling steps associated with the SCM and the dominating step can be determined from the following equations. These equations can also serve as a test to verify the validity of the SCM (Levenspiel, 1999:580).

Film diffusion controlling:

$$\frac{t}{\tau} = X \qquad \textbf{Equation 2.3}$$

Ash layer diffusion controlling:

$$\frac{t}{\tau} = 1 - 3(1 - X)^{2/3} + 2(1 - X) \qquad \textbf{Equation 2.4}$$

Chemical reaction controlling:

$$\frac{t}{\tau} = 1 - (1 - X)^{1/3} \qquad \textbf{Equation 2.5}$$

The value of τ (time for complete conversion) in each equation has distinct values and is represented in table 2.1 (Levenspiel, 1999:580).

Table 2.1: Equations for the time necessary for complete conversion (Levenspiel, 1999)

Rate controlling step	**Equation**
Film diffusion	$\tau = \frac{\rho d}{3bk_g C_g}$ (**Equation 2.6**)
Ash layer diffusion	$\tau = \frac{\rho d^2}{6bDC_g}$ (**Equation 2.7**)
Chemical reaction	$\tau = \frac{\rho d}{bk_s C_g}$ (**Equation 2.8**)

The SCM is a theoretical model and therefore a few errors are inevitable. It is highly unlikely for a reaction to occur at a specific sharp interface between spent and fresh reactant. It is assumed that the particles remain the same size during reaction and temperature gradients are negligible. This is however not realistic for very fast reactions where temperature gradients are major role players (Levenspiel, 1999:581). Although there are a few errors associated with the SCM, many researchers found it to accurately describe gasification behaviour. Kwon *et al*. (1989) found that the SCM is sufficiently accurate for non-catalyzed reactions and concluded that these reactions are chemical reaction rate limiting which is in accordance with literature. Lee & Koon (2009) indicated that ash layer diffusion becomes significant as the reaction proceeds and a combination of chemical reaction rate limiting and ash layer diffusion rate limiting behaviour is apparent.

The random pore model (RPM)

The RPM is also a theoretical model and presupposes the following assumptions (Zhang *et al.*, 2008).

- Pores are represented as cylinders that have random sizes and distribution across the char surface area
- The pores converge in random places as the reaction progresses

The equation for the RPM is presented by Zhang *et al.* (2008) as follows:

$$\frac{dX}{dt} = k_s(1-X)\sqrt{1-\Psi\ln(1-X)} \qquad \textbf{Equation 2.9}$$

The structural effects are incorporated in equation 2.9 by the structural factor Ψ, which is given in equation form below (Bhatia and Vartak, 1996).

$$\Psi = \frac{4\pi L}{S^2} \qquad \textbf{Equation 2.10}$$

The RPM is very adaptable and many researchers have exploited this feature of the RPM to derive very specific forms for very specific situations. When Ψ = 0, the RPM approximates the volumetric model and when Ψ = 1, the RPM approximates the shrinking core model (Zhang *et al.,* 2008). Lu and Do (1992) derived a version of the RPM that is applicable to coal with high mineral contents, to consider the carbon matrix and the mineral as separate entities.

Gupta and Bhatia (2000) also used a modified version of the RPM with an additional rate constant, to take into account the effect of the initial reactivity of the pore surface area when there are functional groups and hydrogen attached to it. The RPM was used by various researchers to model the gasification reaction successfully, including Weeda *et al.* (1993) and Bhatia & Vartak (1996).

Other models that can be used to model steam gasification kinetics

All the abovementioned models are the more popular ways to predict gasification kinetics, but there are many other models that are used by researchers as indicated in table 2.2 that will not be discussed in detail.

Table 2.2: Other models proposed by researchers

Model	Special feature	Reference
Percolation model	Modeling disordered porous media reactions	Lu & Do, 1992
Chemical reaction diffusion model	Models internal diffusion and reaction with special emphasis on pore structure	Bhatia and Gupta, 2000
Semi-empirical	Models are based on homogeneous rate expressions	Johnson, 1979

2.3 Ionizing radiation as imaging tool

The basic concepts of ionizing radiation and how radiation is utilized as an imaging tool, is discussed in the following paragraphs.

2.3.1 Ionizing radiation

Radiation energy comprises two forms i.e. wave-like electromagnetic radiation in which no mass is transferred and particle-like corpuscular radiation in which mass is propagated (Herz, 1969:2). The distinction between wave- and particle-like radiations is not complete and should be considered as different aspects of the same property (the duality of radiation) (Bertin, 1978:4).

According to Herz (1969:2) a particle in motion can indeed display wave-like properties with the frequency dependent on the momentum, whilst electromagnetic waves can be considered as particles since they are emitted in discrete packets of energy (photons). Radiation is called ionizing radiation when it has the ability to directly or indirectly result in electrons being released and consequently in negative and positive charges being created.

2.3.2 Electromagnetic wave-like radiation

X- and gamma-rays are two types of electromagnetic wave-like radiations and although they are seen as different and distinct they are essentially the same. The only true difference is the source of radiation. X-rays are produced by electrical equipment in events outside the nucleus of the atom, whilst gamma-rays are the result of natural processes and is produced by events from inside the nucleus of the atom (Herz, 1969:3).

X-rays

X-rays are essentially produced when fast moving electrons are focused onto matter and have typical wavelengths of between 10^{-5} to 100 Á (Bertin, 1978:4). The kinetic energy from these fast moving electrons is predominantly converted into heat energy during collision, whilst the remainder of the energy is used to form X-rays. The most popular way of producing X-rays is with an X-ray tube which can be modified to suit various different applications. Figure 2.2 is a schematic representation of a basic X-ray tube (Xradia, 2010).

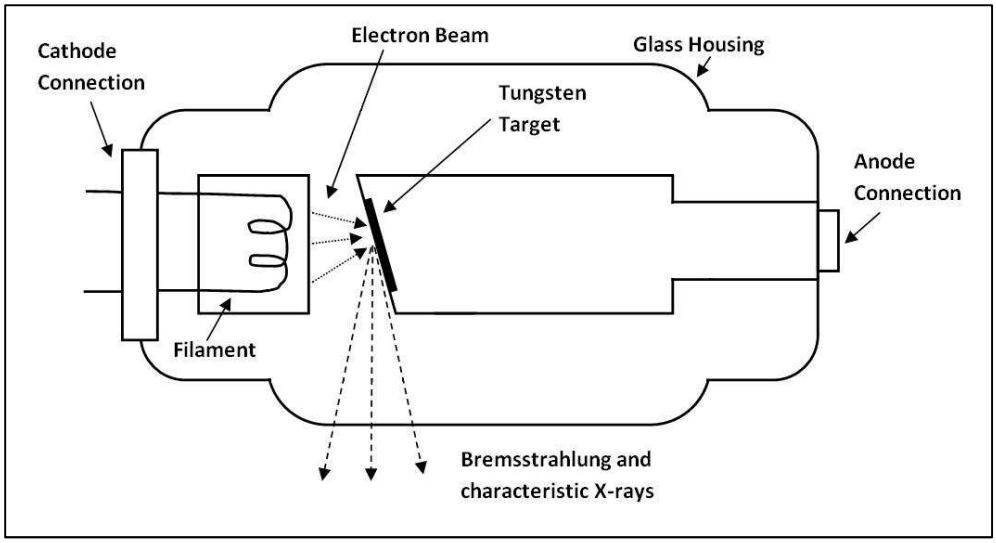

Figure 2.2: Schematic representation of an X-ray tube (Xradia, 2010)

The glass housing is to maintain a vacuum in the tube so that maximum insulation is achieved and is usually covered in a heavy ray proof metal head that confines the X-rays. At the spot where the X-rays exit the glass tube, a beryllium window permits the useful X-ray beam to exit.

The helical tungsten filament is heated by passing an electrical current through it, resulting in the emission of electrons focused by a filament focusing cup. Due to a significant voltage difference between the cathode and the anode, the electrons are accelerated towards the positive anode where the electrons bombard a metal target which emits X-rays (Bertin, 1978:8).

The target is a thin disk or plating of a specific material (usually tungsten) that is imbedded in a heavy water-cooled copper block that removes the heat away from the target area to avoid damage to the target. The filament target space is enclosed by a cylindrical metal shield that has an opening over the beryllium window. Its purpose is to intercept electrons that are incorrectly focused from the filament and electrons that are scattered from the target as well as to minimize metallization of the window by sublimed metal from the filament and target areas. An X-ray tube is an extremely inefficient piece of equipment with roughly 1% of the energy introduced being converted to X-rays and 99% to heat. The target material depends on the application or the desired wavelength of the X-rays produced.

Tungsten is usually used because it provides short X-ray wavelengths whilst chromium can be used to achieve long X-ray wavelengths (Bertin, 1978:8). A rotating anode and target is a new development which increases the heat capacity of the system and consequently increases the ability of the system to produce a higher photon flux over a longer period of time.

The focal spot on the target is essential for the quality (clarity) of images created with X-rays because it is directly the cause for the penumbra or unsharpness (see figure 2.3). The penumbra causes the edge of the sample to appear distorted and therefore lowers the resolution of the image by giving the edge a density gradient (Schena *et al.*, 2007). Eliminating the effect of the penumbra is possible if the focal spot is sufficiently small, as is the case with a microfocus X-ray system. Commercially available micro-focus X-ray scanners have a typical focal spot sizes between 5-20 µm. This is a much better resolution than that obtained with other available systems like a costly medical X-ray CT scanner with a typical resolution of 500 µm (Van Geet *et al.,* 2001). Appropriate focus spots are characteristic to the X-ray tube design and depends specifically on the design of the filament focusing cup (Schena *et al.*, 2007).

The best way to minimize the penumbra or unsharpness would be to minimize the distance between the sample and the detector resulting in no geometrical enlargement but also no unsharpness.

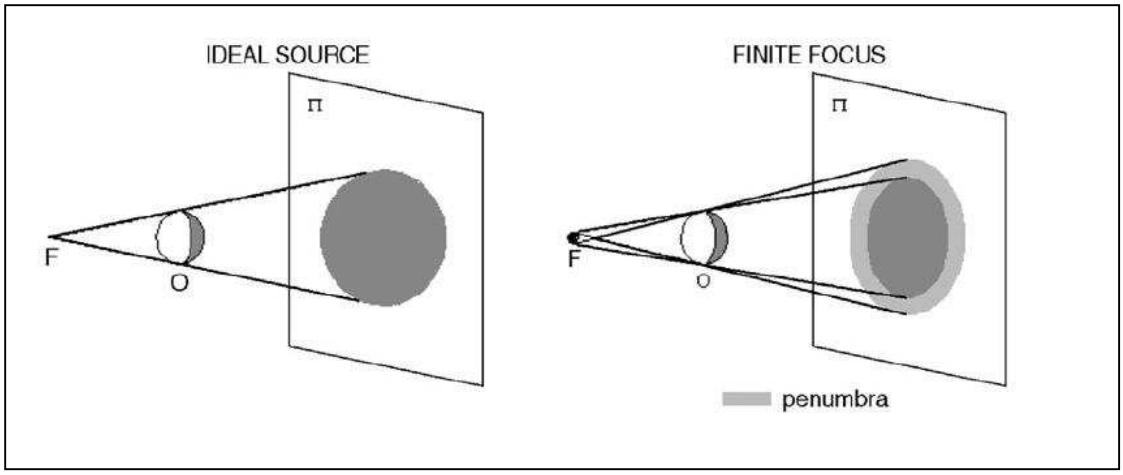

Figure 2.3: Effect of focus spot on unsharpness (Schena et al., 2007)

Two types of X-rays are emitted by an X-ray tube i.e. continuous and characteristic X-rays and are discussed in the following sections. The X-ray spectrum is composed mainly from the continuous X-ray spectrum on which the characteristic X-ray spectrum is superimposed (Herz, 1969:6).

Continuous X-rays (Bremsstrahlung)

The atoms that form the material of the target have a strong Coulomb field surrounding the nuclei. When electrons interact with this strong field one of two situations can occur i.e. the electrons can be stopped or they can be deflected. This deceleration in this electrical field causes a pulse of radiation to be emitted in the form of a continuous X-ray. The electrons that are deflected travel deeper into the target material and consequently loose their energy gradually. The electrons that are stopped immediately upon entering, loose all their energy instantaneously. Therefore, the X-ray energy spectrum is broad and is called the white spectrum (Herz, 1969:4).

Characteristic X-rays

It is known that electrons move in orbits around the nucleus of the atom, each with its own discrete energy. Characteristic X-rays are the direct product of a collision between one of these discrete energy electrons and the high velocity electrons from the filament. The fast filament electron knocks a target electron from its orbit leaving a vacant orbital which can be filled by an electron from another outer orbital as long as the energy of the vacant orbital is lower.

A quantum of electromagnetic radiation (characteristic X-rays) is emitted to balance out the energy that needed to depart in order for the shift of electrons to occur. The voltage required to remove an electron from its orbit is called the excitation voltage and depends on the material involved.

There is a clear relationship between atomic number and excitation voltage, and X-rays produced with high atomic number materials require high voltages (Herz, 1969:5). Characteristic X-rays may also be produced in a process called electron capture where an unstable nucleus with too many protons may capture an electron (e^-) from a nearby orbital. During this process the proton (*p*) is converted into a neutron (*n*) according to the following reaction where *v* is a very small uncharged particle called a neutrino (Herz, 1969:10).

$$p + e^- \rightarrow n + v$$ **Reaction 2.11**

Sometimes when the electron is removed from an orbital that is vacant after capture, an electron from another higher energy orbital can fill it whilst emitting a characteristic X-ray. Some radioactive decay processes may lead to the emission of gamma-rays which can knock out the electrons in the same atom as the source nuclei in a process called internal conversion. The removal of these electrons will lead to the formation of excited atoms resulting in the formation of X-rays as described earlier (Herz, 1969:11).

Synchrotron radiation

A synchrotron radiation source is a special kind of X-ray source with the main advantage being the significant increase in radiation energy, flux and resolution. The X-ray beam is produced by using very powerful bending magnets that alter the path of accelerated particle beams, and can be utilized either as a filtered white spectrum or it can be made mono-energetic with a multilayer spectrometer (Jones *et al.,* 2003).

Gamma (γ)-rays

X-ray photons and gamma-ray photons having the same energy are identical except for their origin. Unstable radioactive isotopes are produced when the amount of neutrons and protons in an atom are tampered with and the resulting radioactive nuclei will emit radiation to restore its stability. In many of these radioactive decay processes the nuclei are left in an excited state and the excess energy is emitted as gamma-ray photons.

Gamma-rays can also be emitted from electron capture where the nucleus is in an exited state after the proton-to-neutron conversion is complete (Herz, 1969:9). Gamma-rays have a few advantages over X-rays, including the weaker dependence on the nature of the sample due to higher energy. With respect to X-rays, gamma-rays can be used to determine the density of samples more accurately since gamma-ray energy more closely approximates that of a mono-energetic beam (Duliu, 1999).

2.3.3 Attenuation

There are many different processes that occur when X-rays and gamma-rays interact with matter, depending on the energy of the radiation and the type of material involved. Note that due to the similarity in the properties of X- and gamma-rays, the absorption processes are similar.

Photoelectric absorption

X-ray photons can sometimes knock out electrons in orbit around the nuclei of atoms when X-rays (specifically low energy X-rays) interact with a material of high atomic number. This will lead to more X-rays being formed as discussed in the previous sections. The electrons ejected in such a fashion are called photoelectrons (Herz, 1969:15).

Coherent or Thomson Scattering. This happens when the incident X-ray photons are deflected or scattered upon interaction with the electrons around the nuclei. This change in direction is associated with an energy transfer to the orbital electrons, which begin to oscillate with the same frequency as the incident radiation. This effect is also predominantly seen with low energy X-rays and high atomic mass materials (Herz, 1969:15).

Incoherent or Compton Scattering. A different process can occur when the incident X-ray energy is sufficiently high with respect to the binding energy of some of the orbital electrons. In this process the incident X-ray photon may collide with a loosely bound orbital electron and is not only scattered but may also lose part of its energy to become radiation with different (increased) wavelength. The energy that was lost by the X-ray photon is transferred to the electron it encountered (recoil electron) (Herz, 1969:16).

Pair production

Energy can be converted into mass in a process called pair production when the energy of the incident radiation is high enough (>1.02 MeV) and the material involved is of high atomic mass. This is more common with gamma-rays that have high enough energy so that the photon passing through the material resembles a nuclear field, resulting in the disappearance of the photons and appearance of an electron-positron pair. This is very basic evidence that there is a distinct relationship between mass and energy (Herz, 1969:17).

Mass-absorption coefficients

Consider a beam of monoenergetic X-rays passing through a material of thickness t and density ρ, it is found that the exit intensity (I) of radiation can be related to the incident intensity (I_0) by the following equation, called the Beer/Lambert law (Bertin, 1978:60; Herz, 1969:18; Duliu, 1999; Cho *et al.,* 1993:148).

$$I = I_0 exp\left[-\left(\frac{\mu}{\rho}\right)\rho t\right] \qquad \textbf{Equation 2.12}$$

The parameter (μ/ρ) is the mass absorption coefficient (cm^2/g) of the absorbing material and is an atomic property of chemical elements that indicates their ability to attenuate X-rays. The mass absorption coefficient is also easily calculated for compounds by considering the concentrations and coefficients of their constituents (Bertin, 1978:60). The attenuation coefficient depends strongly on the effective atomic number and the density of a material, so in theory a researcher should be able to obtain a considerable amount of information regarding chemical composition and density from a tomogram (Duliu, 1999).

The mass absorption coefficient is the sum of all the components from photoelectric absorption (τ^*), coherent scattering (σ_0), Compton scattering (σ) and pair production (π) according to equation 2.13.

$$\frac{\mu}{\rho} = \frac{\tau^*}{\rho} + \frac{\sigma_0}{\rho} + \frac{\sigma}{\rho} + \frac{\pi}{\rho} \qquad \textbf{Equation 2.13}$$

Modern day X-ray computer tomography systems generally produce X-rays with energy in the ranges of 30 – 200 keV which is less than that needed for pair production (Duliu, 1999).

Detectors for imaging with wave-like electromagnetic ionizing radiation

Detectors can be regarded with good authority as being current pulse generators (Cho *et al.,* 1993:134). X-Ray detectors (scintillation counters) make use of special materials (typically gadolinium oxysulphide, cadmium tungstate, cesium iodide, bismuth germinate and barium fluoride) that emit visible light upon excitation by ionizing radiation in a process called scintillation.

The efficiency of these detectors depend on the X-ray energy i.e. the higher the energy the better the efficiency because the high energy X-rays are more penetrative, resulting in more radiation being converted to visible light (Ketcham & Carlson, 2001). There are other methods to detect the transmitted radiation including ionizing chambers, but due to a decrease in resolution of these chambers, the scintillator counter remains the superior technology. Advantages of using scintillator counters include high-detection efficiency, large amplitude of output signals and high speeds (Cho *et al.,* 1993:130).

2.3.4 Corpuscular particle-like radiation

Radioactive nuclei may emit an alpha (α) or beta (β) particle to form a new daughter nucleus of a different atomic number. If this daughter nucleus is in its lowest energy state then the process is finished otherwise gamma-ray photons are emitted to balance the energy. Alpha-particles are helium atoms consisting of two protons and two neutrons, whilst Beta-particles are electrons (Herz, 1969:12).

Neutrons

Neutrons are uncharged particles with a mass slightly heavier than pure protons and most elements interact with neutrons. Neutrons are primarily produced in a nuclear reactor with the fission of uranium or any other fissile material (Herz, 1969:14). The best way to imagine the fission process (refer to figure 2.4) is with the collective model that was formulated by Niels Bohr and John Wheeler (Halliday & Resnick, 2005). Neutrons are classified according to their energy and include cold, thermal, epithermal, fast and relativistic neutrons as indicated by table 2.3.

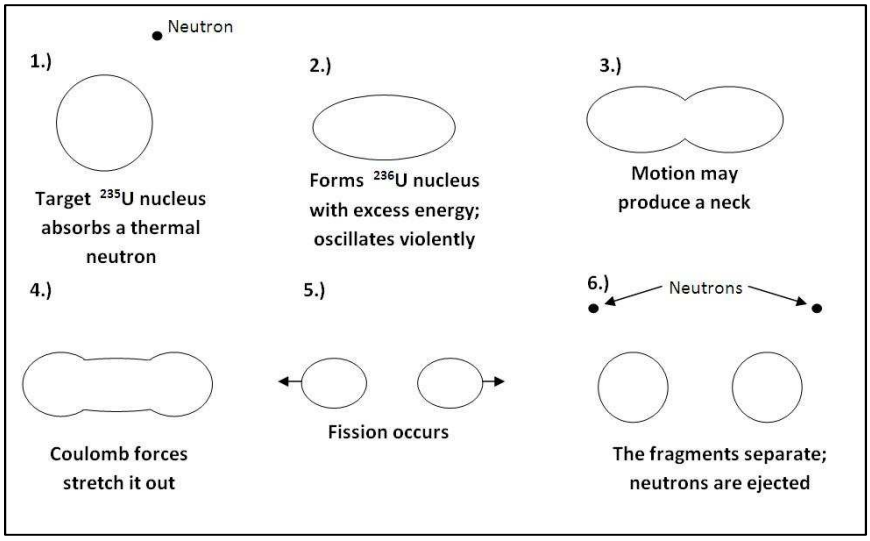

Figure 2.4: Neutron Production (Halliday & Resnick, 2005)

Table 2.3: Neutron energy and classification (Herz, 1969)

Neutrons	**Energy Range (eV)**
Cold	< 0.01
Thermal	0.01-0.3
Epithermal	0.3-10k
Fast	10k-20M
Relativistic	>20M

The first three classes in table 2.3 are referenced as slow neutrons and are produced by slowing fast neutrons down with a moderator such as water or graphite (Herz, 1969:15).

Attenuation

Neutrons are uncharged particles that cannot interact with electrons to ionize matter directly, but there are two other ways in which neutrons can indirectly initiate ionization.

Neutron Absorption. Neutrons that have a specific kinetic energy are captured by the nuclei of atoms to form compound nuclei (Herz, 1969:34).

Neutron Scattering. Neutrons may also experience scattering by undergoing elastic and inelastic collisions with the nuclei of atoms.

It is interesting to note that neutrons will transfer more energy to a light nucleus in an elastic collision than to a heavy nucleus, thus fewer collisions are necessary to stop a fast neutron in hydrogen than with heavy nuclei. Inelastic collision result in excited nuclei and is more common among the heavy nuclei and high energy neutron collisions (Herz, 1969:35).

Neutron imaging should not be viewed as separate from X- and gamma ray imaging but rather as complimentary, since neutrons can highlight certain distinct aspects that are impossible with X- and gamma rays. The attenuation of neutrons is completely different from X- and gamma rays as indicated by figures 2.5 and 2.6 (Grünauer, 2005). The relationship between X-ray attenuation and atomic mass is approximately linear whilst that of neutron attenuation and atomic mass is random. That is why X-ray attenuation can be used to visualize density distributions by converting the CT numbers to grey values.

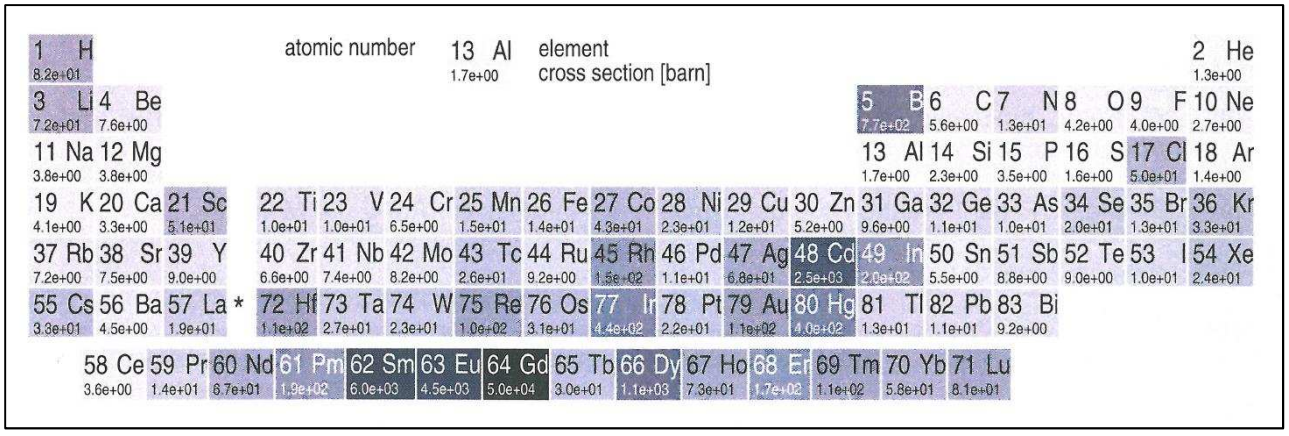

Figure 2.5: Total microscopic cross section for neutrons - 25 meV (Grünauer, 2005)

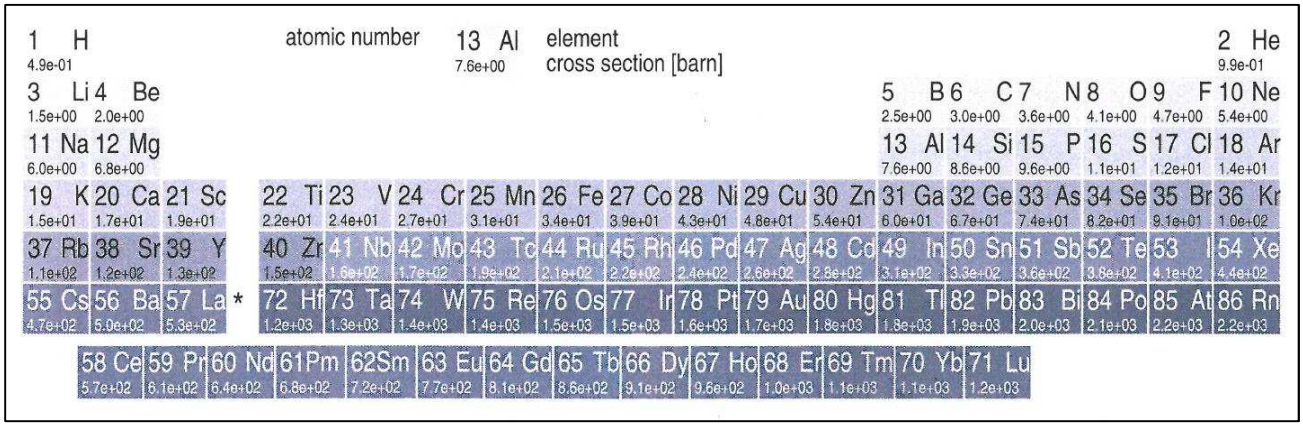

Figure 2.6: Total microscopic cross section for photons - 100 keV (Grünauer, 2005)

SANRAD (South African Neutron Radiography and Tomography) facility

Beam line no 2 at the SAFARI-1 research reactor at Necsa (Pelindaba, Church Street, Pretoria) is specifically designed and optimized for neutron radiography (see figure 2.7) (De Beer, 2005). The SANRAD facility is located between a small angle neutron scattering facility (beam line no 1) and a neutron diffraction experimental facility (beam line no 5). The neutrons utilized for radiography and tomography are thermal neutrons since a bismuth filter removed the fast neutrons and gamma rays. A radial collimator is installed to direct and focus the beam.

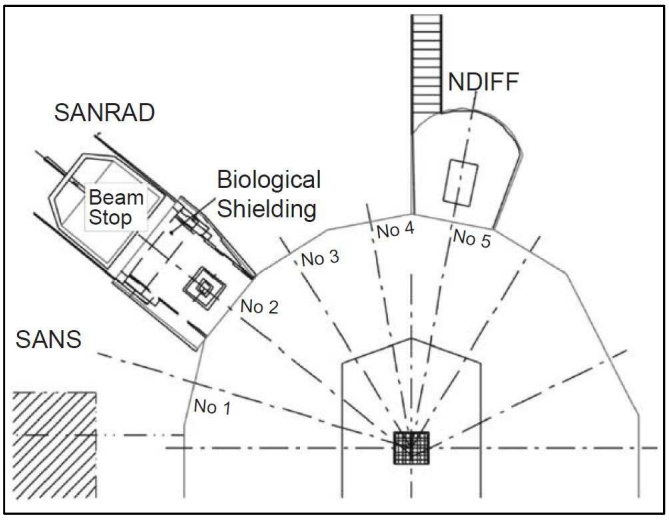

Figure 2.7: Location of the SANRAD facility at SAFARI-1 (De Beer, 2005)

The walls of the SANRAD facility are 45 cm thick high density concrete, covered with 2 cm thick polyethylene and 2 cm thick boronated wax (with 5% Boron by weight). These layers were chosen for their neutron stopping characteristics (they have high neutron attenuation). At the open-end of the facility is an access door which seals the facility and stops the beam when a radiography or tomography experiment is in progress.

This 1.5 m thick door consists of iron and polyethylene enclosed in a 0.5 cm thick steel shell. The inside surface area of this door is covered with 4 cm thick Boron wax (also 5% by weight). This door is the only access point to the facility whilst there are small openings on the top of the facility for very long samples which are analyzed in sections (De Beer, 2005). The SAFARI-1 research reactor usually operates at 20 MW power which results in a neutron beam with a flux (in the middle of beam) of 1.2×10^{7} neutrons cm^{-2} s^{-1}. The flux is adequate for radiography and tomography when the image exposure time is long enough – about 30 – 50 seconds to obtain a high dynamic range (up to 60K grey levels).

The scintillator screen utilized at the SANRAD facility has the elemental composition of 6LiF/ZnS:Cu,Al,Au. The ideal neutron beam would be completely parallel, but this is not the reality at the SANRAD facility and some beam divergence is unavoidable. The divergence ranges from 0.9° at a beam opening of 6 mm to 3.2° at a beam opening of 21 mm (De Beer, 2005).

The SANRAD facility also has the capabilities for X-ray radiography and tomography by inserting a 100 kV X-ray tube in the beam opening with a specialized jig. The neutron scintillation screen is replaced by an X-ray sensitive gadolinium oxysulfide scintillation screen at the bottom of the camera box (refer to figure 2.8). This camera box is made from aluminium and basically contains a mirror which redirects the visible light beam 90° towards the Andor Technology digital camera (De Beer, 2005). This is necessary in order to protect the sensitive electronic components of the digital camera from radiation exposure. Andor also provided the software for image acquisition and camera operation.

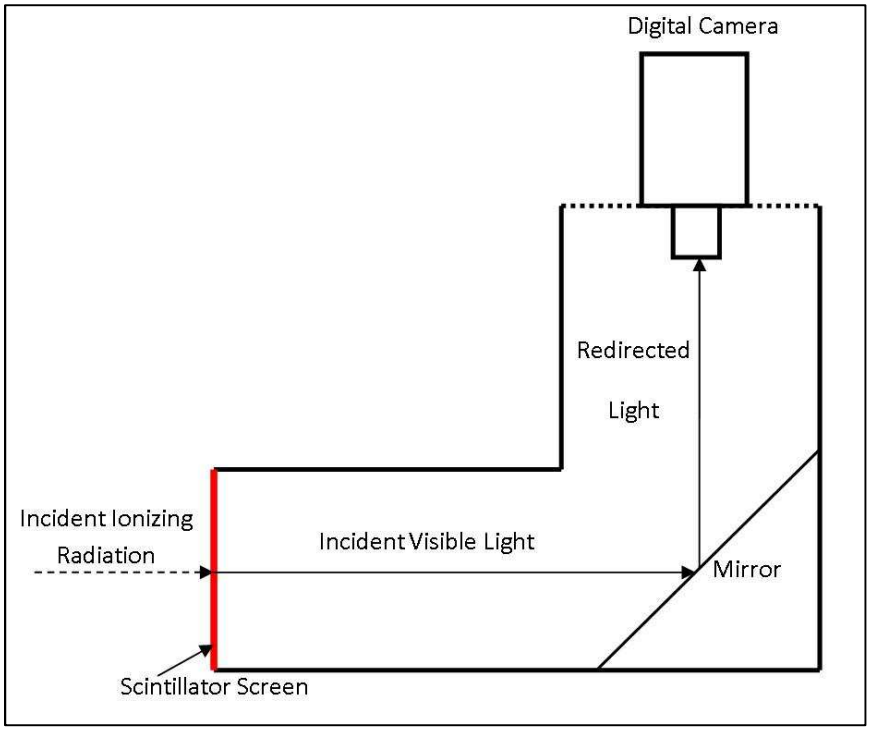

Figure 2.8: Camera box at the SANRAD facility

The camera inside the light tight camera box is a special scientific camera with a Peltier-cooled CCD which has low noise and direct output to a PC. The temperature of the CCD chip can go down to -75 ℃ where the noise is less than 0.05 electrons $pixel^{-1}$ s^{-1}.

The output of the camera is 16 bit images (tiff format) at readout of 2.2 seconds per frame. There are also two lenses which can be interchanged to increase or decrease the field of view. The type of lens used, influences the time of each scan and consequently the time for the smallest field of view lens is five times that of the largest field of view lens. The CCD chip of the camera has a dynamic range of 65535 grey scales per pixel (De Beer, 2005).

Samples are positioned on top of a sample manipulator that can rotate and translate the sample in one direction with Berger Lahr stepper motors. The sample manipulator is controlled from a dedicated PC with a Labview software interface. The two PCs that acquire images and manipulate the sample are linked and can communicate with each other. This ensures that the images are acquired at exact intervals and when the sample is stationary.

The PCs at the SANRAD facility are not utilized for volume reconstruction in order to ensure that the image acquisition is precise and no frames are dropped due to limited memory. All reconstructions are performed at a specific PC laboratory in another building on state of the art 64 bit reconstruction workstations (De Beer, 2005).

The quality and accuracy of quantitative measurements derived from a tomographic scan depends strongly on the clarity of the radiographic images obtained from the experimental equipment. The tomographic system at the SANRAD facility is optimised by optimally focusing the lenses. This is done by placing a very thin Gadolinium foil against the scintillator detector and fine-tuning the focus of the lens so that the edge of the foil is clearly defined by the least number of pixels. The experimental measurements can commence after this procedure (De Beer, 2005).

2.4 Computer tomography

Computerized axial tomography (CAT), or computed tomography (CT), is the process in which a digital map of the spatial distribution of the attenuation coefficient is obtained and has the following characteristics.

- CT is a complete nondestructive imaging technique that is applied in numerous processes from medical imaging to industrial research (Duliu, 1999; Kuper *et al.,* 2007).

- The images that result from a CT scan are digital in nature and can be converted and processed with image processing software (Duliu, 1999). Typical techniques include filtering of noise, smoothing, contrast enhancing, etc.

The principle concept of how a CT scan can result in 3D images of the object lies in the properties of the attenuation coefficient as described in section 2.3.3. The first step in the CT process is to create 2D radiographic images of the radiation that is transmitted through the sample (refer to figure 2.9 – top left). It is these images that represent the distribution of the attenuation and consequently density of the sample (Duliu, 1999). The next step entails the conversion of the 2D data into a usable 3D data set through a process called image reconstruction. Reconstruction is the mathematical process in which a sinogram is transformed into 2D data that can be used to represent a 3D volume and one of the methods most frequently used is the filtered back projection technique (Van Geet *et al.*, 2001; Remeysen & Swennen, 2006).

A sinogram (refer to figure 2.9 – top right) is the representation of the data in the initial 2D radiograph on a logarithmic scale (Kuper *et al.,* 2007). The reconstructed images (refer to figure 2.9 – bottom left) are 2D slices of the scanned sample in the scan plane, perpendicular to the axis of rotation and are a distribution of the so-called CT-numbers or Hounsfield number (Ketcham & Carlson, 2001; Mazumder *et al.*, 2006). The CT-number of air is taken as 1000 whilst that of water is taken as 0.

$$CT_N = K\left(\frac{\mu-\mu_w}{\mu_w}\right) \qquad \textbf{Equation 2.14}$$

The CT-numbers are to voxels (volume elements) in the reconstructed 3D volume what the grey values are to pixels in the original radiographic images. Reconstructed images are usually displayed as negative images i.e. the areas which have the highest density and consequently the highest attenuation value are displayed with the lowest or lightest intensity (Duliu, 1999).

This general rule is not applicable to neutron scans because the relationship between attenuation and density is not as ordered (linear) as with X-rays. Reconstructed images can be stacked together in dedicated software and viewed as a 3D volume of the sample (refer to figure 2.9 – bottom right). This 3D volume is analyzed by different techniques like segmentation where a greyscale threshold is isolated as representative of a certain material (Kuper *et al.,* 2007).

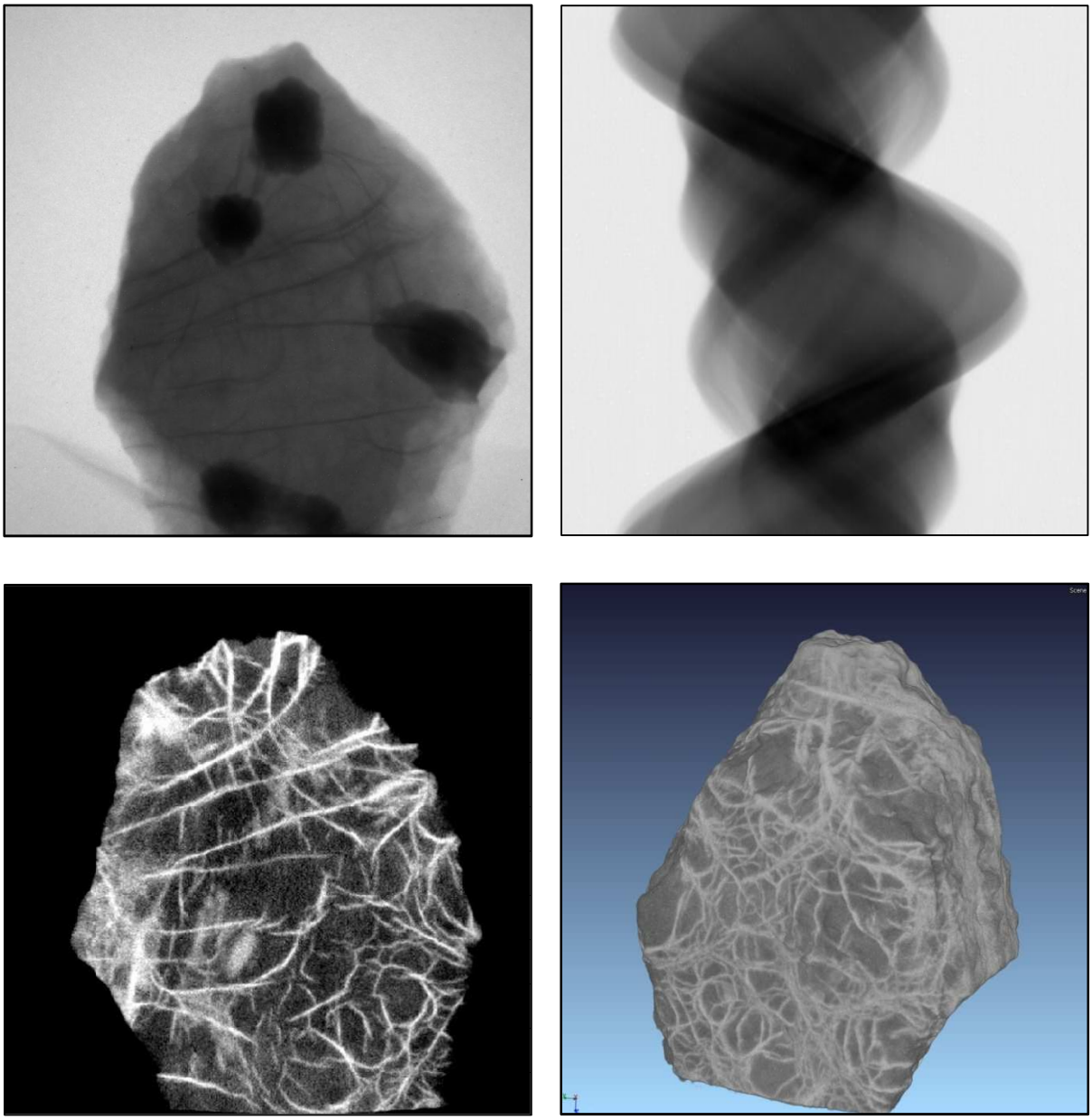

Figure 2.9: The Reconstruction Process

Like all technology CT has a few disadvantages. Some artifacts (and errors) are associated with CT scanning and are discussed in the next section. It is sometimes difficult to distinguish between the grey values of materials with closely related densities.

To distinguish the constituents of samples that have components of near densities are very complicated (Duliu, 1999). This problem can sometimes be overcome by image processing, but this leads to the systematic build-up of errors. There can be a negative correlation between the attenuation coefficient and the spatial resolution, especially with medical CT equipment.

This can be overcome by using a microfocus (μCT) system that has improved spatial resolution (Duliu, 1999). Defrise (2001) stated that all 3D tomographic techniques have the disadvantage of an increased background due to X-ray photons being scattered. The resolution is also highly dependent on the sample size, especially with microfocus X-ray CT i.e. the smaller the sample the better the resolution (Long *et al.*, 2009).

X-rays have been used extensively in the past to reveal the inside structure of many objects through a process called X-ray radiography. This method comprised using radiographic film to present 3D information on a 2D surface and has a few major disadvantageous (Duliu, 1999). All the detail in the sample, irrespective of their position, is projected onto the same plane and consequently a significant amount of spatial orientation and distribution information is lost. There is a non-linear relationship between the optical density of the film and the attenuation coefficient which can lead to a systematic build-up of errors. That is one of the reasons why radiography cannot be used to calculate the density of materials.

Neutrons have also been extensively used in imaging of geological and other non-living materials. There are a clear relationship between atomic number and, consequently, the density of atoms, and their respective X-ray attenuation coefficients, whilst the same cannot be said about neutrons. That is why neutron tomography should not be seen as an alternative to X-ray tomography, but rather as complementary to it (Winkler *et al.,* 2002).

2.4.1 Artifacts associated with CT

Beam hardening

The most common artifact is beam hardening which provides the illusion that the material on the outside edges of a sample is denser than the material on the inside, whilst the material is in fact homogeneous (Cho *et al.,* 1993:156).

This is the direct result of the average X-ray energy increasing as the beam passes through the sample i.e. the lower energies being absorbed by the sample. Beam hardening can be a serious problem in the sense that it will change the CT value of a specific voxel and therefore it is erroneous to deduce density or composition information from that specific sample.

Beam hardening is also sample structure specific with irregular shaped samples being the most affected since the beam hardening is difficult to observe and its extent, differs from slice to slice. Ketcham & Carlson (2001) proposed that the easiest ways to cure beam hardening would be to ensure that the incident X-ray energy is sufficiently high or the sample size should be sufficiently small. The increased X-ray energy will lead to a decrease in attenuation contrasts and consequently it will become more difficult to distinguish different densities.

Another remedy includes providing a pre- or post sample filter (typically copper, brass or aluminium) which removes this effect by eliminating the lower energy photons of the X-ray beam. An appropriate filter will reduce beam hardening in high attenuating material and will almost remove beam hardening in low attenuating material like the coal matrix (Van Geet *et al.,* 2001). This remedy too has problems since it affects all energy ranges in some way or another, thereby increasing the noise (Ketcham & Carlson, 2001). The sample can also be placed in a calibration material which should eliminate the low energy photons by letting beam hardening form in the calibration material instead of the sample, but this too would add noise to the already noisy system (Ketcham & Carlson, 2001). The previous methods included physical methods of removing beam hardening whilst there are software packages that correct for this artifact, although aggressive correction can also lead to data loss.

Ring artifacts

A ring artifact appears as rings in the vicinity of the axis of rotation and is the product of a shift in the output of a detector which is amplified during the reconstruction process i.e. the no-linear response of the detector (Ketcham & Carlson, 2001; Kuper *et al.,* 2007). Factors causing this shift include temperature changes and beam intensity changes, amongst others. These physical experimental conditional changes can be eliminated by implementing sensitive controllers and regular calibrations that ensure a stable experimental environment. Ring artifacts are closely related to beam hardening in the sense that they occur when the detector incorrectly responds to changes in beam intensity and can also be eliminated or minimized in the same way but more frequently it is dealt with by converting to polar coordinates (Ketcham & Carlson, 2001). Ring artifacts are seen as lines when the reconstructed image is converted to polar coordinates, and can therefore be easily removed (Kuper *et al.,* 2007).

Streak artifacts

When a highly attenuating object with an irregular shape is scanned, it is possible for an artifact in the form of streaks to appear at sharp edges. The difficulty with streak artifacts is that they can amplify the effect of other artifacts (like ring artifacts) so that they are eventually more difficult to remove (Ketcham & Carlson, 2001). Due to their link with ring artifacts it is possible to minimize the effect of these streaks by using the same methods as with ring, and consequently beam hardening artifacts.

Partial-volume effects

The partial-volume effect occurs due to the limitations of the resolution (Ketcham & Carlson, 2001). The CT numbers are representative of the volume distribution and are derived through reconstruction from the grey values of the pixels. So if the resolution is low, the voxels would be bigger and they would be derived from relatively large pixels that may span more than one detail. The CT value is derived by averaging the properties of the data that completes one voxel i.e. the software would average the pixel values to obtain the voxel CT number. Partial-volume effects are responsible for the blurring effect of the edges especially where there is a transition between high and low attenuating material. Any analysis and specifically the quantitative analysis with extreme partial-volume effects are very difficult. Partial-volume effects are directly related to the resolution of the scanning system used, and consequently a system with a better spatial resolution (i.e. a smaller voxel) will minimize the effect of partial-volume artifacts.

2.4.2 Optimal operation

Various researchers studied the optimal operating conditions and optimization procedures for CT. Sleutel *et al.* (2008) compared different CT setups, ranging from microfocus to nanofocus systems and concluded the following with respect to optimal operating parameters:

- A medium energy scanning setup present the best results regarding phase segmentation although low energy is the best theoretically
- A high amount of noise leads to significant loss in image quality, especially in the low energy ranges.

Increasing the exposure time per projection can be beneficial in situations like this, but this will add strain to the X-ray tube filament and target. Software based filters and corrections can also be useful.

- Filters can be used to aid in phase segmentation, although the use of it should be with caution since filters can lead to discrepancies.

2.4.3 A review of the results obtained in geosciences research by using CT

Many of the properties and characteristics described here are the desired outcome of coal investigations, as will be discussed in the next five chapters.

Mineral distribution

One particular research field that utilised the non-destructive nature of the CT technique extensively is the geosciences (of which coal research is a subsection). Kuper *et al,* (2007) studied the 3D distribution of minerals in diamondiferous eclogites with synchrotron X-rays and concluded that this technique can be utilized to view the mineral distribution of several sample sizes. Diamondiferous eclogites are very rare and therefore the non-destructive nature of the CT technique was appreciated during this investigation. Determining the grey value interval that corresponds to the material of interest was particularly difficult for the authors, since partial volume effects due to relatively low spatial resolutions (approximately 100-200 µm) were present.

But even with these limitations it was possible to observe the diamonds within the eclogite matrix. By knowing the spatial relationship between the diamonds and other minerals it is possible to have a better understanding of the processes that govern diamond formation. Neutron tomography was used by Winkler *et al.* (2002) to determine the mineral composition, mineral grain size and spatial distribution of mineral grains of rock samples. The conclusion of the study was that neutron tomography does not currently have the spatial resolution of X-ray µCT and it is anticipated that neutron systems will be available in the near future with spatial resolutions of 5-10 µm.

Petrographical analysis

Long *et al.* (2009) applied µCT as a petrographical tool to characterize Westphalian C sandstone samples and compared the result to a thin sectioning process. Thin sectioning is the usual method that is used to perform petrographical analyses and do not produce accurate information concerning the shape, size and spatial distribution of objects in 3D. It was found that a major drawback of µCT is the limiting sample size that determines the optimal resolution. The magnification of a µCT scanner is directly related to the sample size and the smaller the sample the better the resolution and consequently the enlargement.

A small sample is not necessarily representative of the bulk material. Long *et al.* (2009) found it difficult to determine the optimum resolution and sample size that would both be adequate and representative of the bulk material. The sample size (8 mm) was therefore kept sufficiently small to ensure that the best spatial resolution (6.2 µm) could be obtained. They concluded that µCT is indeed a complimentary research technique and porosity and distinct mineral phases were determined. They did however fail in distinguishing different clay minerals present due to the close attenuation coefficients of these minerals.

Mineral liberation analysis

Schena *et al.* (2007) designed a high resolution CT system to study the mineral liberation of fine multi-phase particles and found that the CT technique is a powerful way of extracting liberation information (Miller *et al.,* 2003), and proposed a dedicated system specifically for this purpose. The primary goal of the investigation was to obtain information on the liberation spectrum of a system of particles – an important parameter for plant optimization. The time that it takes for this information to be available is crucial since the specific process is rarely interrupted and the sooner the information is available the sooner it can be corrected for mistakes.

SEM of polished sections (which is time and labour consuming) was the predominantly used method to obtain this liberation spectrum information prior to CT. It was further reported that the system that is proposed will achieve micron and sub-micron resolutions whilst still being faster and cheaper than current industrially available systems. The characteristics of multiphase particles are of significant importance when mineral processing operations are considered.

The performance of these operations depends on the characteristics of the microstructure of individual particles and typical characteristics include composition distribution, surface exposure of mineral grains, phase continuity, interfacial areas, particle shape, etc (Miller *et al.,* 2009). The multiphase particles of packed beds were characterized in 3D by Videla *et al.* (2007) with µCT. During this study the density of different particles in a packed bed were calculated and the volumetric grade distribution of multiphase mineral particles were determined.

Porosimetry measurement

It is sometimes needed to not only study the current porosity of a specific sample but also the development and progression of the porosity network due to certain physical and chemical processes. De Gryze *et al.* (2006) studied the changes in pore morphology of soil by using µCT. Decaying plant material inside soil influences the amount and type of microorganisms that are present within soil at any particular time. The pores that are in close contact with the decaying material are of particular importance since these pores contain the most microorganisms. Little is known about the effect of decaying organic material on the porous architecture and the CT technique allowed the researchers to gather crucial information. Obtaining information on soil porosity at an aggregate level was very impractical before CT, since data obtained via thin sectioning was for very thick cross sections of samples. The system that was utilized enabled the researchers to identify pores with mean diameters of approximately 27-40 µm, and they concluded that aggregate samples from natural and artificial origins differ significantly. The reason for the latter difference can be ascribed to the formation of micro-cracks (± 100 µm) in the (artificial) soil structure, which could only be visualized through µCT. A mass fractal dimension was also calculated to quantify the changes in pore sizes and it was concluded that pore stability, rather than pore morphology, was responsible for the formation of stable aggregates.

Van Geet *et al.* (2003) measured the porosity of sedimentary rocks with a µCT system and compared the results to data obtained from polished surfaces. Porosity data obtained via the common mercury porosimetry measurement technique is inaccurate and in reality not actually a pore size distribution but rather a distribution of the effective radii of pore openings (throats). It was observed that the average value for porosity obtained with µCT is slightly larger than the average values obtained through mercury and vacuum porosimetry. The reason for that indicated one of the major advantages of using µCT to determine porosity, and that is µCT includes all the pores and not only the connected pores.

It was however concluded that μCT is not necessarily the most appropriate way to study permeability due to this total pore volume representation. Therefore, μCT is an additional tool for studying porosity in conjunction with other techniques.

A synchrotron radiation source have has increased resolution (typically less than 5 μm) and provide even more detail regarding the porosity of sandstone, as was investigated by Jones *et al.* (2003). Estuarine sediments were analyzed with synchrotron CT because understanding these types of samples will lead to an understanding of the sandstone formation process, as well as the transport of manmade contaminants. The porosity characteristics (including mechanical properties) of the samples were determined and the results were comparable to that those found with more conventional methods. The research conducted by Jones *et al.* (2003) also demonstrated the ability of CT to be applied in environmental studies that aims to prevent unnecessary pollution. Auzerais *et al.* (1996) also studied the transport in sandstone samples with extremely small samples in a μCT system. Typical parameters that were determined included geometrical parameters, permeability constants, electrical resistivity and residual saturation. By using the non-destructive capabilities of CT it was possible to directly compare the theoretical calculations and laboratory measurements.

Fracture and cleat analysis

Fluid flow in fractures and fracture networks are currently forming integral parts of scientific fields including hydrology and petroleum and civil engineering. Vandersteen *et al.* (2003) characterized fracture apertures for limestone samples with μCT and concluded that the apertures obtained is are in accordance with optimal microscopy measurements. A previous method of quantifying the variability of fracture apertures included injecting hardening resins and metals rendering the sample unusable for further experimentation. Zabler *et al.* (2008) used synchrotron radiation to study the formation of cracks and voids in rocks by acquiring and comparing a 3D image of the rock sample prior to and after compression.

Moisture content

Neutrons are ideal when determining the moisture content of coal since neutrons are highly attenuated by hydrogen. It is proposed by Sowerby *et al.* (1988) that the neutron attenuation coefficient should be split for solids and water when determining the moisture of coal with neutrons. The following equation represents how this is done:

$$\mu_{neutron} = \mu_w C_w + \mu_s C_s \qquad \textbf{Equation 2.15}$$

Here μ_w and μ_s refer to the neutron attenuation of water and the solids (in this case coal) respectively, whilst C_w and C_s refer to the concentration of water and solids respectively. The error for calculations from neutron applications in coal are lowest when the ratio I/I_0 (equation 2.12) is between 0.005-0.1. It should also be noted that calculating moisture values based on Beer Lambert's equation will always differ from measurements since the equation does not bring scattered neutrons into account. It is therefore advisable that the researcher uses a large source to detector distance and a small sample and detector to minimize the effect of scattered neutrons.

The main objective in the investigation performed by Sowerby *et al.* (1988) was to evaluate different setups, with numerous distinct neutron detectors, in order to minimize the error associated with moisture content measurements. The emphasis was therefore on determining the best neutron equipment to perform the measurement and not on the coal properties that determine the coal behaviour. Therefore, neutrons still have to be used in coal research, with emphasis on coal characterization by determining chemical and physical coal properties.

It was however found that the error associated with the determination of hydrogen content in coal was in the order of 0.-0.15 wt%, which is comparable with that obtained from a chemical laboratory hydrogen analysis. The results were even better for lump coke since an error of less than 1 wt% could be achieved with neutrons and the results were not as dependant on variations in hydrogen content. This is however only achievable if the bound hydrogen (hydrogen that forms part of the coal matrix and not moisture) is less than 0.14 wt%. Typical errors obtained from chemical laboratory analyses were in the order of 0.08-0.26 wt%, which is also comparable (Sowerby *et al,.* 1988).

The following chapter will discuss transport properties in the macrostructure of coal with emphasis on carbon dioxide sequestration and methane production.

3. Carbon dioxide sequestration and coal bed methane production

The cleats, fractures, voids and macro and micropores that constitute the porosity of coal are vital in facilitating transport of gases in and out of the coal structure. Two research topics that currently enjoy a vast amount of attention and are based upon coal void structure transportation, are carbon dioxide sequestration and coal bed methane production.

3.1 Background information

The burning of fossil fuels is still the single most important energy production method in the world, even though alternative methods exist. Burning all these fossil fuels result in enormous amounts (22×10^9 ton/year) of carbon dioxide being emitted into the atmosphere and it is general knowledge that carbon dioxide is a major contributor to global warming (Holloway, 2005). It is therefore natural to search for ways in which carbon dioxide production and disposal can be controlled. The first obvious thing to do would be to regulate the amount that is being produced and consequently many laws limit the carbon footprint of individuals and institutions. But a far more difficult thing to do is to deal with the already produced amount of carbon dioxide in the atmosphere. That is where carbon dioxide sequestration comes to play since it is a viable method in which produced carbon dioxide can be stored in a section of the earth that is unused (Holloway, 2005). This is however easier said than done since it would have to be performed at a significant scale and it should not pose any more risk towards man and the environment. That is why “carbon dioxide sequestration” is a buzz word amongst the scientific community.

The underground volume that would be needed for sequestration would need to have characteristics that would permit storage of carbon dioxide for hundreds to thousands of years until the carbon dioxide levels in the atmosphere has dropped (Holloway, 2005). Pilot and experimental operations conclude that it is definitely technically possible to store vast amounts of carbon dioxide underground (up to 1×10^6 tons/year for the Sleipner West gas field in the North Sea). There are in fact numerous natural carbon dioxide gas fields around the world which enclosed its carbon dioxide for tens of millions of years.

The proposed sequestration locations would however have to comply with very strict geological guidelines or considerations (Holloway, 2005). The process of carbon dioxide sequestration begins with capturing and transporting carbon dioxide. This is however easier said than done because carbon dioxide is usually not the only emission from industrial processes. Separation of carbon dioxide from other flue gases is therefore vital since the volume in which it can be stored is limited and compression of all the flue gases will add drastically to costs. Separated carbon dioxide is primarily transported by pipeline or in some cases by ship where the sequestration site is offshore.

There are four types of underground sequestration locations, including coal beds, spent oil and gas fields, natural and man-made caverns, porous and permeable rocks (Holloway, 2005). Man-made caverns like mines are not necessarily appropriate since they have very limited capacity and they tend to fill with water and gases will consequently be forced out. Storing of carbon dioxide in unused porous and permeable rocks is very appropriate since it is estimated that up to 400 to 10000 giga tons of gas can be stored in this way (Holloway, 2005). Storing carbon dioxide in depleted oil and gas fields have the added benefit of increasing oil and natural gas production.

Some coal beds are ideal for sequestration projects since many coal beds do not have coal that is economically important. These coal beds do however have a network of cleats and fractures (and microporous structure) that make them ideal for large scale gas storage (Holloway, 2005). Many coal beds that contain coal that is not mineable, have significant amounts of methane and consequently still economic value. Due to the small size of the molecules they are closely packed and coal beds can consequently contains large amounts of methane (up to 20 m^3/ton of coal) (Holloway, 2005).

The methane molecules are adsorbed onto the surface of the cleats and micropores and are held in place by weak electrostatic forces that are very sensitive to temperature and pressure changes (Karacan & Okandan, 2000; Holloway, 2005). Factors that influence the amount of adsorbed methane and the kinetics of adsorption include coal composition, porous structure and mineral matter characteristics (Karacan & Okandan, 2001). Wang *et al.* (2007) reported that the amount of methane that can be extracted from a coal bed with conventional depressurization before extraction becomes uneconomical typically ranges between 50-60 % of the total methane volume.

Carbon dioxide has a higher affinity for adsorption on coal than methane and consequently sequestration in coal beds not only disposes of unwanted carbon dioxide, it also aid in extraction of useful methane (Holloway, 2005). Methane typically constitutes about 95 % of all gaseous material within the coal structure (Karacan & Okandan, 2000). The methane recovered could be used to partially fund for the costs associated with the sequestration.

It is sometimes very difficult to extract all the methane from the coal bed, especially when the gas flow becomes low and consequently further extraction becomes uneconomical. It is because of the environmental impact that carbon dioxide sequestration has and the financial benefits of methane extraction that it is crucial to obtain knowledge on how these gases flow within the pores and fractures in the coal structure. CT is an attractive research technique to obtain this knowledge as the following paragraphs will indicate.

3.2 Sorption and desorption of carbon dioxide

The adequacy of possible sequestration sites depend on many characteristics of coal, including porosity, permeability, sorption capacity and the quantification of swelling due to carbon dioxide uptake and shrinkage due to water and methane loss (Pone *et al.,* 2009). The two last mentioned characteristics are especially important since the injection of carbon dioxide decrease the sorption ability of a possible sequestration site. The reason is that the increase pressure experienced by injecting carbon dioxide into the coal will lead to the fractures and pores being compacted and consequently, a decrease in permeability. The opposite is true for desorption of methane and water where the permeability is increased (Pone *et al.,* 2009a).

The first step that is necessary to investigate a possible sequestration location is modeling the chemical and physical processes that occur during sequestration, especially keeping aforementioned characteristics in mind. It has been found that modeling coal swelling and shrinkage under in-situ stress conditions (under confining stress) with conventional, basic volumetric models does not adequately represent coal behaviour. These models, typically, do not consider the effect of coal heterogeneities, compression and compaction, softening, collapse, rearrangement and rebound phenomena of the coal structure. The dissolution of carbon dioxide may result in the softening and rearrangement of the coal structure and consequently, a lower diffusion rate.

This is because a softening or relaxation of the coal structure may decrease the effective volume due to the compaction and compression of lithotypes (especially among bituminous coals) (Pone *et al.,* 2009a). The heterogeneity of the coal is responsible for non-uniform deformation and kinetic effects of adsorption and desorption of carbon dioxide (Pone *et al.,* 2009a). Penetration into different regions would commence at different rates and compaction would also occur at distinct time intervals due to the distinct composition of all the lithotypes in the coal. Regions that are easily accessible would swell first and with the effect of the confining pressure would compress adjacent regions that have slower adsorption kinetics.

Conventional strain measurements that were used to obtain information on the deformation of the coal structure under stress conditions gave only limited insight of the internal structure and associated changes. This is because strain measurements are usually done on the surface and it is impossible to deduce a relationship between deformation and microstructure in this way. However, three dimensional X-ray CT allows the visualization of permeability, gas sorption, the development of cracks and fractures as well as the swelling and compacting in three dimensions. Another reason why previous attempts at modeling the swelling and shrinking of the coal structure was so unreliable is the incorrect sample size. Some researchers attempted to describe swelling and shrinking of coal by using powders which is not comparable to the behaviour of a coal core due to the locally heterogeneous nature of coal (Pone *et al.,* 2009a; Karacan & Okandan, 2001).

A sample can be prepared perpendicular or parallel to the bedding plane for strain evaluation, but it is advised to choose it parallel to the bedding plane (Pone *et al.,* 2009; Pone *et al.,* 2009a). The reason for that is the overburden (typically sandstone) on top of the seam would inhibit swelling in a direction perpendicular to the bedding plane (Pone *et al.,* 2009). Both ends of the sample should be level and polished to ensure that the strain is applied uniformly along the direction of the bedding plane.

It is also very important to evacuate the sample prior to gas strain experiments to remove any remaining gases and water. Dry carbon dioxide can dehydrate the coal sample with the direct result being a shrinkage that could be approximately equal to the swelling induced. Since sequestration sites are deep underground it will be necessary to simulate the resultant pressure at that depth by applying equivalent hydraulic pressure uniformly around the sample (typically pressurized with water) (Pone *et al.,* 2009).

Reference images should be taken prior to and after pressure (confining stress) has been applied (the sample should be left for a few days to achieve pressure equilibrium). The pressure at which the gas should be injected should be carefully regulated and kept at a constant value which would be representative of the pressure at which the gas would be injected at the sequestration site. The injection process should conclude when the pressure in the sample remains constant. An appropriate amount of time should also be given for the gas to escape from the coal matrix during desorption experiments where the shrinkage can be assessed (Pone *et al.,* 2009).

It is possible to identify distinct entities within the coal structure and consequently the movement of these entities can lead to strain evaluations (feature tracking). It is thus possible to see how stress and strain can alter the coal structure by just tracking certain features. The feature tracking technique is especially applicable to coal investigations since there are usually distinct clusters of high attenuating material that can be tracked. The chosen material should have a lower reactivity to carbon dioxide, water, etc. and a sufficiently higher density than the rest of the coal matrix. South African coal contains significant quantities of the minerals calcite, dolomite and koalinite (Falcon & Falcon, 1987) which are ideal features to track with CT since they have sufficiently high X-ray attenuation values. The CT numbers of calcite, dolomite and koalinite are respectively 4521, 3924 and 3096 which is much higher than the 1254 of the coal structure (with an assumed formula of $C_{49}H_{43}O_7SN$ and density of 1.3 g/cm^3) and should therefore be easy to distinguish (Maylotte *et al.*).

Each cluster of high attenuating material could be used as a reference point in three dimensions and can be easily followed after strain has been experienced. It is easy to fully quantify the location of each reference point in three dimensions since most commercial visualization software packages can calculate the Cartesian coordinates in all directions. A discrete displacement vector field can be compiled by recording the coordinates in the different levels of applying strain. From the vector field it is possible to quantify the effect of stress and strain on the coal structure. A potential problem that may be associated with the feature tracking method is the inability to visualize the heterogeneity of the coal structure due to low contrast between constituents that have similar densities (Pone *et al.,* 2009a). By visualizing the digital volume of the sample, it is possible to identify the different reference points (as discussed in the previous paragraph).

Four of these neighbouring reference points can be grouped to form a tetrahedron from which the geometric centre (centroid) can be calculated (refer to figure 3.1). The centroids are used to quantify the amount of deformation that each tetrahedron experiences. The displacement of each centroid is quantified by noting the change in the Cartesian coordinates of each centroid.

Sharing tetrahedron boundaries can ensure that there is continuity in the strain calculations due to elimination of localized effects (i.e. different regions will deform differently). The complete mathematical procedure and equations used in quantifying the movement of each centroid are discussed in Pone *et al.* (2009a). In summary the movement of each centroid is quantified in three dimensions by calculating the translation on each axis (x, y and z). Quantifying the direction and magnitude of the total displacement requires simultaneous solution of linear polynomials representing all directions whilst the total volumetric strain is the sum of strains in all directions.

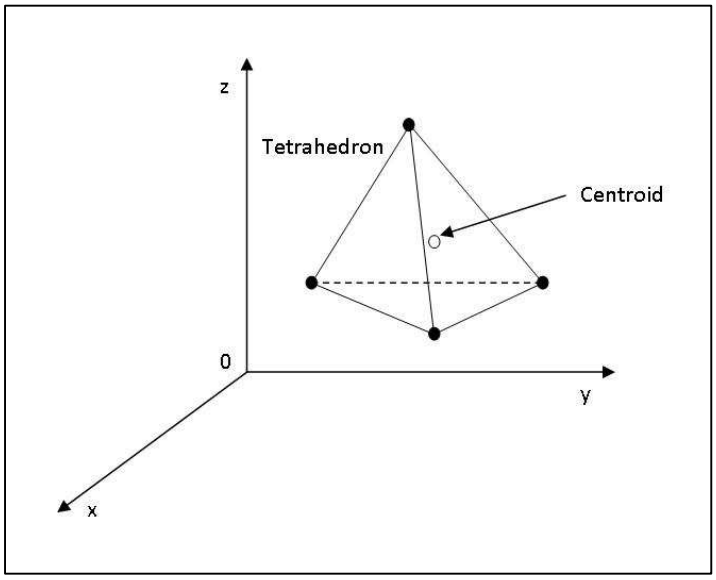

Figure 3.1: Calculating a centroid (Pone et al., 2009a)

An interesting observation that can be concluded from strain evaluations of carbon dioxide sequestration analyses is that the coal structure is altered irreversibly. Pone *et al.* (2009) concluded that the coal structure swelled irreversibly when carbon dioxide is injected, even under confined pressure, whilst another investigation concluded a net compression of the coal structure (Pone *et al.,* 2009a).

The reason for this difference could be ascribed to the heterogeneity of the coal structure since different levels of fracturing and different lithotypes and macerals react distinctly to the confinement and carbon dioxide induced pressures. Another possible reason why there is this distinct difference in behaviour, although the experimental conditions were similar, would be the presence of water and methane. Care has been taken to remove free water in all cases although some residual water remained as was evident from a proximate analysis conducted at the end of the experiment (Pone *et al.,* 2009).

Another method that enables researchers to investigate the alteration of the coal structure is by correlating the digital images of different stress levels. This is usually done in two dimensional images, but can be extended to three dimensions if enough images are analyzed. In this method successive images are taken at a specific position as strain is applied to the sample. Markers (lines or points) are identified prior to and after strain has been applied - Kang *et al.* (2007) followed this technique with steel samples. The change in the location of these markers will then be used to quantify the strain experienced during the evaluation. A SEM is usually used to acquire the images of such a strain evaluation but micro-focus X-ray imaging can also be used. After acquisition the images are imported into commercially available software which utilizes the digital image correlation methodology i.e. the automatic comparison of successive images to quantify movement of markers. This method can be accurate and spatial resolutions of 0.3 μm were reported for steel (Kang *et al.,* 2007).

3.3 Adsorption and gas transport

The heterogeneous nature of coal extends to seams and layers as well, where the predictions made with respect to gas transport flow rates and kinetics will not apply to different regions within the same seam. There is therefore a definite need for information concerning the flow and storage behaviour of coal that is representative of the whole seam. This information is typically not obtainable by crushing different coal samples (as is usually the case) where the results obtained would be an average of the seam. Karacan and Okandan (2001) reported that the transport of gases like methane in the coal microstructure depends on various factors including the type of microstructure, the orientation and distribution of these microstructures and the amount and type of minerals present in the walls of voids (fractures and pores).

It was also concluded that gas transport in bright-banded (vitrinite rich) bituminous coal tends to be more dependent on the macro fracture structure than dull-banded coal (inertinite rich). A SEM was used to investigate how many different types of microstructure, which can facilitate gas transport, were present in the coal samples (Karacan & Okandan, 2000a). Small irregular pores with low permeability are present in the organic matrix and are mainly perpendicular to the bedding plane. Some regions in the organic matrix contain phyteral pores that are partially filled with mineral matter and to some degree provide directional permeability. The degree to which phyteral pores offer permeability to the coal matrix depends on the specific mineral matter present. Clay minerals and calcite typically lower the permeability although it is still higher than other regions of the organic matrix with irregular pores that are mineral free. Typical minerals that raise the permeability include koalinite and illite. Regions that contain many phyteral pores tend to have higher densities due to these mineral inclusions that are associated with this type of pores, but they still have high levels of porosity. Phyteral pores are also connected to each other with small microfractures crucial for gas transport in the regions containing these microstructures (Karacan & Okandan, 2001).

It was demonstrated in the previous section how information can be obtained about how much deformation occurs within the coal structure during adsorption and desorption of gases. The following paragraphs will show how gas transport and adsorption occur within the coal structure and what the limiting factors are (Karacan & Okandan, 2001). Kinetics of adsorption studies are usually performed on crushed coal samples that are not representative of the natural state of coal. To study the effect of gas flow would require visualizing the gas within the coal structure and this can be difficult, since methane and carbon dioxide is virtually invisible during CT due to the very low densities. That is why an alternative gas, like xenon, which has a higher X-ray attenuation, should be used (Karacan & Okandan, 2000a). There is however a problem with this approach since the adsorption and transport characteristics of xenon, methane and carbon dioxide vary significantly. It is therefore only an assumption but the accuracy of the assumption can be improved by investigating the adsorbed amount of xenon at different times at all the different locations.

The mechanism with which adsorption occurs begins with the gas molecules diffusing into the macro and mesoporous space. This process is governed by molecular and Knudsen diffusion mechanism. Once inside the macro- and meso porous volume, the gas molecules adsorb to the walls of the entrance of the micropores. Once a certain energy barrier is overcome the gas molecules will diffuse into the micropores in a process called micropore diffusion.

The aforementioned mechanism is only valid if the pore size distribution is accepted to be multimodal (Karacan & Okandan, 2001). Calculating the porosity of a specific region in a coal sample would aid in calculating the amount of an adsorbed xenon gas. This is how the amount of xenon adsorbed was quantified by Karacan and Okandan (2001). First the sample is evacuated so that X-ray scans (dry scans) can be performed at predetermined locations. This step is necessary to remove any residual gases in the coal structure and to obtain data that is representative of only the coal structure. Secondly nitrogen is then injected in the coal until saturation where after scans are performed at exactly the same locations as the dry scans. The CT numbers for the coal structure and nitrogen-saturated porous regions can be calculated from the dry and nitrogen-saturated scans, respectively. Equation 3.1 is used for calculating the matrix CT number for a specific region (CT_m).

$$CT_{coal} = CT_N(1 - \varphi) + \varphi CT_{gas} \qquad \textbf{Equation 3.1}$$

In equation 3.1 CT_{coal} is the CT number of the coal that is evacuated of any gases i.e. determined from the dry scans. CT_{gas} is the CT number of nitrogen-saturated porous regions and φ is the average coal porosity measured with mercury intrusion experiments. Once CT_N is known it can be used to calculate the region specific porosity by using equation 3.1 a second time. This time however CT_{coal} is the CT number of the nitrogen-saturated coal structure whilst CT_{gas} is only that of nitrogen (determined in a calibration experiment without any coal). It is advised that the sample should be evacuated again before xenon is introduced, to eliminate the effect of residual gases (including nitrogen) and moisture content (Karacan & Okandan, 2001).

The coal sample can now be scanned at two different energy levels once xenon is injected so that the actual amount that is adsorbed can be calculated. The dual energy method enables a researcher to calculate the density much more accurately (more on the topic in section 5.1). With the density and volume known from the CT scans it is relatively easy to determine a mass distribution along any plane in the sample. This is very helpful in visualizing how the porosity varies with respect to materials with different densities on the same plane.

It is easy to calculate the total amount of stored gas once the density of a specific region at any given time during adsorption and the density of that same region prior to xenon adsorption are known (Refer to equation 3.2).

$$Stored\ gas = \frac{\rho_t V - \rho_d V}{\rho_d V} \qquad \textbf{Equation 3.2}$$

In this equation ρ_t is the total density of any given region at any time during gas uptake and V is the volume of the region of interest. The density of the same region prior to gas uptake is represented by ρ_d. Note that the region of interest can even be as small as a single voxel. Calculating the amount of free gas requires the pressure-density relation of xenon gas and the density of the region of interest prior to gas adsorption (Refer to equation 3.3).

$$Free\ gas = \frac{V\varphi(0.0788P - 0.00863)}{\rho_d V} \qquad \textbf{Equation 3.3}$$

In this equation P is the pressure during any time during gas uptake. The amount of free gas in the pore volume will decrease as time goes by since the free gas will diffuse into the coal structure (and consequently the pressure of the free gas will also diminish). The total amount of adsorbed gas is the difference between the total stored gas and the amount of free gas in the pore volume (Karacan & Okandan, 2001).

Qualitatively Karacan and Okandan (2001) observed that the areas in the coal where there are higher density materials like mineral rich regions tend to contain (store) more xenon than the coal organic matrix which had a lower density, when gas equilibrium has been achieved (i.e. no more gas has been adsorbed or stored). A possible reason could be that the organic matrix contains pores that are not connected and consequently the permeability and diffusion would be very low in these regions. Regions where there are distinct mineral layers that are in close contact with the organic matrix proved to be more effective than only the organic matrix, when it comes to storing gas. This may be because the organic material in close contact with distinct mineral layers tends to have different characteristics than in regions of organic material only. It should be noted that regions that contain only mineral matter usually have low porosity and some regions of organic matrix exhibited high levels of porosity. Last mentioned is probably due to some fractures and macropores in the organic matrix.

3.5 Summary

The regions that contained the most phyteral pores have the highest adsorption of gasses due to the large void volume present. The rate at which adsorption occurs is also faster than in other regions since the phyteral pores are connected with microfractures.

Therefore, the permeability and connectivity of these regions are much higher than any other in the coal samples. The regions in the coal sample that had the second best adsorption were the coal matrix regions that are in close contact with mineral matter. The regions with the worst adsorption were the regions that contained only coal matrix samples with limited and unconnected pores. Crushed coal is not the best sample type when determining adsorption kinetics, since it is representative of the average properties of a coal seam.

A plot of adsorbed amount versus time indicates the adsorption rate kinetics regarding the different microstructures, minerals and lithotypes. From such adsorption curves it is possible to see what the limiting step in adsorption kinetics is. The coal matrix regions tend to only have one slow gas uptake and consequently the limiting factor is matrix penetration through micropore diffusion. Regions where there were phyteral porosity tend to have a fast initial gas uptake when the gas diffuse within the macropore structure, followed by a slower but still fast micropore diffusion (the limiting step).

4. Cleat spacing and aperture in coal

Various aspects of micropores, which constitute most of the porosity in coal, were discussed in the previous section. Now the structure responsible for the primary permeability of a specific coal sample will be discussed i.e. the cleat and fracture network.

4.1 Cleat characteristics

Cleats are fractures in the coal bed and typical cleat characteristics that need to be known in order to model gas flow within a coal bed include size (length and height), spacing, extent of connectivity, aperture and typical minerals present in cleat walls. It is however easier said than done since it is very difficult to obtain accurate information about these characteristics (Karacan & Okandan, 2000a). This is due to the sample size and destructive methods in which characterization information is usually obtained like cuttings and image analysis. Mazumder *et al.* (2006) reported that attempts have been made to determine the cleat angle distribution and cleat spacing distribution of coal seams.

Cleat spacing distribution information is also difficult to obtain with cuttings and therefore a method that calculates the difference in fracture behaviour between macerals and minerals was used (Mazumder *et al.,* 2006). Numerous assumptions have to be made when modeling fluid flow in coal, due to the difficulty in obtaining information regarding cleat size and spacing. Typical modeling assumptions include assuming a very small cleat size in terms of length, height and aperture although in reality the cleats can be centimetres to meters in size (Karacan & Okandan, 2000a). Not only is information concerning the cleats and fractures important when considering fluid flow within coal beds, but also when considering the density of the sample. A true quantitative density analysis can only be performed when the wide range of cleats is considered, since some cleat aperture can be of the order of millimetres to centimetres.

There are two types of cleats in coal called face and butt cleats that form the orthogonal joint system and usually occur perpendicular with respect to type and bedding plane (Refer to figure 4.1) (Mazumder *et al.,* 2006).

Cleats that extend through the coal bed are referred to as face cleats whilst smaller cleats that ends in the through-going face cleats are called butt cleats (Laubach *et al.,* 1998).

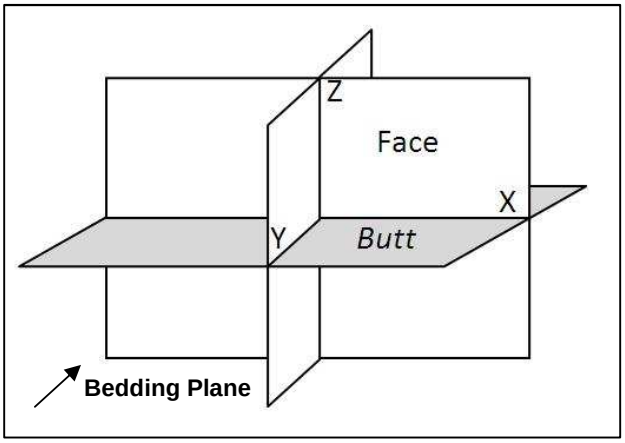

Figure 4.1: Orthoslices and sample orientation (Mazumder *et al.,* 2006)

Cleat spacing varies with coal type, mineral content and coal rank (specifically decreasing from lignite through medium-volatile bituminous coals and increasing through the anthracite range) (Mazumder *et al.,* 2006; Karacan & Okandan, 2000a). Therefore, most coal samples have a bell-shaped cleat spacing distribution. Face cleats are of the order of 22 cm in lignite and decrease to about 0.2 cm in anthracites and it is apparent that bright coal lithotypes have smaller cleat spacing than dull coal lithotypes. High mineral content value coal tends to have larger cleat spacing than low mineral content value coal and it is apparent that the lithotype layer thickness is linearly proportional to cleat spacing.

X-ray CT will be an ideal method to investigate cleats due to the non-destructive nature of the technique and the possibility to investigate relatively larger sample sizes (than with previous methods). The samples can also be scanned as obtained from the source and therefore would require very little pre-experimental preparation (Mazumder *et al.,* 2006). There is however a drawback in the sense that this method is greatly limited by the resolution of the equipment as was discussed in previous chapters. A low resolution would limit the researcher to detect small cleats that are especially present under in-situ conditions (Mazumder *et al.,* 2006).

With that in mind many researchers who analyzed cleat characteristics did so under non-stressed conditions (Mazumder *et al.,* 2006; Karacan & Okandan, 2000a). Luckily there are numerous mathematical and physical filters and techniques that can be used to enhance the contrast so that it is easier to distinguish between a cleat and low density materials.

4.1.1 Data processing

The best way to investigate cleats and fractures would be to create a binary volume of the X-ray scan data. This means all material would be assigned a data value whilst all voids would be set to zero data. Care should be taken to include all the cleats and fractures whilst excluding pores and other voids (Mazumder *et al.,* 2006). Obviously, this method would include some entities that are not cleats and omit smaller cleats, but when appropriate software is used this bias could be minimal. Software like VGStudio Max 2.1 can easily perform this task because the researcher can specify where material is prevalent and where cleats begin and end. A number of imaging processing software, such as Image-J (free-ware), which can handle an entire image sequence (typically a direction), can also perform this task. Calibration of experimental equipment is also vital especially where CT numbers are calculated. Using water as calibration material is sufficient but using a coal analogue (like carbon) is better since it will be easier to observe the cleats due to attenuation differences (Mazumder *et al.,* 2006). Care should however be taken since using an analogue calibration material like carbon will enhance the desired features, as well as the noise and artifacts. A manufactured calibration standard with a fracture of known aperture can be beneficial when making sense of cleat aperture data. Such calibration standard can be made by cutting a coal sample in two halves and then combining them with spacers (of specified thickness) between the two halves. Cleat apertures are also calibrated by using optical microscopy (Kumar *et al.,* 2011).

4.2 Cleat orientation and spacing distribution

A sequence of images in a specific orthogonal direction (face or butt) can be compiled once the cleat identification is finished and the binary volume has been created. The cleat spacing analysis is performed on the image sequence and it should be noted that a better resolution would not only detect smaller cleats but will also provide more images in the image sequence and consequently better data. The cleat spacing measurements can commence once an orthogonal direction is established (Mazumder *et al.,* 2006). Any cleat that is not parallel to the specified direction is disregarded and is not considered during this particular direction's measurements. Gridlines perpendicular to the chosen orthogonal direction are added to the image connecting parallel cleats.

It is advised that the distance between consecutive gridlines should be carefully chosen so that not even cleats with very small lengths are omitted. The cleat spacing and frequency distribution can be obtained by measuring each gridline that connects parallel cleats. The cleat length can be estimated by summing the distance between all the gridlines that defines the entire cleat. Cleat spacing and orientation distributions are usually negatively skewed and thus log-normally distributed. The reason for that is still unclear (Mazumder *et al.,* 2006).

4.3 Quantifying fracture apertures

A binary volume and image stack made the determination of the cleat spacing distribution easier since the cleats had to be identified visually. The cleats will be identified directly from the reconstructed scans when determining the cleat apertures. The CT numbers for the coal matrix and cleat is necessary for quantifying the cleat aperture. A dip in the CT number profile will clearly indicate the presence of a cleat although it might be difficult to distinguish it solely on the CT images (Mazumder *et al.,* 2006). From these CT versus pixel value plots it is possible to quantify cleat and fracture apertures with several parameters (Vandersteen *et al.,* 2003; Mazumder *et al.,* 2006) (Refer to figure 4.2). The missing attenuation value (MA) is a parameter which incorporates the integrated loss of attenuation in the region of the cleat or fracture due to the absence of material. Another parameter is the full-width-half-maximum (FWHM) of the attenuation profile of the cleat. Both MA and FWHM methods require the researcher to measure the attenuation profile perpendicular to the cleat direction.

The peak height (PH) value is a parameter that incorporates the entire attenuation value range of a cleat. The advantage of using PH above MA and FWHM is that the direction of measurement is not as important since the absolute attenuation coefficient range is considered. The disadvantage is that the attenuation value should be higher than that of air, which means that it would be difficult to use this parameter with very high resolution scans (possibly micro-focus X-ray tomography).

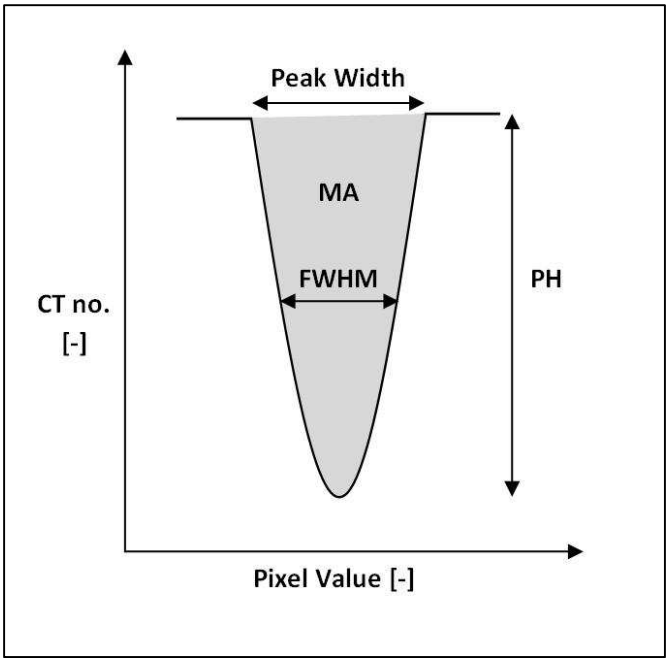

Figure 4.2: Different parameters to quantify cleat aperture (Mazumder et al., 2006)

MA is the better parameter to use when considering MA and FWHM, and together with PH is also the most frequently used (Vandersteen *et al.,* 2003). It was discussed in chapter two that artifacts like beam hardening and noise can lead to incorrect quantitative data and misinterpretation. So it is necessary to process the tomography scans prior to calculating the MA and PH values, especially for scans with a low SNR and for very small cleats. This pre-analysis processing entails fitting the attenuation profiles with a Gaussian function, since the cleat can be seen as a combination of a rectangular cleat profile and a Gaussian point spread function (Mazumder *et al.,* 2006; Vandersteen *et al.,* 2003). The noise in an attenuation profile can be described by a sine function.

The MA and PH values can be calculated once the attenuation profile has been determined with the following two equations (Mazumder *et al.,* 2006; Vandersteen *et al.,* 2003). Equation 4.1 represents the attenuation profile and enables the researcher to calculate PH whilst MA follows directly from equation 4.2. MA is thus a derived parameter from PH and peak width and any error occurring with PH and peak width is amplified. Note that the width of the peak should be within a 68 % confidence interval.

$$Y = PHexp\left[-\frac{1}{2}\left(\frac{X_p - xp}{\Delta xp}\right)^2\right] + CT_{coal} + Asin\left(\frac{2\pi}{\lambda}X_p + \omega\right) \quad \textbf{Equation 4.1}$$

$$MA = \sqrt{2\pi \cdot PH \cdot \Delta xp} \quad \textbf{Equation 4.2}$$

Table 4.1: Parameters and description for equations 4.1 and 4.2

Parameter	Description
Y	The attenuation value
X_p	The pixel value
Δxp	The peak width (refer to figure 4.2)
xp	Pixel position of peak minima
A	Amplitude of sine function
λ	Wavelength
ω	Phase angle

Mazumder *et al.* (2006) removed the noise (the third term in equation 4.1) and concluded that the Gaussian points spread function estimate the data very well as indicated by figure 4.3.

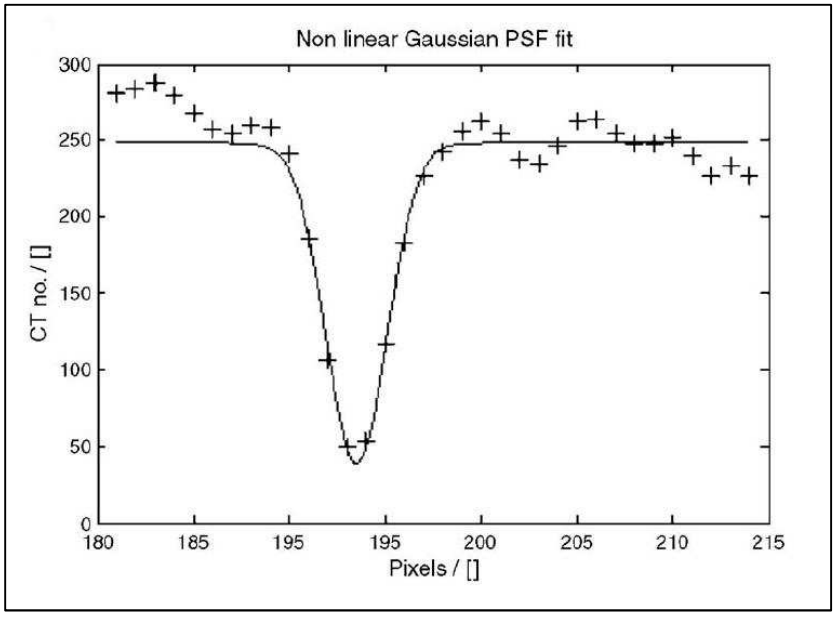

Figure 4.3: Fitting technique approximating measured data (Mazumder et al., 2006)

To calculate the optimized values of PH, MA and xp required minimizing the least square error i.e.

$$E_r = \sum_{k=0}^{n} \left(PH exp\left[-\frac{1}{2} \left(\frac{X_p - xp}{\Delta xp} \right)_k^2 \right] - Y_k \right)^2 \qquad \textbf{Equation 4.3}$$

MA is a very sensitive parameter because it is a derived parameter (dependant on PH and peak width). This means that for vertical cleats MA is adequate whilst MA has to be multiplied with the cosine of the angle of the cleat plane for non-vertical cleats. Mazumder *et al.* (2006) stated that MA is the best parameter to use when the cleats have large aperture widths whilst PH is the best for smaller aperture widths. This is because at smaller aperture widths the error for MA is significant and due to the sensitivity of this parameter the apertures calculated in this way are possibly inaccurate.

4.5 Fracture surface analysis

A vast number of minerals are present in coal as was discussed in chapter two. The importance of these minerals in fluid flow dynamics can be investigated by studying the cleat surface. Iron bearing minerals like illite and chlorite are in close contact with gases flowing in coal and can possibly interact physically and chemically with these gases. Other minerals within the coal matrix can migrate to the cleat surface and affect gas flow at a later stage (Karacan & Okandan, 2000a).

Karacan and Okandan (2000a) also investigated coal from Turkey macroscopically (since the resolution was more than a millimetre) and found that the mineral matter in fractures is clearly visible even under these conditions. The mineral matter in cleats and fractures are epigenetic since they are deposited vertically and horizontally throughout the coal structure and are deposited from groundwater (Stach *et al.,* 1982). Mineral ions in the groundwater moves through the coal structure and consequently deposit on the surface of major cracks. From here the minerals can move into microcracks and even the coal structure through diffusion. The mineral matter is sometimes seen as layers and clusters in coal with very little or no fractures (autochthonous coal). Coals that exhibit these bands are usually not sufficient for gas transport unless the permeability of the mineral bands is higher than that of the surrounding coal matrix. Minerals that deposited in this way is said to be syngenetic (Karacan & Okandan, 2000a).

4.6 Summary

CT enables the researcher to investigate the orientation of the cleat and fracture structure for coal specimens of different origin. This can in effect be used to model flow and fracture systems within coal. Although the size of these samples is bigger than the sample size of other experimental procedures for studying cleats and fractures, it is by no means representative of the seam. Another problem with the CT method is that the finite pixel size can limit the accuracy of data obtained. It is therefore advised to use more modern equipment like microfocus X-ray CT with smaller pixel sizes. Another recommendation is that the voxel volume should have a cubic shape with the same dimensions so that measurements in all directions can be compared.

5. Non-destructive characterisation

The importance of the fracture and pore network in the permeability of coal and coal seams were discussed in chapter three along with methods for quantifying the fracture and/or cleat network (chapters three and four). Now the focus moves from macrostructures such as fractures (or cleats) to microstructures such as porosity and identifying mineral matter, in a discussion on non-destructive coal characterization. Microfocus X-ray CT is especially important when considering microstructures since the increase in spatial resolution enables the researcher to identify samples that were previously averaged out.

5.1 Segmentation

Yao *et al.* (2009) characterized coal in a non-destructive manner with density, helium porosity, air permeability and water saturation analyses. It is not necessary to pre-process the samples in any way and random drill cores from pre-determined sources were investigated. The distribution and type of mineral matter present in the samples were determined with a normative chemical analysis. CT scans are very sensitive and case specific and therefore calibrations should be performed continuously. Typical calibration techniques are offset, gain and wedge calibrations of which the last mentioned is probably never used (Yao *et al.*, 2009; Ketcham & Carlson, 2001). To obtain a more accurate grey value reading of the material of interest it is necessary to account for materials (or voids) that are not of interest.

An offset calibration is when the detector values in a CT image are corrected for by subtracting the background i.e. when there is no beam. So a detector image is acquired under the exact same conditions as the normal CT image but with no beam. This image will typically correct for the effect of dead pixels etc. A gain calibration is when a correction is made for air i.e. when an image is acquired under the same conditions as the normal CT image but without a sample. It is difficult to distinguish between the constituents of a sample when the densities of these constituents are closely related. That is why researchers like Ketcham and Carlson (2001) propose that a different calibration material than air should be used under conditions where the density is closely related (Miller & Lin, 2009).

A cylinder of material that has the same attenuation properties as the material of interest should make a good choice. This is called a wedge calibration and enables the researcher to distinguish more clearly between constituents. Once the scanning is finished, it is easy to resolve the corresponding images with the segmentation method (also called the threshold technique) i.e. where different entities are separated by specifying a grey value interval. Identifying the grey value interval is not always as straightforward since an interval usually contains material that is not of interest.

A line profile across an image can possibly aid in distinguishing the different grey value intervals but care should be taken. The upper and lower thresholds of the grey value interval of each component should be carefully chosen so that it is applicable to all images and consequently be representative of the three dimensional volume. Software like VGStudio enables the user to specify the grey value interval directly in three dimensions whilst software like Mimics permits only two dimensions (Yao *et al.*, 2009). It is easy to obtain 3D information regarding the sample from 2D data by considering the volume to be many 2D slices. All the slices can then be averaged to obtain an approximation for the entire sample.

Although the grey values of a reconstructed image (slice) is representative of the density and atomic number of the material involved, there are exceptions to the rule. For instance Yao *et al.* (2009) found that although the density of a particular sample can be higher than that of another, it does not mean that the averaged grey value would be necessarily higher. The sample with the lower density can have clusters of material with higher density, like inertinite resulting in a higher average grey value whilst the higher density sample can have significant pores that lowers the average grey value.

So it is vital that the region of interest should be carefully investigated so that the grey value interval should represent the desired constituent rather than an average of the desired and undesired constituents. Another factor that influences the grey values of coal constituents is the state of the coal samples and should be kept constant (Yao *et al.*, 2009). The samples may contain different levels of saturation (or dryness) when mined and should be sorted accordingly or pre-scan processed with drying, or evacuated. Resolving geological samples like coal with segmentation is difficult and cumbersome since components with closely related densities are difficult to distinguish. A dual energy method has been proposed specifically for that reason and should be used when dealing with samples like coal (Van Geet *et al.,* 2001; Karacan & Okandan, 2001).

The technique enables the researcher to calculate density and atomic number of components in a sample with closely related density materials. It is sometimes difficult to distinguish different materials with similar densities since the resulting grey values are also similar. These grey values emerge as one peak on the histogram of all the grey values of the sample. The dual energy method provides a grey value distribution that comprises distinct peaks of which each is representative of a specific material. Beer Lambert's law (equation 2.12) can be rewritten for a high and low energy X-ray scan as follows:

$$\mu_{high} = \rho\left(a_{high} + b_{high}\frac{Z^{3.8}}{E^{3.2}}\right) \qquad \textbf{Equation 5.1}$$

$$\mu_{low} = \rho\left(a_{low} + b_{low}\frac{Z^{3.8}}{E^{3.2}}\right) \qquad \textbf{Equation 5.2}$$

The parameters *a* and *b* (high and low energy) can be calculated from a calibration with a material of known density since these parameters are properties of the energy of the scan and not the material present.

5.2 Porosity

The porosity and mineral distribution is important for most physical and chemical processes associated with coal. Typical processes include coal bed methane extraction and carbon dioxide sequestration (discussed in chapter three) but also gasification since most reaction sites are within the pores. Mercury porosimetry, gas adsorption and water-saturation are typical analytical methods with which porosity is measured (Yao *et al.,* 2009). There are however a few drawbacks to using these methods because they are destructive and represent information for connected pores only.

Complex interactions of the adsorbate with the coal structure can also lead to misleading results (Clarkson & Bustin, 1999). These methods are also inadequate when investigating the coal heterogeneity in three dimensions. Segmentation can also be used to determine porosity by defining an upper and lower threshold that is representative of pores. Ideally a pore would have no grey value in the reconstructed image since it is a void and has no material, but this is not realistic and a pore can be considered as material with a very low density.

The pores are predominantly filled with air and consequently should have the same value as the air directly outside the sample, but this is not the case. The reason for the grey values of pores is the way in which the X-ray spectrum interacts with matter and the way in which the X-ray photons lose energy. A binary sample volume rendering can aid in calculating porosity of a specific sample and it is easy to create such a binary volume with volume rendering and image processing software. The air inside a pore and outside the sample will have the same value after converting the digital sample volume to a binary volume i.e. it will have a zero grey value whilst material will have a value of one. The porosity of the sample can then be calculated by equation 5.3.

$$\varphi = \frac{Volume\ of\ pores\ (regions\ inside\ sample\ with\ value\ 0)}{Total\ volume\ (total\ sample)} \times 100\% \qquad \textbf{Equation 5.3}$$

Porosity calculated by CT is in close correlation with data obtained via other methods usually used for porosity measurements, as indicated by figure 5.1 (Yao *et al.*, 2009). It is expected that the porosity measured with CT should be the highest since it includes single pores that are not connected to other pores and the outside. Water-saturated porosity and helium porosity approximates the total porosity by considering connected pores.

Another reason why there is such a significant difference between the three methods may lie in one of the artifacts associated with CT. CT data is prone to partial volume effects that may be included in the porosity calculation and consequently an overestimation of the porosity. Low density material can also be considered a pore when the resolution is limited, further adding to the overestimation.

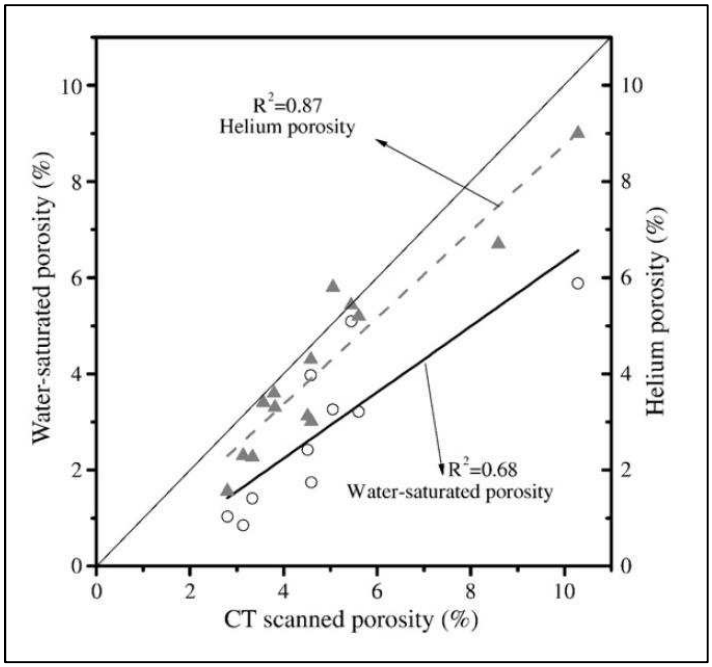

Figure 5.1: Comparison of porosity measurements with different techniques (Yao *et al.*, 2009)

5.3 Mineral and maceral distribution

The spatial distribution of fractures (and cleats), pores and minerals is important in evaluating a specific coal bed as a possible carbon dioxide sequestration or methane extraction site. Volume rendering software enables the researcher to orient the sample with three planes that aids in distinguishing different features. It is the only non-destructive way in which data can be obtained on the three dimensional distribution of features within the sample. Yao *et al.* (2009) also found that the mineral matter within coal is mostly closely related to fractures. It confirms the conclusion of the previous chapter in which it was stated that the minerals are deposited on the walls of fractures due to the movement of mineralized water. There are however cases in which a particular coal sample has a well-developed fracture structure that is mostly connected and mineral free. In this case the permeability of the coal is usually very high and the mineral matter in the coal matrix is distributed as spherical aggregates (like pyrite).

5.4 Correlation between CT and colour image analysis

Colour image analysis (CIA) is an image analysis technique that is used to distinguish between different materials based upon a difference in their colour. The difference in colour is basically a quantification of fluctuations in hue, saturation and intensity (Van Geet *et al.,* 2001). The upper and lower colour levels that represent a specific material are also determined through segmentation. Van Geet *et al.* (2001) were able to clearly distinguish between vitrinite, liptinite, inertinite and pyrite with segmentation of colour images. Care should also be taken when choosing the upper and lower thresholds since the same problem occurs with colour image analysis as with CT i.e. it is difficult to distinguish between materials with similar colour characteristics. Pyrite and inertinite have similar colour characteristics and is sometimes difficult to distinguish in CIA. The complete procedure is discussed in detail by Van Geet *et al.* (2001).

5.5 Density of constituents

The density can be calculated fairly accurately using the dual-energy CT-method and a correlation between CT and CIA and the results of such a calculation are represented in table 5.1 (for high volatile A bituminous coal), as well as values obtained from literature. The dual-energy technique is however sensitive to noise and therefore, it is necessary to average a few successive slices of the same position to obtain a smooth signal (Van Geet *et al.,* 2001). Lin *et al.* (2000) developed an on-line coal washability analyzer which determines the specific gravity amongst other properties.

Table 5.1: Density comparisons

Component	**Calculated density – CT data (g/cm^3) (Van Geet *et al.,* 2001)**	**Reported density (g/cm^3) (Stach *et al.,* 1982)**
Vitrinite	1.31	1.3
Liptinite	1.74	<1.3
Inertinite	5.64	1.6
Pyrite	1.21	5

The reason why the values for inertinite and pyrite are completely different is because of the difficulty in distinguishing the colour values of inertinite and pyrite during CIA segmentation. The inertinite regions can also be filled with minerals which can be another reason why the density value is so much different. There is also a slight deviation in the liptinite density value due to the close association with clay minerals (Van Geet *et al.,* 2001).

5.6 Summary

The CT technique enables the researcher to investigate and view the spatial distribution of fractures, pores and minerals in a non-destructive way. In addition to spatial distribution it is possible to calculate the porosity of a particular sample and it was found that the CT technique compares with other techniques such as helium porosimetry and water-saturation tests. The value obtained by CT will always be higher than obtained by other techniques since CT includes unconnected pores and some artifacts can occur. One of the key aspects of this chapter was the thresholding method utilized to identify certain desired materials. This method requires the scientist to qualitatively distinguish upper and lower grey values that should include the desired material. This can be cumbersome and difficult and may include materials closely related but not of interest. It is however easier to distinguish between such materials by using the dual-energy method. Correlating CT data with CIA data enables the researcher to calculate the density more accurately than by just using CT data and the results are comparable to that found in literature.

6. Experimental

A clear description of the CT technique and micro-focus X-ray CT were given in chapter two. This chapter will add to that in the sense that real equipment utilized, will be discussed. The capabilities of the MIXRAD facility will also be compared with that of two leading German research facilities, with special emphasis on coal research.

6.1 MIXRAD (Micro-focus X-ray Radiography and Tomography) facility

The next chapter presents a preliminary investigation on the capabilities of a micro-focus X-ray machine in coal research and therefore it is justified to discuss this type of equipment in detail. A state of the art micro-focus X-ray machine was installed at Necsa in 2011 and consequently the MIXRAD facility for the national (and international) research community was instigated. This machine will enable students from various research disciplines to do research on a micro-focus machine. This was previously very difficult since all similar machines in South Africa are privately owned and consequently, it is very expensive to work on this type of equipment (if even possible). Micro-focus X-ray investigations also form the basis of most tomographic synchrotron investigations and consequently the MIXRAD facility enables students from South Africa to do research on synchrotron light sources.

The Nikon XTH 225 ST micro-focus X-ray system is fully assembled in Europe and meets very stringent quality standards (Nikon Metrology). The system basically consists of a lead-lined cabinet, an external control module, an external chiller and a reconstruction PC. The lead-lined cabinet houses the X-ray tube, sample manipulator and flat panel detector. The system voltage ranges between 30 and 225 kV whilst the beam current ranges from 0 to 1 mA. This ensures that a wide variety of samples can be investigated with the system, even if the density is very high. The specific X-ray tube that is installed in this system is easy to maintain and cost effective since off the shelf filaments are used. The spot size is about 3 micron and therefore the geometrical unsharpness associated with cone beam enlargement is minimized (Nikon Metrology). A multi-metal reflection target enables the researcher to utilize a specific X-ray energy spectrum depending on the specific sample that is being investigated.

The multi-metal target comprises molybdenum, copper, silver and tungsten (which is mostly used in X-ray sources). Due to the small focal spot and high energy the target is eventually burned (> 80 hours) and forms a small hole in a process called electron drilling or pitting. This pit is small and the target can be indexed so that the beam is always at an optimum energy.

X-rays are generated in a vacuum and therefore the system is supplied with a turbo-molecular pump as well as a two-stage rotary vane pump. The time needed for operational vacuum is approximately 10 minutes. The X-ray tube filaments can be replaced easily and cost effectively by eliminating the vacuum and opening the X-ray tube at quick-release latches. The tungsten filaments are relatively cheap to acquire and last about a hundred hours under normal operation. The detector is a flat panel detector with a 16 bit dynamic range and is manufactured by Perkin Elmer. This detector is state of the art and uses a scintillator material in conjunction with a direct output digital panel. The size of the detector is 400 mm x 400 mm and could consequently accommodate a sample of approximately the same size at lowest magnification.

A 5-axis sample manipulator is installed in the lead-lined cabinet and is completely controlled with the acquisition PC (installed in the external control module). A maximum sample weight of 50 kg is permitted on the sample manipulator which extends the capabilities of the system to large samples (Nikon Metrology). Joysticks as well as a CNC user interface on the image acquisition software enables the researcher to obtain the optimum sample position before experimentation begins. The sample manipulator can move 200 mm in the horizontal plane, 300 mm in the vertical plane and 610 mm in the beam direction.

Last mentioned movement is directly responsible for a large amount of geometrical enlargement (zoom) of up to 150 times. The rotation movement is extremely accurate up to 1/1000th of a degree and consequently a vast number of projections are possible. The number of projections influences the resolution of the final scan. The system is delivered with pre-installed image acquisition and sample manipulation software and is fully automatic once the sample has been placed in the sample holder. The software that is used to acquire a CT scan is called Inspect-X and has been developed completely by Nikon.

This software acquires the projections, manages the vacuum, operates the sample manipulator, communicates with the X-ray controller and determines the safety status of the system. This software is installed on the 32 bit image acquisition PC which is housed in the external control module with the power supply and power distributor to the system. This image acquisition PC is connected to a 64 bit reconstruction PC with a 1 GB per second CAT 6 data cable.

So the images can be directly acquired to the reconstruction PC and therefore eliminates data transfer time. The software that is used by the two PCs to communicate is called CT Agent and has also been completely developed by Nikon (Nikon Metrology).

6.2 Tomographic process at the MIXRAD facility

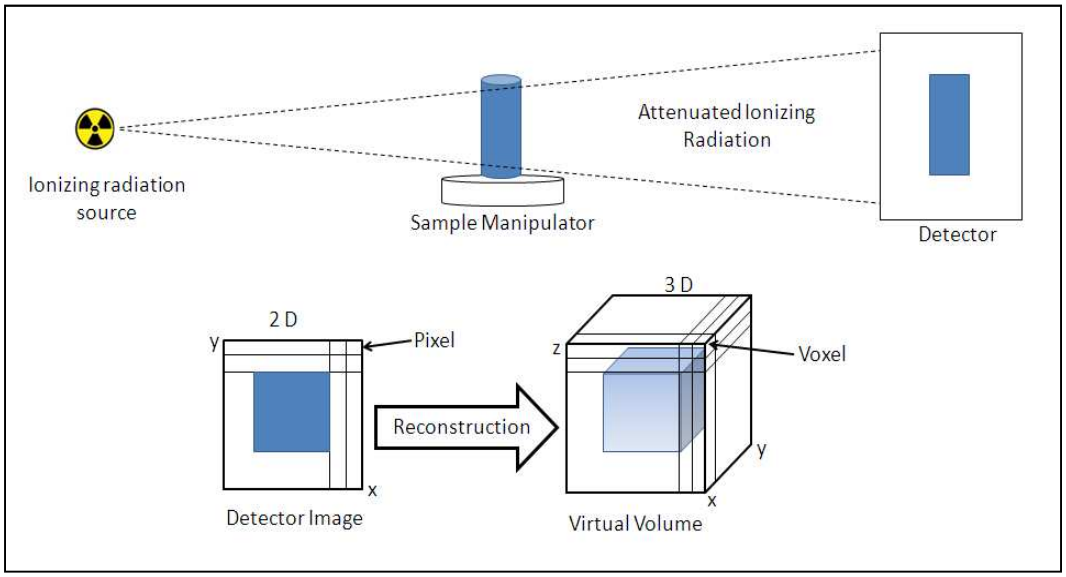

Figure 6.1: Tomographic process

The tomographic process of the MIXRAD facility is approximately the same as that of the SANRAD facility (figure 6.1). The biggest difference is probably the amount of automation, with the SANRAD facility being the least automated. The sample is placed on the sample manipulator in the micro-focus X-ray scanner and optimally adjusted automatically via the image acquisition PC. The amount of flat field and dark images can be specified when doing a shading correction. One flat field image and one dark image are usually used to do the shading correction and this may be inadequate since the general rule is to use at least three of each. This is not applicable here since around 128 flat field and 128 dark images where averaged to obtain one of each. The Inspect-X software incorporates these images in real-time so that the projections obtained from a CT scan are already normalized. The software also enables the researcher to correct for beam hardening artifacts and reconstruct in real time but this is not desired since it will be a lengthy process. Micro-focus data sets are very large (~20 GB) and it takes a long time to reconstruct on a 32 bit PC.

The projections are directly acquired to the 64 bit reconstruction PC and the reconstruction process can commence the moment the scan is complete. The format of the projection images (tiff) are already in the appropriate format and therefore no conversion is necessary. CT-Pro software is preinstalled on the reconstruction PC and is also fully developed in-house by Nikon. This is highly specialized software and reconstructs the projection images very quickly with limited input from the user. The basic function of CT-Pro is to specify the parameters for the reconstruction process since the actual reconstruction is performed by CT-Agent.

The major difference between CT-Pro and Octopus software (described in the previous section) is the way in which reconstruction parameters like the centre of rotation is specified. The user decides visually on most parameters in Octopus whilst the software decides on edge clarity in CT-Pro. This basically means that the quality of a scan that has been reconstructed with Octopus software depends strongly on a qualitative opinion of the user, which is not the case with CT-Pro. The final product from a reconstruction in CT-Pro is a RAW 3D volume file which can be directly imported in visualization software like VGStudio Max.

6.3 Safety of the MIXRAD facility

The lead-lined cabinet meets international radiation standards and is shielded so that the total hourly dose is less than 1 microsievert. Numerous dual safety switches and interlocks protect the user when the access doors are open. This means that the X-ray beam current is switched off the moment the access door is opened. There is no decay rate for X-rays and the sample can be removed or adjusted immediately after opening. The lower part of the cabinet also houses the safety system that cancels the X-rays when the access door is opened, as well as the power supply, vacuum pump and transformer. There are lights on the side of the lead-lined cabinet that indicate whether X-rays are generated and if the trip switches have been activated. These lights inform the user that the machine is in use and that the access door should not be opened.

6.4 Comparison between the MIXRAD facility and similar facilities in Germany

As part of this project, the capabilities of the MIXRAD facility were evaluated against two leading German facilities in Berlin. The facilities were the Helmholtz Zentrum-Berlin and BAM (Bundesanstalt für Materialforschung und –prüfung), which are both government funded research facilities. Numerous different types of samples were used, ranging from anatomical to geological samples including a few coal samples. Unfortunately only one coal sample was used at all the facilities since there was limited time in doing the experiments. This coal sample consisted of small particles taken at a specific stage during gasification, and includes some particles that had a high mineral content value.

It was specifically chosen so that a wide range of density materials could be visualized and was therefore representative of a wide range of coal constituents. Only one particle was scanned at BAM at maximum magnification. Both systems visited in Germany were custom-made and are consequently vastly different from each other and the MIXRAD facility. The Helmholtz facility's micro-focus X-ray machine had the major advantage of a higher resolution detector. The detector pixel size is 0.05 mm whilst those of the MIXRAD facility and BAM are 0.2 mm.

There is however a major disadvantage of the Helmholtz facility when it comes to sample size, since the detector is a quarter of the size of that of the MIXRAD facility. Figure 6.2 is a comparison between a scan obtained at the Helmholtz facility and MIXRAD facility. It is evident from this figure that the capabilities of the MIXRAD facility are comparable to that of the facility at the Helmholtz Zentrum-Berlin. The image obtained at the MIXRAD facility is even less noisy. This is to be expected, since the detector utilized at the MIXRAD facility inherently has low noise.

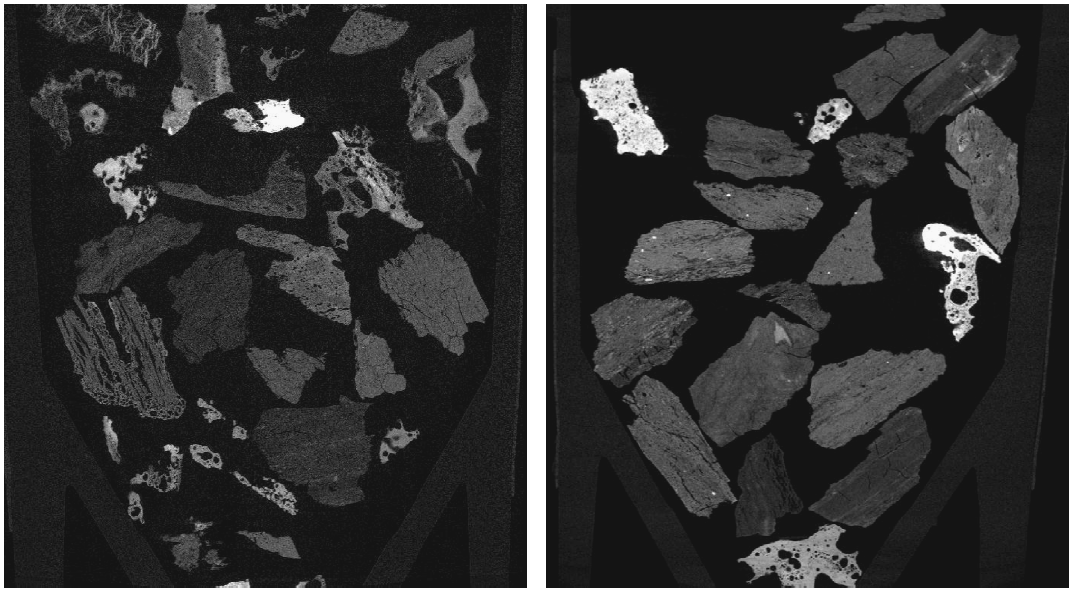

Figure 6.2: Coal particles - Helmholtz facility (left) and MIXRAD facility (right)

The voxel size of the image on the left was 0.0062 mm^3, whilst that of the image on the right was 0.0087 mm^3, although the magnification was approximately the same. This indicates that the resolution of a scan is more dependent on the enlargement capabilities of the source at very high magnifications than on the detector pixel size. The opposite is obviously true for very low magnifications.

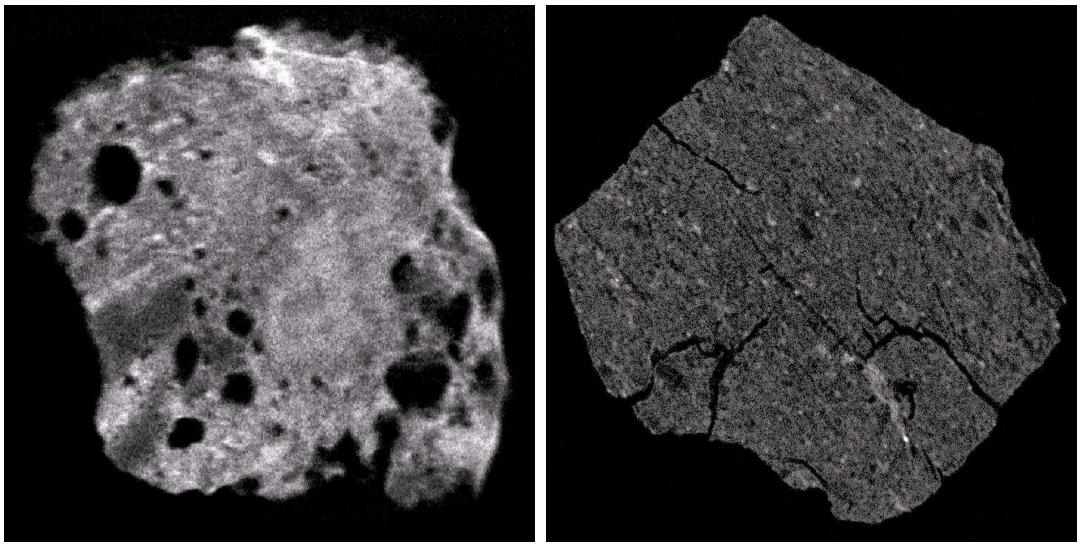

Figure 6.3: Coal sample - BAM facility (left) and MIXRAD facility (right)

Figure 6.3 is a comparison between a scan obtained at BAM and that obtained at the MIXRAD facility. It is of one of the particles in the sample described above and the highest magnification possible was investigated. Note that the particles used in figure 6.3 originate from the same sample subset, but the particles have completely different characteristics. The minimum voxel size that can be obtained (and that of the left image in figure 6.3) at BAM is approximately 20 µm whilst that of the MIXRAD facility is approximately 5 µm. These images prove again that the resolution is highly dependent on the focus spot size of the source, when the magnification is very high, since the difference between these images is not all that significant. The level of noise is also comparable since both facilities utilize flat panel detectors.

6.5 Summary

The specific tomographic equipment used in this investigation was discussed in this chapter with special emphasis on the capabilities of the MIXRAD facility at Necsa. The possibilities and limitations of the MIXRAD facility were described by comparing two coal related scans with those from leading German research facilities. The next chapter will present results and discussions of a pyrolysis and gasification investigation.

7. Investigating pyrolysis and gasification with µCT

CT experimental method and results are discussed in this chapter for two types of coal samples. The first type will be coal particles that are rich in inertinite and pyrite whilst the second type is rich in volatile matter and vitrinite. All the particles were used to study pyrolysis whilst only the inertinite rich particles were used for additional gasification experiments (up to a level 30%). Various interesting parameters could be seen and determined from the CT data, including the development of the fracture network, as well as the density.

7.1 Experimental

7.1.1 Materials used

Carbon dioxide and nitrogen

High purity carbon dioxide was used as primary reaction gas whilst high purity nitrogen was used as an inert gas which can quench the reaction at desired levels. All the gases were supplied by Afrox in Potchefstroom and had the following purities:

- CO_2 > 99.999%
- N_2 > 99.995%

The gas flow rate was set between 5 L/min and 6 L/min for all experiments.

Coal particles

Three inertinite and pyrite rich coal particles from the Highveld region and three volatile and vitrinite rich coal particles from the Waterberg region, were selected. The samples were specifically chosen from these two regions since it is known that the Highveld region contains mostly inertinite rich coal, whilst the Waterberg region contains mostly vitrinite rich coal. All the coal samples were taken from a conveyor belt and shaped (using a hacksaw for primary and rasp for final shaping) into spheres of roughly 20 mm diameter.

A size of 20 mm was considered appropriate since the sample holder of the thermo-gravimetric analyzer (next paragraph) utilized at the North West University, is optimized for 20 mm diameter particles. The Highveld coal samples were named H1, H2 and H3 whilst the Waterberg coal samples were named W1, W2 and W3. All the samples were randomly picked by hand from the respective coalfields located in the Highveld and Waterberg regions of South Africa.

7.1.2 Experimental setup

a. Thermo-gravimetric analyzer (TGA)

Everson *et al*. (2005) reported that the TGA is the most widely used experimental equipment when determining information regarding the reaction mechanism during gasification. The basic function of a TGA is to enable a researcher to observe a change in mass during a certain process. The primary elements of a TGA are a heat source and mass balance as depicted in figure 7.1 (A and B, respectively). TGA experiments can be isothermal or non-isothermal depending on the requirements and in this particular investigation the actual gasification experiments were performed under isothermal conditions. The quenching phase with nitrogen was non-isothermal but this is not part of the gasification experiments.

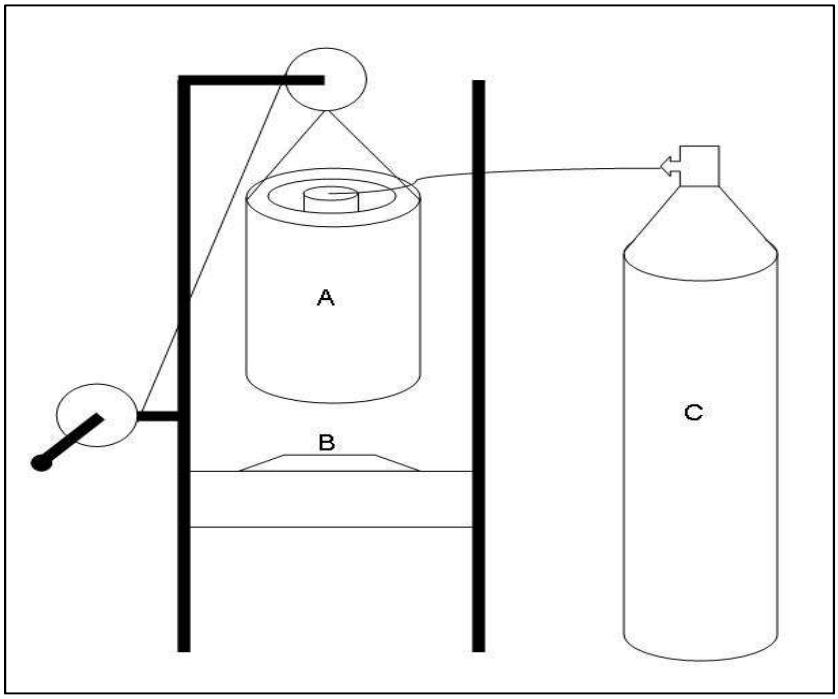

Figure 7.1: TGA setup (A – heat source, B – mass balance, C – gas cylinders)

Discussion of TGA setup

The tube furnace (heat source) is controlled by an external control module and the mass balance is connected to a PC with a RS-232 cable. The temperature in the tube furnace is monitored with a thermocouple which is also connected to the PC. Everything is therefore controlled automatically once an experiment commences. The PC logs the mass data from the mass balance and the temperature data from the thermocouple at specific user defined intervals, which in this case was 2 seconds. The software used was Visidaq Runtime and the output was a text file containing the time, mass and temperature. The data on this text file was imported into Microsoft Excel where all further processing was performed.

The tube furnace basically comprised four silicon carbide heating elements that were evenly spaced around a steel alloy inner tube (50 mm diameter). The operating temperature range of this type of furnace is from ambient to 1200 ℃ and is carefully controlled by a control module. The whole furnace assembly is installed in a steel jig and can be raised and lowered with a cable and pulley system as indicated in figure 7.1. The furnace was raised and lowered whenever the sample holder needed to be loaded or removed from the mass balance. Safety pins were inserted once the sample holder was in place so that the furnace remained stationary during operation and as a safety precaution.

The tube furnace was sealed at the top with an aluminium block and the gases were introduced here through two pipes. The steel alloy inner tube was sealed at the top to avoid air entering the system and consequently prohibit combustion when the sample is at high temperatures. The flow rates of the gases (C in figure 7.1) were controlled by regulators which were connected to a manifold that permitted switching between the two different gases without interrupting the experiment. This limited the chance of accidental combustion due to air entering the system.

The sample holder has two distinct parts including an aluminium base and a quartz top where the sample was placed. The aluminium section contains three legs with rubber ends to ensure that the sample holder remains stationary during experimentation. The top cylindrical part of the aluminium section has a hole in which the quartz section is inserted. The top section of the quartz rod was tapered into a conical holder that kept the sample in place during the experiment. This conical container has a hole where the conical section meets the quartz rod which is inserted in the aluminium section. This hole is basically a passage for the volatiles, tars and phenols to escape in during pyrolysis.

b. Microfocus CT

A microfocus X-ray CT scanner with similar specifications to the scanner discussed in chapter six was used during this investigation. This micro-focus CT scanner was located at X-Sight in Stellenbosch, South Africa. The only difference is that the detector had a size of 24.4 x 19.5 cm^2 instead of the 40.0 x 40.0 cm^2 that was discussed in chapter seven. This also meant that the number of pixels was (1920 x 1536) instead of (2048 x 2048). The reconstruction software and process were also the same as discussed in chapter seven.

7.1.3 Experimental method

Each coal sample was CT scanned prior to any TGA experimentation. The furnace assembly was raised manually with the cable and pulley system to a height that permitted the researcher to load the sample holder (with the sample in place) on the mass balance. Nitrogen was used in the pyrolysis experiments whilst carbon dioxide was used for gasification. The gas flow regulator was set to the desired flow rate and the furnace assembly was lowered over the sample holder on the mass balance. The furnace control module was set to reach the temperature set point (refer to the next paragraph) with a heating rate of 5 ℃/min. The experiment commenced at the specified temperature (Appendix A1) until no further mass loss could be observed. The furnace was switched off once the mass stabilized whilst still maintaining a constant nitrogen flow rate. This nitrogen/carbon dioxide flow rate was maintained until the sample had sufficiently cooled down so that combustion would not occur once the furnace was raised. The samples were then taken to a micro-focus X-ray scanner (X-Sight, Stellenbosch) where the samples were CT scanned. This whole procedure was repeated twice for complete pyrolysis and an additional time for gasification (only for the inertinite rich coal).

Each sample was placed (uncovered) on a piece of foam that is transparent to X-rays when scanned. This served as the sample holder for the scans and was placed on the sample manipulator. All the samples were just placed on the sample manipulator with no specific orientation since the samples were digitally oriented during the analysis phase. The sample was then manoeuvred into position by using the electronically controlled sample manipulator. Once the sample was in position the scans commenced at the following conditions:

- Voltage - 100 kV
- Current - 10 μA
- Pixel size - 0.127 mm
- Voxel size - 0.017 mm^3
- Projections - 2000
- Exposure time - 1 second

7.1.4 Experimental program

It was decided to study pyrolysis at three different levels as indicated in table 7.1. To obtain this level meant that the particle had to be subjected to a nitrogen environment at a specific temperature until no further mass loss could be observed. So calibration experiments were conducted to determine the specific temperatures at which only the desired percentage of pyrolysis was obtained. Two similar coal samples were used during the calibration experiments in two test runs. The same experiments were performed to determine the time for the desired percentage conversion during gasification. The complete procedure can be found in Appendix A1 whilst the appropriate temperatures are presented in table 7.1.

A total of 19 CT scans were performed at Stellenbosch.

Table 7.1: Experimental program

	Highveld Coal Samples			**Waterberg Coal Samples**		
	H1	**H2**	**H3**	**W1**	**W2**	**W3**
Percentage pyrolysis (%)	0, 50, 100					
Final Temp for 50% pyrolysis (℃)	554	559	536	650	650	650
Final Temp for 100% pyrolysis (℃)	1000	1000	960	1000	1000	1000
Percentage gasification (%)	30	-	30	-	-	-
Time for percentage gasification (min)	65	-	65	-	-	-

The resolution for each scan is listed in table 7.2.

Table 7.2: Spatial resolution of scans performed

Sample	Scan	Spatial resolution (mm)
H1	Baseline (0% Pyrolysis)	0.0171
	50% Pyrolysis	0.0239
	100% Pyrolysis	0.0239
	30% Gasification	0.0205
H2	Baseline (0% Pyrolysis)	0.0182
	50% Pyrolysis	0.0239
	100% Pyrolysis	0.0239
H3	Baseline (0% Pyrolysis)	0.0182
	50% Pyrolysis	0.0239
	100% Pyrolysis	0.0239
	30% Gasification	0.0205
W1	Baseline (0% Pyrolysis)	0.0239
	50% Pyrolysis	0.0239
	100% Pyrolysis	0.0240
W2	Baseline (0% Pyrolysis)	0.0239
	50% Pyrolysis	0.0308
	100% Pyrolysis	0.0239
W3	Baseline (0% Pyrolysis)	0.0239
	50% Pyrolysis	0.0308

7.2 Results and discussion

This section will present the results of the pyrolysis and gasification experiments described above. Each coal sample will be discussed individually with comparisons between consecutive scans. The Highveld coal samples will be discussed first and the Waterberg coal samples will follow.

H1

Characteristics: Mineral matter will have the lightest colour in micro-focus X-ray images whilst the organic matrix will have the darkest colour. It is evident from figure 7.2 that a significant fraction of the minerals in coal H1 occurs parallel to the bedding plane. This is indicative of the movement of mineralized water as described in chapter five, typical of epigenetic intrusion. The matrix of coal H1 therefore had a high permeability in order for the minerals to be deposited on the walls of the pores. Most of the mineral matter is however located in bands which is indicative of previous fractures that have been filled with mineral matter over time. The current fractures are however relatively free of mineral matter.

Inertinite is distributed in bands and layers as indicated in figure 7.2. The inertinite layers are represented as grey layers whilst the mineral matter is represented as white dots and streaks.

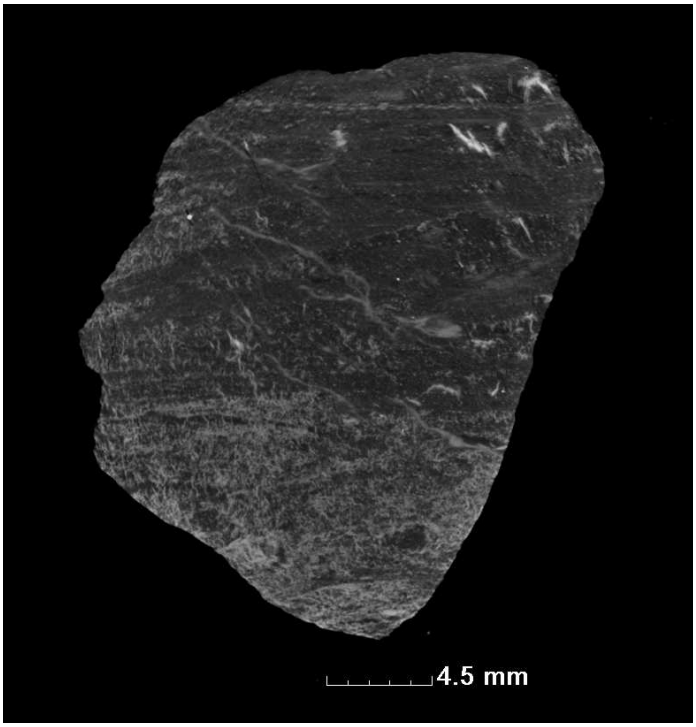

Figure 7.2: Coal H1

Pyrolysis: The total volume of coal H1 increased from 6066 mm^3 to 6527 mm^3 (7.1% increase) in the first pyrolysis experiment i.e. up to 50% pyrolysis. The increase in total volume is defined here as the increase in fracture and pore volume. VGStudio Max software enables the user to close a fracture and a pore on the outside surface of coal particle so that the total volume includes all the organic matter, as well as the volume of pores and fractures. This means that the density decreased due to this swelling and due to the loss of gases. This is consistent with the first and second stages of pyrolysis as described in chapter two (literature). At this stage the particle has a plastic nature and the escaping gases have difficulty passing through the matrix. This is the driving force behind the swelling of the coal structure and the resultant cracks that form (refer to figure 7.3). Note that the images are digitally oriented so that the location of the cut in the images is approximately in the same region. The swelling occurs mainly in the more reactive parts of the coal structure which in this case is probably vitrinite. The inertinite and the mineral matter did not influence the origin or development of the fractures.

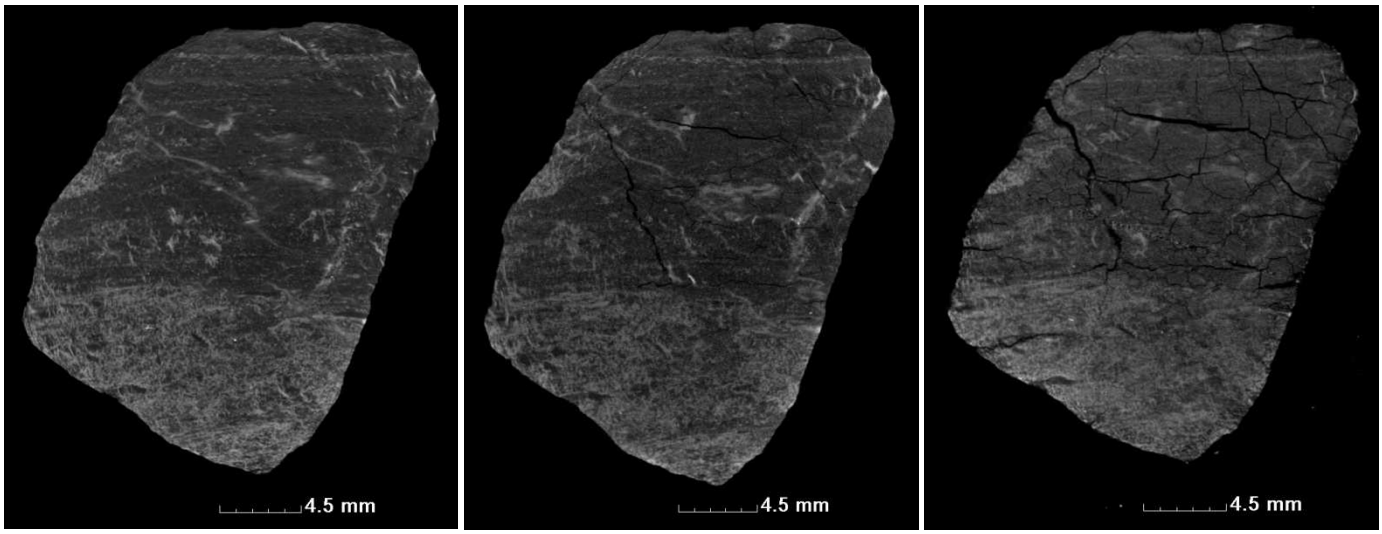

Figure 7.3: Pyrolysis of H1 (left = 0%, middle = 50%, right = 100%)

The volume of coal H1 decreased to 5663 mm^3 at 100% pyrolysis (13.2% decrease). This is typically the third stage of pyrolysis where all the gases are driven off and the coal becomes a brittle char. The decrease in volume can be ascribed to small sections of the particle breaking off from the char. This breakage probably occurred during transport and loading and removing the sample from the CT scanner.

Development of the fracture network: It was possible to identify a fracture that had been present in the coal particle prior to any experimentation and follow the associated change during pyrolysis (refer to figure 7.4). This fracture probably originated during the pre-experimental processing of the coal sample. The crack increased significantly from 0% pyrolysis to 50% pyrolysis, but a drastic change was observed when a 100% pyrolysis was achieved.

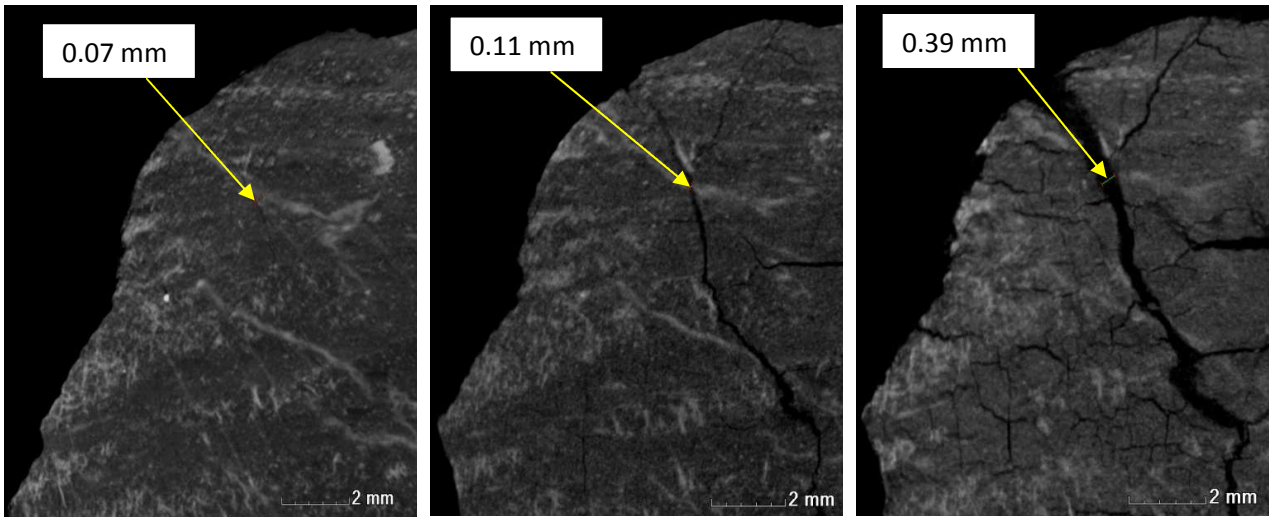

Figure 7.4: Fracture development of H1 (left = 0%, middle = 50%, right = 100%)

Gasification: The volume of coal H1 decreased from 5663 mm^3 at 100% pyrolysis to 5130 mm^3 at 30% gasification. This slight decrease in volume (9.4%) was expected since the char did not become significantly more brittle after pyrolysis. The sample reacted according to the mechanisms proposed by the SCM as described in chapter two. It is clear from figure 7.5 that there was a core of unreacted material enclosed in a layer of reacted material.

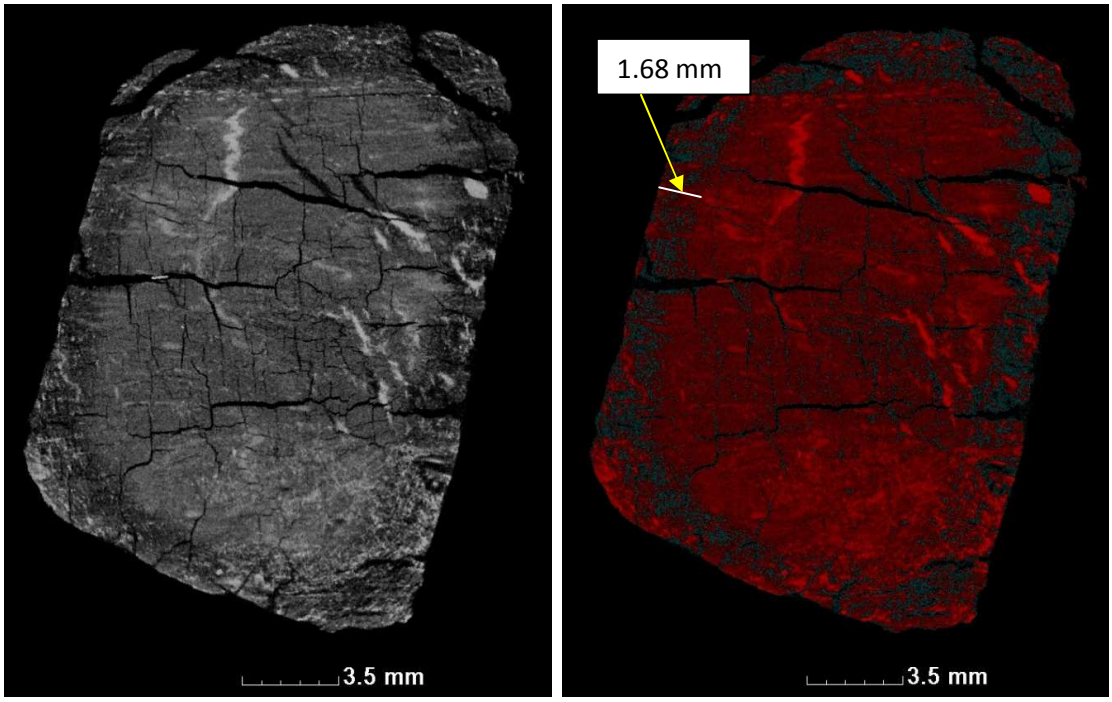

Figure 7.5: 30% Gasification of coal H1

Note that the reaction occurred predominantly in the layer on the outside of the particle and not in the cracks as expected. Figure 7.5 indicates the layer and unreacted core (with red making the difference more visible) with the outside layer minimized. There are regions where gasification occurred within the core, especially where significant numbers of small fractures were present (in the middle of the right image of figure 7.5). The thickness of the reacted layer was measured to be around 1.5 mm at 30% gasification. Another interesting aspect is that the mineral matter inclusions have very little effect on where the reaction occurred. The reacted layer was however slightly thicker at the bottom part where mineral matter was in abundance.

Kwon *et al*. (1989) stated that the SCM is especially applicable to non-catalyzed reactions, which is the case here. Therefore, it is justified to think that the reactions are chemical reaction rate limiting at this stage. Ash layer diffusion will have a greater effect once the reaction has progressed, but Lee & Koon (2009) concluded that a combination between ash layer diffusion rate limiting and chemical reaction rate limiting will be the prevalent rate limiting mechanism.

H2

Characteristics: The mineral and inertinite distribution in coal H2 is well dispersed and there is no layering parallel to the bedding plane as with coal H1. It is possible to distinguish clearly between inertinite regions and mineral regions as indicated in picture 7.6. The inertinite regions are the localized grey regions whilst the minerals are present in spherical aggregates. This also indicates that the organic matrix of coal H2 is highly permeable and consequently mineralized water deposited the mineral matter on the pore walls.

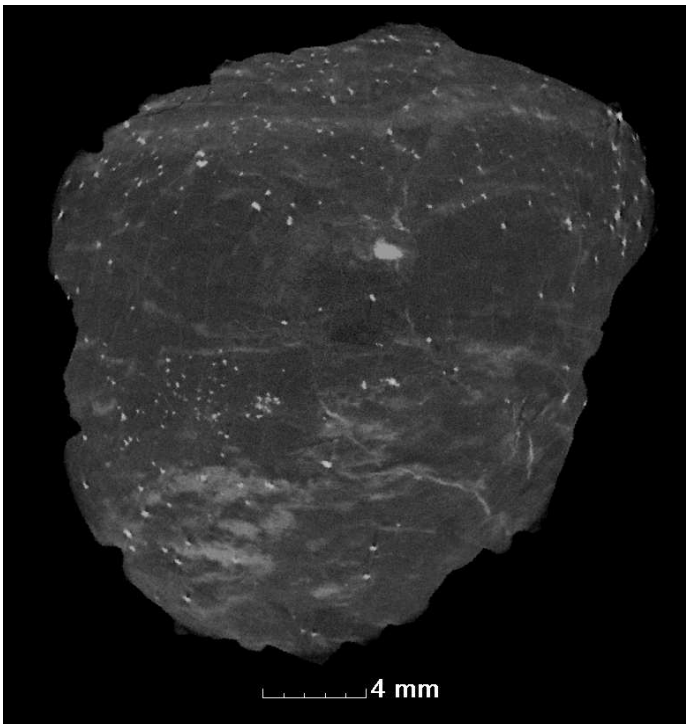

Figure 7.6: Coal H2

Pyrolysis: The volume of particle H2 increased from 7339 mm^3 to 7355 mm^3 (0.2% increase) when a 50% pyrolysis level was achieved. The density decreased as predicted by the first and second stages of pyrolysis and consequently, the sample weighed less than before the first experiment commenced. The same plastic characteristics were observed as with coal H1 and consequently numerous fractures occurred after the first pyrolysis experiment. There are however a clear distinction between the inertinite regions, the organic matrix and the minerals. The localized inertinite regions are much larger than that of coal H1 and consequently it was difficult to include these regions in volume calculations, and consequently an error was introduced in the volume calculations. The inertinite and mineral rich regions did not change significantly throughout the pyrolysis process and most fractures propagated from the organic matrix.

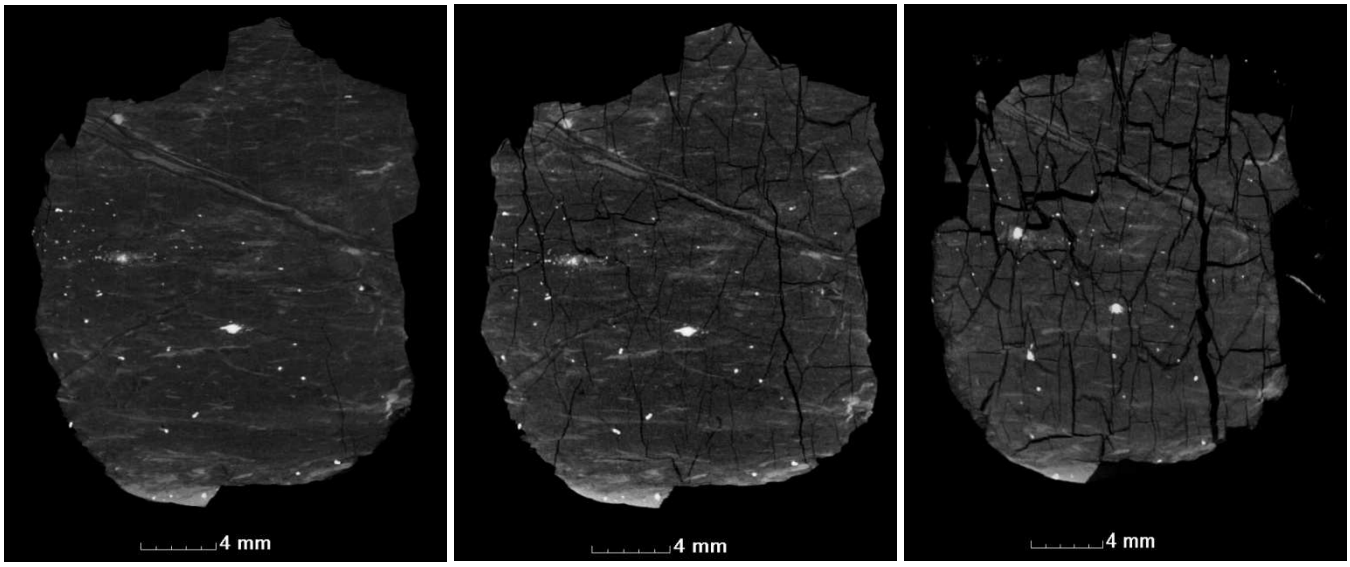

Figure 7.7: Pyrolysis of H2 (left = 0%, middle = 50%, right = 100%)

The volume of coal H2 decreased to 2561 mm^3 (65.2% decrease) when a pyrolysis value of 100% was achieved. This is a significant drop in volume, which indicates that the sample fractured and a few pieces broke off. The same happened with coal H1 but the drop in volume was not this large and consequently it appears that coal H2 was more brittle than coal H1 after pyrolysis.

Development of the fracture network: It was possible to follow the development of a fracture from 0% pyrolysis to 50% pyrolysis. This fracture enlarged significantly when 50% pyrolysis was reached as indicated by figure 7.8. It was however very difficult to identify the same fracture for 100% pyrolysis because the volume changed so dramatically when this value was reached. A measurement of a fracture in the same region is therefore presented in figure 7.8 just to show that the fracture widths did increase significantly from 50% pyrolysis to 100% pyrolysis. Care was taken to measure the fracture at approximately the same point by merging the samples digitally and then cutting the merged volume.

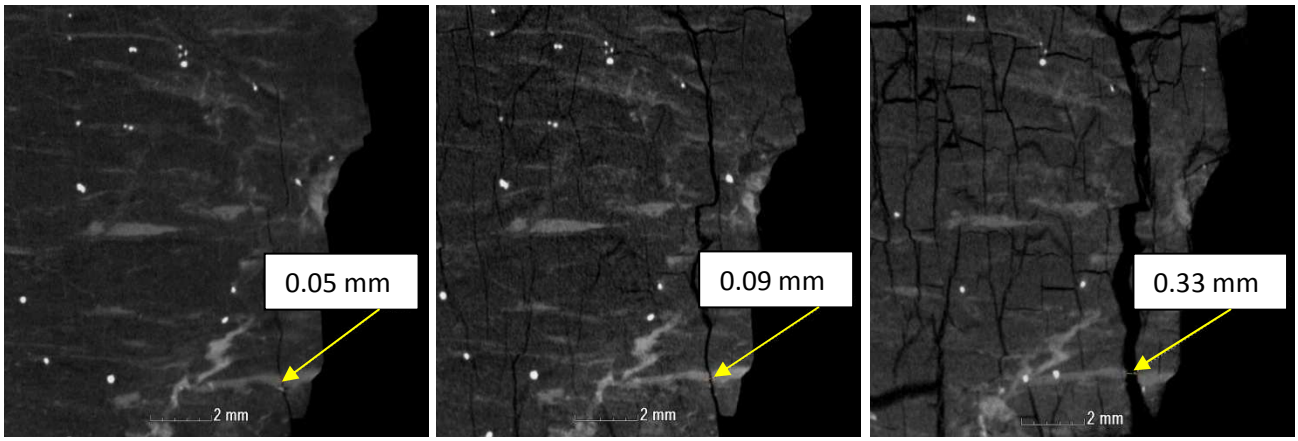

Figure 7.8: Fracture development of H2 (left = 0%, middle = 50%, right = 100%)

Gasification: Coal H2 became too brittle to investigate 30% gasification.

H3

Characteristics: Coal H3 also had a completely random mineral distribution with no layering parallel to the bedding plane. All of the mineral matter present in coal H3 is distributed in aggregates in the coal matrix. This indicates that the organic matrix is highly permeable and the minerals deposited in the pores of the coal matrix (the same as the previous two coals). Coal H3 probably had the best representation of localized regions of inertinite as indicated in figure 7.9. They grey regions are inertinite whilst the small white speckles are a very high density mineral like pyrite. Very few fractures are present and the fractures that are apparent, are probably the result of pre-experimental preparation.

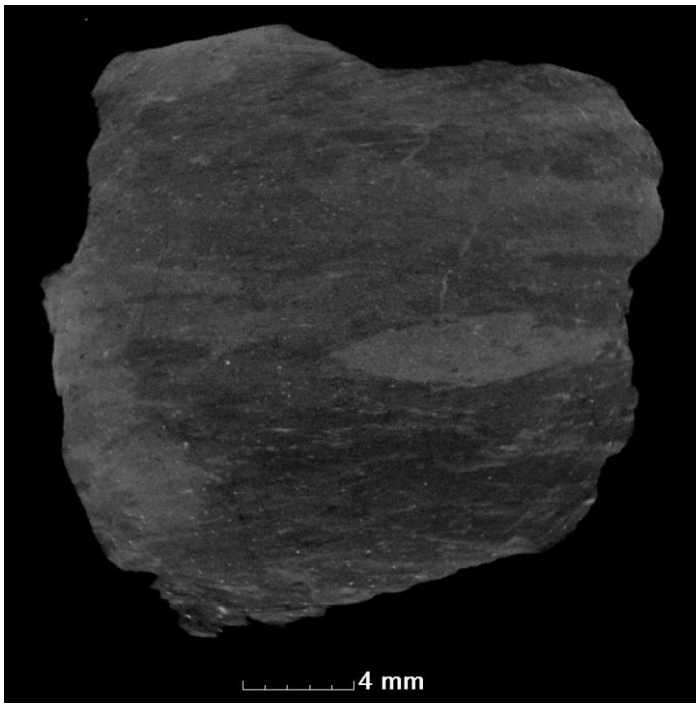

Figure 7.9: Coal H3

Pyrolysis: The volume of coal H3 increased from 6403 mm^3 to 6415 mm^3 (0.1% increase) when 50% pyrolysis was achieved. This is the smallest volume increase in all of the Highveld coals. The reason for that may be because coal H3 has the highest quantity of inertinite and the majority of swelling occurs in the less dense coal matrix. So although the density decreased only a little the same trend of the other two coals were observed i.e. the coal developed a plastic nature and the fractures formed in the organic matrix. The same problem occurred with coal H3 as with coal H2. The inertinite regions were large enough so that it was difficult to obtain an accurate volume calculation. Therefore, there are regions of very high density and regions of very low density and the volume calculation tool in the software (VGStudio) could not merge the two regions accurately. The trend in volume change is still applicable. The inertinite and mineral regions did not change significantly up to 50% pyrolysis as was the case with the other two coals.

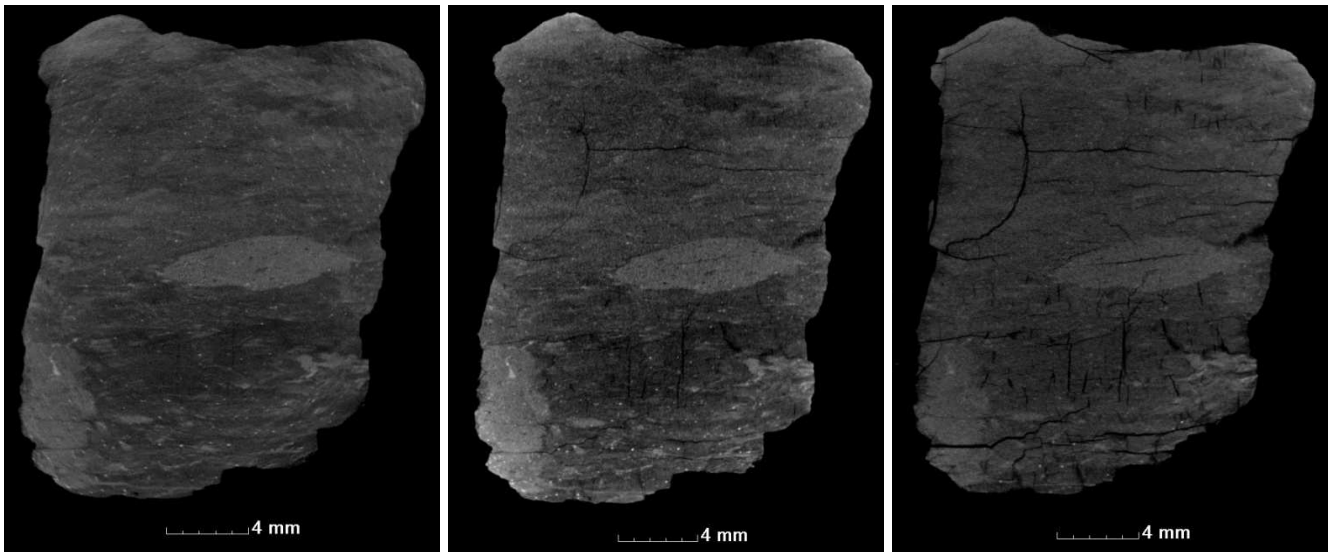

Figure 7.10: Pyrolysis of H3 (left = 0%, middle = 50%, right = 100%)

The volume decreased to 6173 mm^3 (3.7% decrease) when 100% pyrolysis was achieved. Here the decrease in volume was not as much as in the previous two coals. That is primarily because coal H3 has more inertinite regions which are quite stable throughout pyrolysis, whilst the organic matrix becomes brittle. It is the brittle char that breaks easily when handled and therefore the amount that broke off of coal H3 was very little.

Development of the fracture network: A fracture was identified and its progression was followed throughout the pyrolysis process as indicated in figure 7.11. The fracture increased significantly up to 50% pyrolysis where after the size increased very slowly. This is probably because of all the inertinite in the coal that limit the amount of organic swelling and consequently the size of fractures.

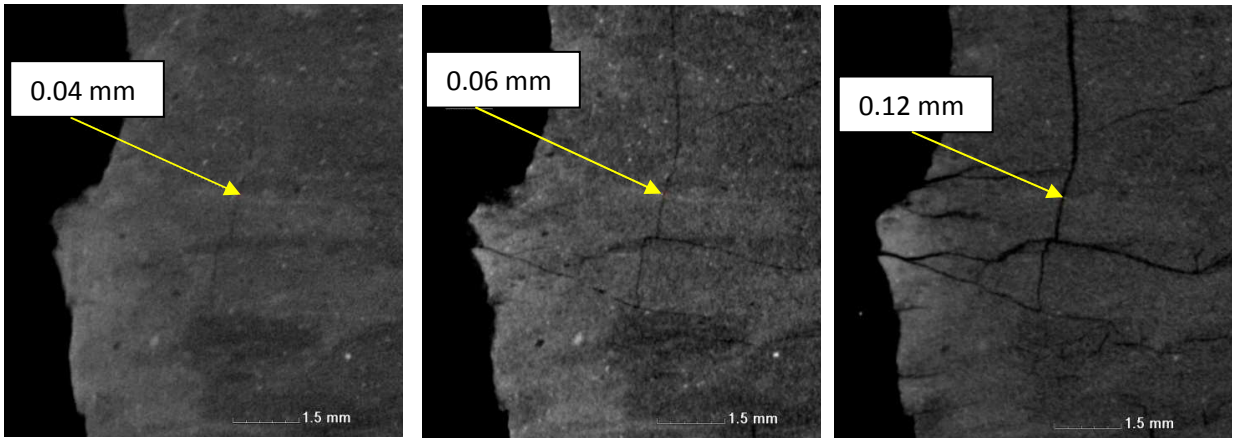

Figure 7.11: Fracture development of H3 (left = 0%, middle = 50%, right = 100%)

Gasification: A volume decrease of 3.9% (from 6173 mm^3 to 5933 mm^3) was observed when coal H3 achieved 30% gasification. This is exactly what was expected, since coal H3 contained large quantities of inertinite and consequently did not become as brittle as the other Highveld coal samples. It was difficult to visualize whether coal H3 behaved like coal H1 and followed the reaction mechanism proposed by the SCM. Figure 7.12 indicates that there is an unreacted core and a reacted layer around the core.

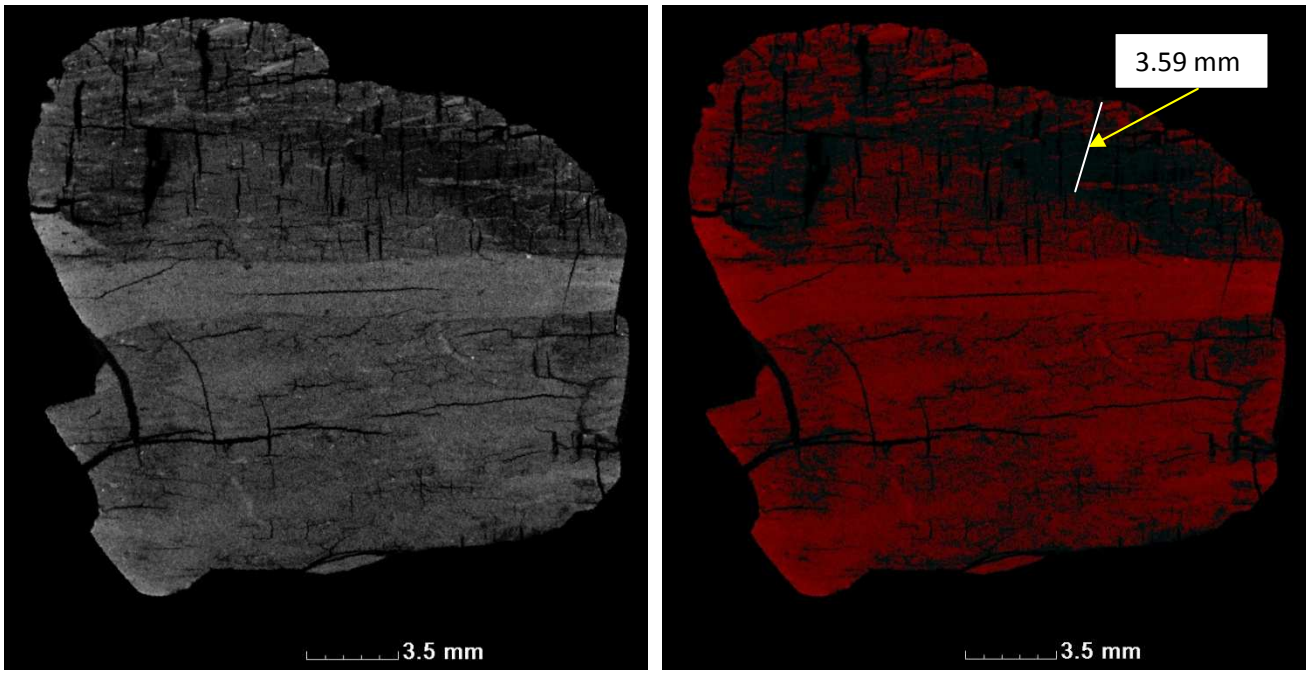

Figure 7.12: 30% Gasification of coal H3

An interesting observation in figure 7.12 (right image) is the localized regions of inertinite (bottom and top left) which did not part-take in the shrinking core behaviour. These regions also contributed to the difficulty in verifying the core and reacted layer and did not have any catalytic or inhibiting effect on the gasification reaction. It was expected that the reaction would predominantly occur in the fractures created during pyrolysis but this was not the case (as with coal H1). The thickness of the reacted shell at 30% gasification was measured to be around 3.5 mm which is much larger than that of coal H1. This was not expected since coal H1 contains more vitrinite than coal H3. No reasonable explanation can be given for this.

W1

Characteristics: Coal W1 is the first of the coal samples of the Waterberg region which is vitrinite and volatile matter rich.

The majority of the mineral matter is arranged in the direction of the bedding plane and in fractures that have been filled with mineral matter. The lack of small aggregates of mineral matter indicates that the organic matrix of coal W1 is less permeable than that of the Highveld coals. It is evident from figure 7.13 that there are regions of very high density material which is probably the inertinite. There are few small fractures (small length and aperture) present in the coal and the fractures that are present are close to the edge of the sample. These fractures probably originated in the pre-experimental preparation of the coal sample.

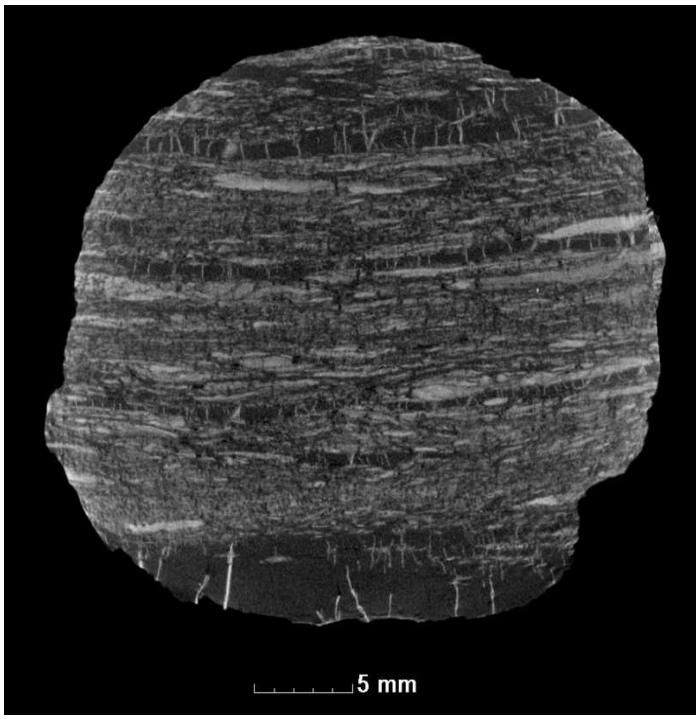

Figure 7.13: Coal W1

Pyrolysis: The volume of particle W1 increased from 16301 mm^3 to 17640 mm^3 (7.6% increase) when 50% pyrolysis was achieved (refer to figure 7.14). This is in accordance with the expected behaviour of a vitrinite and volatile rich coal. This increase in volume is much larger than any of the Highveld coals and is indicative of a char with strong plastic characteristics. The escaping volatiles have difficulty passing through the coal matrix and this resulted in numerous large fractures. The density of the coal particle decreased significantly at this stage of pyrolysis and it would weight less due to the mass loss.

The fractures developed predominantly in the organic structure and the mineral matter and high density parts did not influence the formation of these fractures.

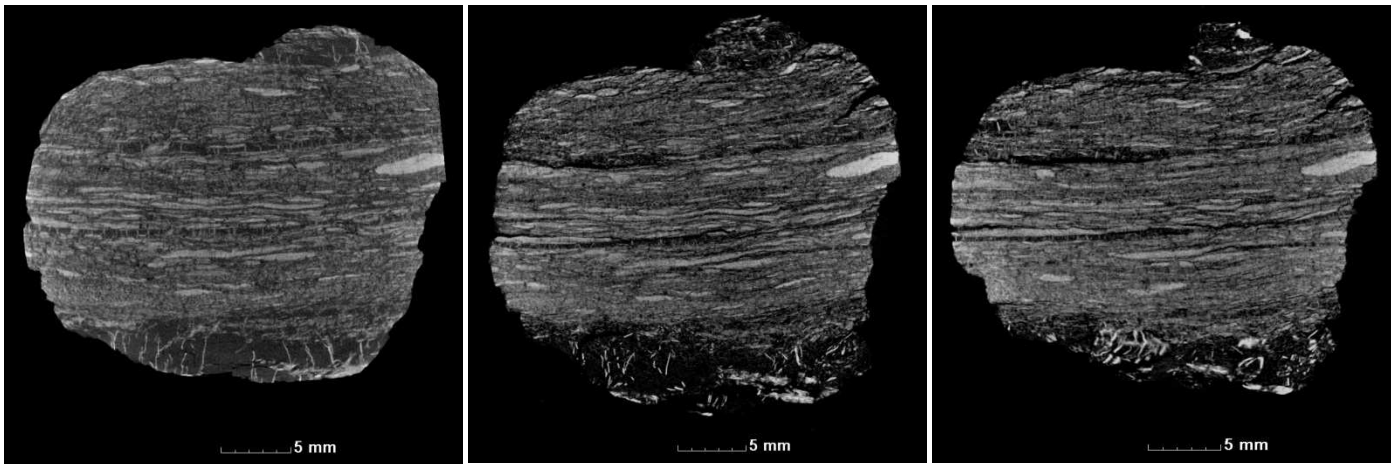

Figure 7.14: Pyrolysis of W1 (left = 0%, middle = 50%, right = 100%)

The volume of coal W1 decreased to 15757 mm^3 (10.7% decrease) when a 100% pyrolysis was achieved. This is not surprising because the coal became very brittle after all the volatiles have been driven off. The plastic nature of the coal diminished and the result was a brittle char. Small parts of the sample broke off when the sample was handled and consequently the volume decreased significantly.

Development of the fracture network: It is evident from figure 7.15 that the fracture network developed primarily during the first stages of pyrolysis. There was no significant change from 50% pyrolysis to 100% pyrolysis.

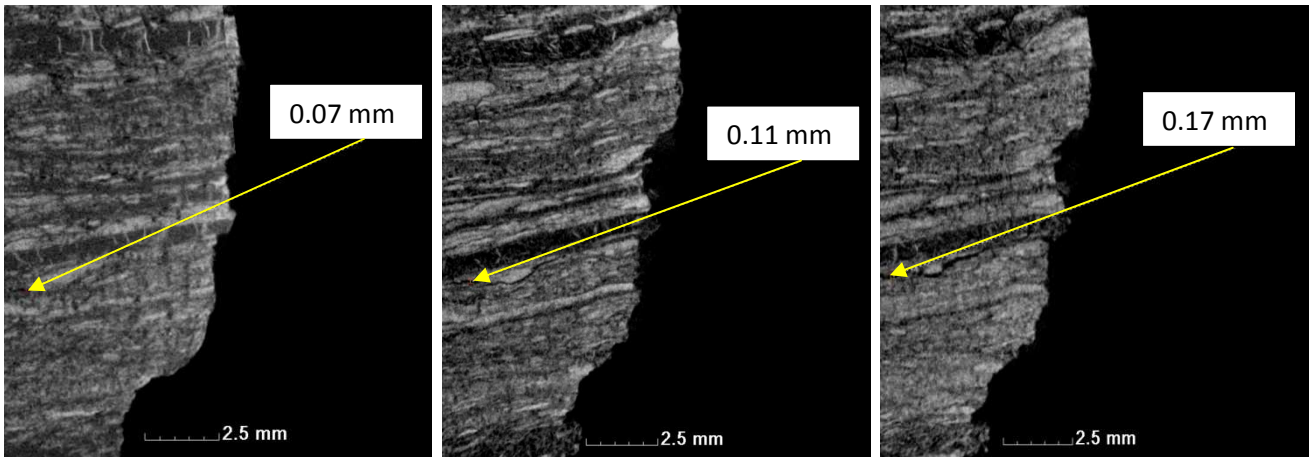

Figure 7.15: Fracture development of W1 (left = 0%, middle = 50%, right = 100%)

W2

Characteristics: The mineral matter arrangement in coal W2 is the same as that of coal W1 with small differences. The biggest difference is that the mineral matter is not present in fractures and there is only a banded structure. There are also small aggregates of very dense particles like pyrite that were not really present in coal W1. This indicates that the coal matrix was probably more permeable than that of coal W1 and consequently some minerals were deposited in the pores. There are also localized regions of high attenuating material that is most probably inertinite regions. The vitrinite is also present in layers that are parallel to the bedding plane. Small fractures were already present and are probably the result of the pre-experimental preparation of the sample.

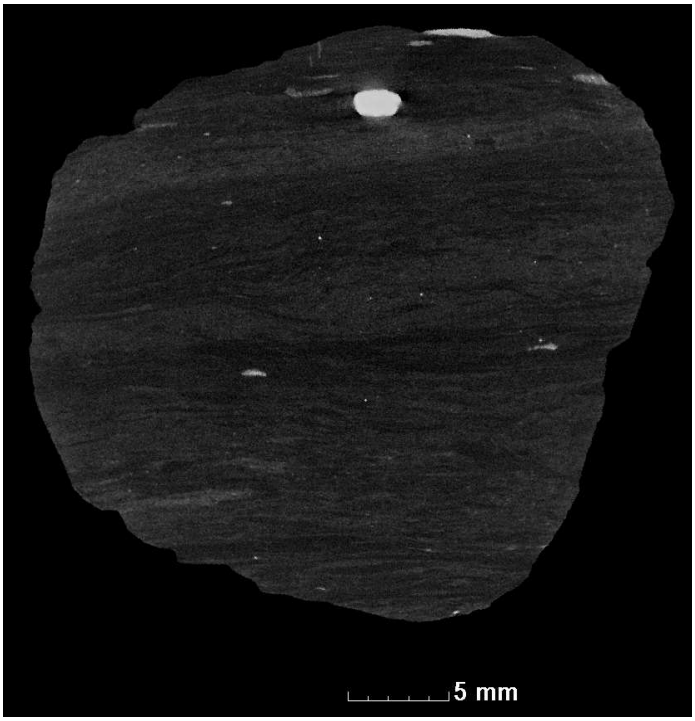

Figure 7.16: Coal W2

Pyrolysis: The volume of coal W2 decreased from 16746 mm^3 to 15996 mm^3 (4.5% decrease) when 50% pyrolysis was achieved. This deviation from the norm can be explained by three reasons. The first and most significant reason is probably that some small part of the sample broke off during transportation. This is possible because some vitrinite regions swelled significantly and even protruded the sample as indicated in figure 7.17. These protrusions are very brittle and small parts of it can easily break off.

Another reason could be that the software did not calculate the volume accurately. The volume is calculated by distinguishing between two extreme grey values which in this case is between that of air and that of sample. It is therefore difficult to calculate the volume accurately when there are prominent bands of high attenuating material in close proximity to bands of very low attenuating material.

The software then excludes small regions of very high attenuating material. The process of volume calculation was however optimized and the effect of this problem should be minimal. The last reason for this deviation could be an incorrectly calculated temperature for 50% pyrolysis. This means that the temperature may have been too high and the plastic characteristics of the coal had been surpassed. A very brittle char was the product. The fractures developed mainly in regions of lower density like vitrinite regions as indicated in figure 7.17.

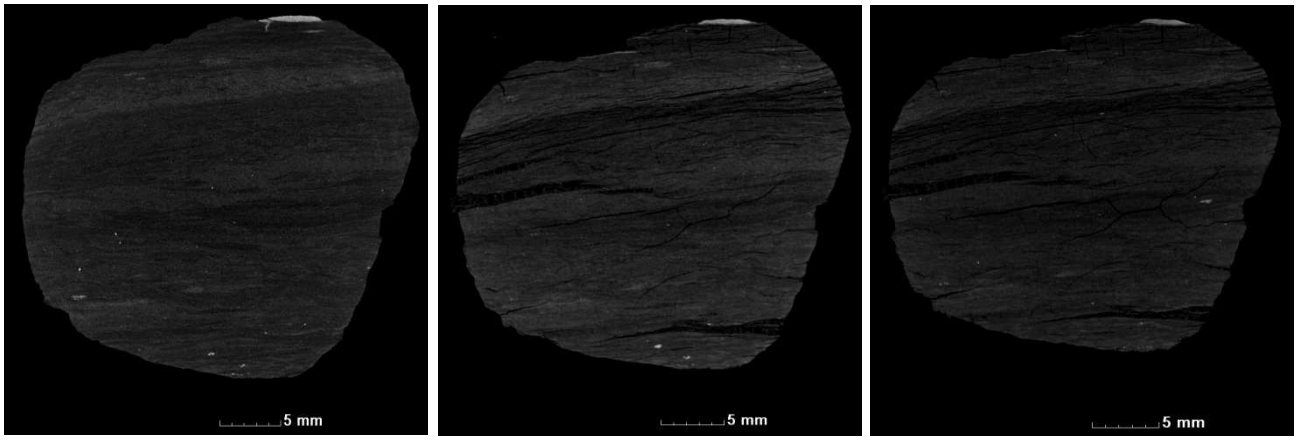

Figure 7.17: Pyrolysis of W2 (left = 0%, middle = 50%, right = 100%)

The volume decreased further to 12913 mm^3 (19.0% decrease) when 100% pyrolysis was reached. The sample probably broke again during handling and transportation. This time it was expected, since the sample was extremely brittle at this stage.

Development of the fracture network: The fracture network progressed from 0% pyrolysis to 100% pyrolysis as indicated in figure 7.18 where after it levelled out. The measurement in figure 7.18 is of a single crack and is approximately in the same location for all images. This indicates that the swelling predominantly occurred from 0% to 50% pyrolysis or that the specific temperature for the 50% pyrolysis level was incorrectly calculated as described in the previous paragraph.

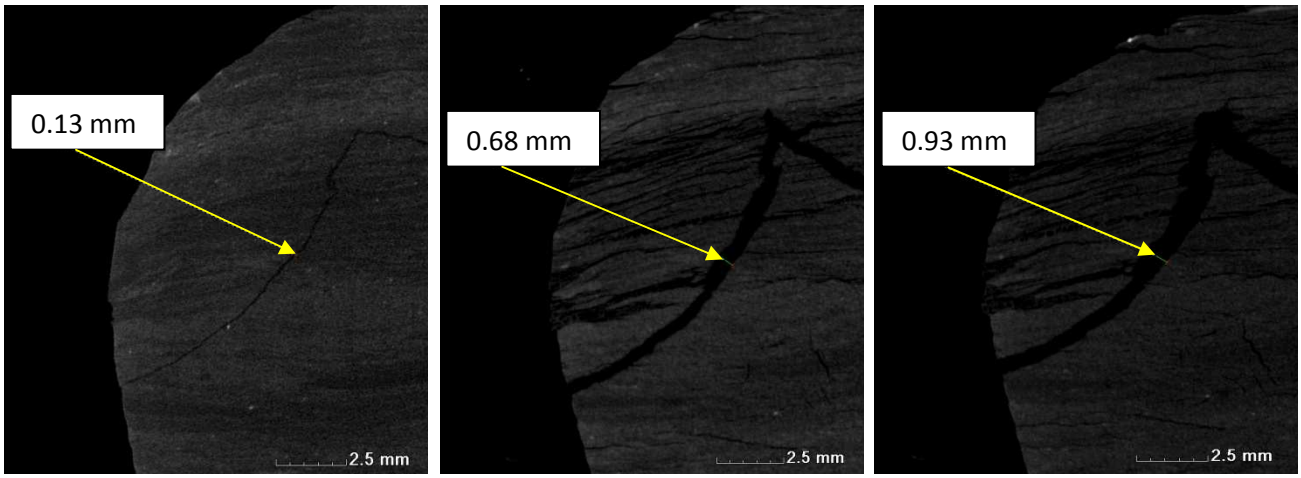

Figure 7.18: Fracture development of W2 (left = 0%, middle = 50%, right = 100%)

W3

Characteristics: The mineral matter arrangement of coal W3 is practically the same as that of coal W2. Most of the mineral matter is arranged in bands whilst a minimal amount is present in the form of small aggregates. The aggregates typically comprise very high density materials like pyrite. There are fewer bands of inertinite and more of vitrinite than present in coal W2, as indicated in figure 7.19. Small fractures were present before any experimentation commenced.

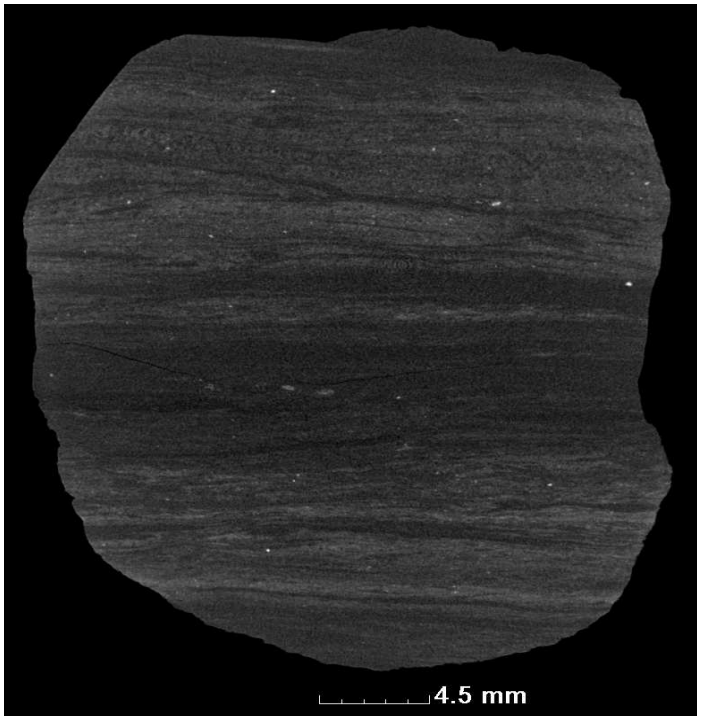

Figure 7.19: Coal W3

Pyrolysis: The volume of coal W3 increased from 15431 mm^3 to 18641 mm^3 (17.2% increase) when a pyrolysis value of 50% was achieved. This is the biggest increase in volume of all the coal particles that have been investigated during this study. The reason for that may be the vast amount of vitrinite present in the sample. The coal sample therefore developed strong plastic characteristics at 50% pyrolysis and could therefore expand to the level that was observed. It can be seen from figure 7.20 that there was what is assumed to be a thick vitrinite band in the sample and this band swelled significantly during the process.

This band formed large pores and fractures in the coal and consequently there was a huge expansion. The regions which was assumed to be inertinite rich, did however limit this expansion and consequently the vitrinite band began to protrude from the sides as can be seen from figure 7.20. The fractures that were present in the beginning of the experiment increased significantly and a few new fractures developed in the vitrinite rich bands. Note that a step towards full pyrolysis was attempted but the sample became so brittle at 50% pyrolysis that it was not possible to perform a third scan.

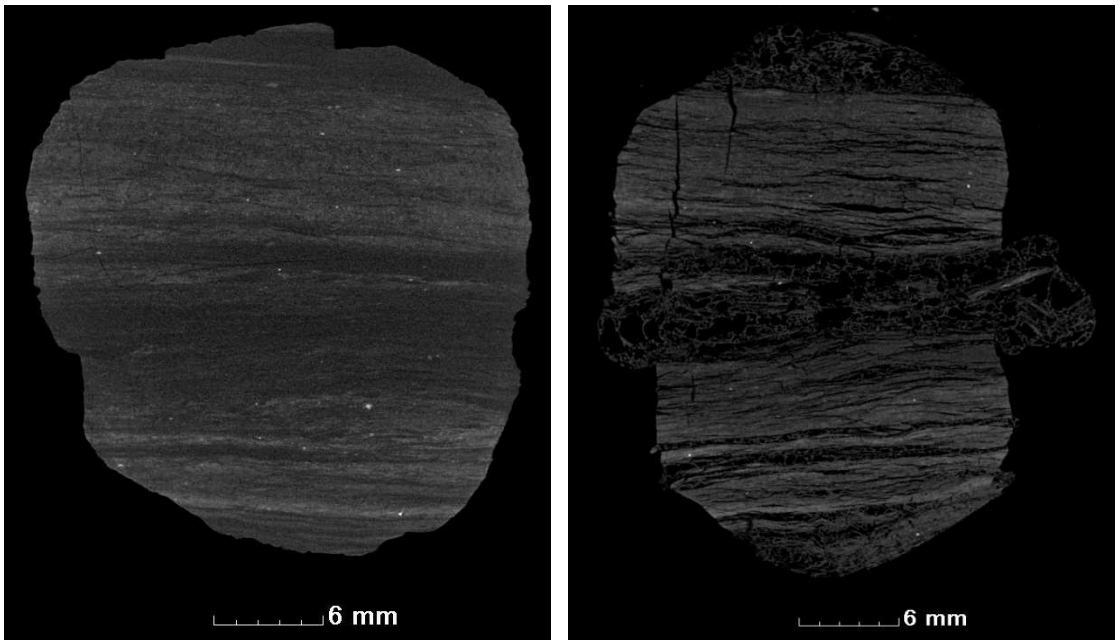

Figure 7.20: Pyrolysis of W3 (left = 0%, right = 50%)

Development of the fracture network: The fractures that were present at the beginning of experimentation developed into large fractures that were prevalent in the vitrinite regions, as well as perpendicular to the inertinite layers (refer to figure 7.21).

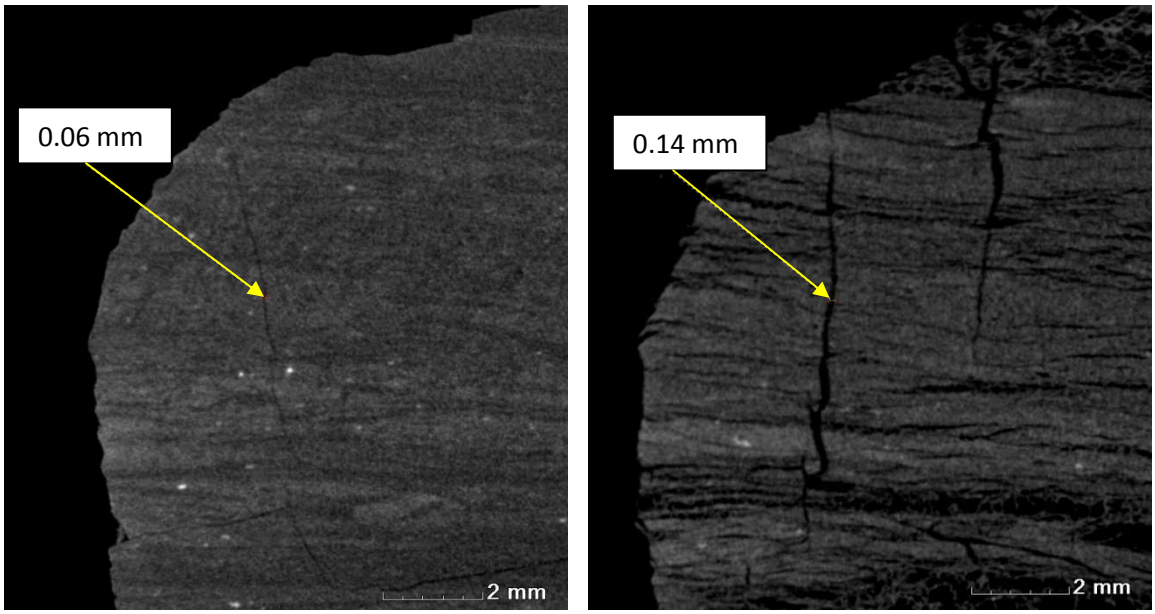

Figure 7.21: Fracture development of W3 (left = 0%, right = 50%)

7.3 Summary

Qualitative and quantitative micro-focus X-ray CT analyses of pyrolysis and gasification of two different types of coal were presented in this chapter. The CT technique made it possible to see the structural changes in the coal undergoing pyrolysis and gasification. This volume change could be quantified with the appropriate software and consequently the density during various stages of pyrolysis could be calculated. It was found that the Highveld coals, which were inertinite rich, did not expand as much as the vitrinite and volatile rich Waterberg coals. The common trend for expansion was that the coal volume increased when 50% pyrolysis was achieved, and decreased beyond that up to 100% pyrolysis.

The increase in volume could be attributed to the plastic nature of the coal under the conditions of 50% pyrolysis whilst the decrease could be attributed to the brittle char that forms after 100% pyrolysis. All the fractures formed and developed primarily in the less dense vitrinite regions whilst the inertinite and mineral rich regions remained largely unaffected. It was also found that the Highveld coals had a less dense organic matrix when compared to the Waterberg coals. The reason for that is the abundance of aggregate mineral matter in the organic matrix of the Highveld coals. This is indicative of mineralized water that deposited minerals on the walls of pores in the coal structure.

The mineral matter was predominantly arranged in clear bands for the Waterberg coals. It was assumed that the coal samples used in this investigation reacted according to the mechanisms proposed by the SCM. This assumption is justified from the clear core and reacted layer surrounding this core. The thickness could also be determined and from the difference between the two values it could be concluded that one coal sample had a higher permeability of the organic matrix. The behaviour observed was in accordance with that proposed in literature and other investigations.

To conclude that the samples did not react in the pores and fractures would require a calculation of the fracture surface area which is easy to do with volume rendering software. It was not done during this investigation since the resolution (0.017 mm) of the scans was significantly larger than the size of the micro-pores (< 2 nm) which constituted the majority of the porous surface area (Koopal, 2001).

8. Summing up

8.1 Conclusions

This paragraph highlights the conclusions made during this investigation, in which the capabilities of ionizing radiation as imaging tool in coal research was investigated.

- The CT technique was predominantly used in previous coal research to investigate carbon dioxide sequestration and methane production from coal beds. In chapter three it was concluded that X-ray CT is a very powerful research technique with which a potential coal bed could be evaluated (for carbon dioxide sequestration and methane production). The CT technique could therefore be used to determine the permeability of a specific coal bed. This permeability was influenced by minerals and the amount of phyteral pores. It was found that the regions with the best permeability were the regions that contain phyteral pores connected to microfractures. Regions with the worst permeability were organic matrix regions with limited or no connected pores. It was observed, by using Xenon gas, that coal with phyteral pores initially had a fast gas uptake that was limited by diffusion into the micropore structure.
- The cleat and fracture network plays an integral role in modeling gas flow within coal and coal beds. Chapter four demonstrates how the researcher could obtain information on the orientation of cleats and fractures and how this orientation was determined when the coal developed during the coalification process.
- The CT technique is ideal to calculate porosity and void volumes, since most commercial volume rendering software include tools to do this. Chapter five discussed how CT was used to quantify the porosity of a specific coal sample and how these pores were spatially distributed. It was found that porosity information obtained with the CT technique is comparable to other more destructive characterization techniques like helium porosimetry. Porosity determined by CT may even be more accurate, since the CT technique is capable of including unconnected pores. The dual energy method may help in identifying different materials more accurately.

- There are very few coal research projects in which neutrons were used to obtain physical and structural information. It was concluded in chapter six that neutrons are ideal to determine the moisture content of coal and that results obtained with this technique were comparable to a chemical laboratory analysis.
- Chapter seven described the capabilities of the SANCRAT with special emphasis on the SANRAD and MIXRAD facilities. It was concluded that the results obtained in the MIXRAD facility is comparable to that of two different leading German facilities.
- The CT technique made it possible to characterize and follow the progression of pyrolysis and gasification in a non-destructive manner as described in chapter eight. The swelling during pyrolysis was quantified with appropriate software and the density change could be observed. It was concluded that swelling occurred mostly in the vitrinite rich regions whilst the inertinite rich regions remained relatively unchanged. The Waterberg coals contained large amounts of vitrinite and swelled much more than the Highveld coals, which were inertinite rich. The coals swelled mostly up to 50% pyrolysis which is indicative of the plastic nature of the coal which is prevalent under these conditions. After 50% pyrolysis the coals became very brittle and it became difficult to handle without breaking. The fractures also primarily developed in the lower density vitrinite regions whilst the inertinite and mineral rich regions remained unaffected.

  It was possible to verify the permeability of the organic matrix in the way in which the minerals were deposited. The Highveld coals had a less dense organic matrix than the Highveld coals because the minerals were distributed in aggregates in the organic matrix. This indicates that the organic matrix was penetrated by mineralized water and the mineral matter was deposited on pore walls. The mineral matter was predominantly arranged in fractures of the Waterberg coals, which indicates that the organic matrix was difficult to penetrate. CT also made it possible to visually see how the first stages of gasification occurred (up to a level of 30%). It was concluded that the reaction mechanism that was prevalent was indeed the SCM with a defined core and reacted layer. The mineral matter and inertinite regions did not have a significant impact on the development of the core. All the conclusions about pyrolysis and gasification were in accordance with that found in literature.

8.2 Recommendations

The following recommendations are made for further investigations.

- It will be interesting to model the flow of process gases in gasification and how the developing fracture structure influences this flow. To do this would require extensive knowledge about the porous and fracture structure of coal, which can be obtained from principles described in chapters three and four.
- Use the best possible resolution for investigations regarding measurements. This was the limiting factor in chapter four where µCT would have delivered more accurate results, since the resolution is better. It is also advisable that the size of a voxel should be uniform in all directions since this will ease analysis and measurements. The sample size should also be considered carefully, since very small samples may not be representative of a seam.
- It is recommended that the dual energy method should be used in future investigations to calculate the distribution and amount of the coal macerals. It was difficult to distinguish during this investigation between the different macerals due to their closely related densities. The dual energy method will however ease this process.
- It is recommended to correlate values obtained with CT with that of more conventional techniques. This will add to the accuracy of values obtained as was demonstrated in chapter five. This is especially important when a quantitative analysis is considered.
- It is recommended that the moisture content of coal should be evaluated with neutron radiography/tomography as well as the flow characteristics of steam during steam gasification.
- It is recommended to perform gasification studies to higher levels than 30% to verify whether the SCM is still applicable. During this investigation it was possible to observe a core of unreacted coal within the particle once a level of 30% gasification was achieved. So it will be interesting to observe the formation of this core as gasification progresses (beyond 30%). It might even be possible to deduce some kinetic and reaction mechanism information. One might be able to conclude which reaction mechanism is applicable at different levels of gasification and whether certain minerals have a catalytic or inhibiting effect.

- It is also recommended that coal samples with different composition should be gasified to determine whether the RPM would be more prevalent in different types.
- Another interesting aspect that should be investigated is how the structural properties (fracture and mineral distribution) can influence the breaking pattern of coal. It should be possible to identify regions where breakage is most likely to occur. Fracture network maps will aid in this regard as well as to provide information for gas flow modelling.
- CT number transformation enables the researcher to quantify certain changes like fracture growth and material loss. It is therefore advised that the CT numbers are determined in future studies.
- The specific minerals present and the spatial distribution of these minerals will give insight into the overall influence on the coal structure - which minerals have a catalytic effect and how do minerals influence the breaking pattern of coal (to name but a few).

References

AUZERAIS, M., DUNSMUIR, J., FERRÉOL, B.B., MARTYS, N., OLSON, J., RAMAKRISHNAN, T.S., ROTHMAN, D.H. & SCHWARTZ, L.M. 1996. Transport in sandstone: A supply based on three dimensional microtomography. *Geophysical Research Letters* 23:705-708.

BAI, J., LI, W., LI, C., BAI, Z. & LI, B. 2008. Influences of minerals transformation on the reactivity of high temperature char gasification. *Fuel Processing Technology* 2009.

BERKOWITZ, N. 1985. The chemistry of coal. Amsterdam, New York.

BERTIN, E.P. 1978. Introduction to X-ray Spectrometric Analysis. New York: Plenum Press. 485p.

BHATIA, S.K. & VARTAK, B.J. 1996. Reaction of micro porous solids: The discrete random pore model. *Carbon* 34:1383-1391.

CHAMBER OF MINES OF SOUTH AFRICA. 2009. Economics and Statistics. http://www.bullion.org.za Date of access: 26 August 2009.

CHEN, H., LI, B. & ZHANG, B. 2000. Decomposition of pyrite and the interaction of pyrite with coal organic matrix in pyrolysis and hydropyrolysis. *Fuel* 79:1627-1631.

CHERMIN, H.A.G. & VAN KREVELEN, D.W. 1956. Calculation of the free enthalpy of formation of hydrocarbons from group contributions. *Fuel* 36:85.

CHI, W. AND PERLMUTTER, D.D. 1989. Reactive surface gasification. *American Institute of Chemical Engineers Journal* 35:1791.

CHO, Z., JONES, J. & SINGH, M. 1993. Foundations of Medical Imaging. New York: John Wiley and Sons.

CLARKSON, C.R. & BUSTIN, R.M. 1999. The effect of pore structure and gas pressure upon the transport properties of coal: a laboratory and modeling study. 1. Isotherms and pore volume distributions. *Fuel* 78:1333-1344.

CLOKE M. & LESTER, E. 1994. Characterisation of coals for combustion using petrographic analysis. A review. *Fuel* 73:315.

CRELLING, L.C., HIPPO, E.J. WOERNER, B.A. AND WEST, D.P. 1992. Combustion characteristics of selected whole coals and macerals. *Fuel* 71:151.

DE BEER, F.C. 2005. Characteristics of the neutron/X-ray tomography system at the SANRAD facility in South Africa. *Nuclear Instruments and Methods in Physics Research A* 542:1-8.

DE GRYZE, S., JASSOGNE, L., SIX, J., BOSSUYT, H., WEVERS, M. & MERCKX, R. 2006. Pore structure changes during decomposition of fresh residue: X-ray tomography analyses. *Geoderma* 134:82-96.

DEFRISE, M. 2001. A short reader's guide to 3D tomographic reconstruction. *Computerized Medical Imaging and Graphics* 25:113-116.

DENIS, J., PONE, N., HALLECK, P.M. & MATHEWS, J.P. 2009. 3D characterization of coal strains induced by compression, carbon dioxide sorption, and desorption at in-situ stress conditions. *International Journal of Coal Geology (2009).*

DULIU, O.G. 1999. Computer axial tomography in geosciences: an overview. *Earth-Science Reviews* 48:265-281.

EVERSON, R.C., NEOMAGUS, H.W.J.P., KASAINI, H. & NJAPHA, D. 2005. Reaction kinetics of pulverised coal-chars derived from inertinite-rich coal discards: Gasification with carbon dioxide and steam. *Fuel* 85:1076.

FALCON, L.M. & FALCON, R.M.S. 1987. The Petrographic Composition of Southern African Coals in Relation to Friability, Hardness, and Abrasive Indices. *Journal of the South African Institute of Mining and Metallurgy* 87:323-336.

FOURIE, C.J.S., DU PLESSIS, S.J. & HENRY, G. 2006. New airborne geophysical data from the Waterberg coalfield-South Africa's major future energy source. www.csir.co.za/nre/mineral_resources/pdfs/CPO-0024.pdf Date of access: 27 July 2009.

GAN, H., NANDI, S.P. AND WALKER, JR., P.L. 1972. Nature of the porosity in American coals. *Fuel* 51:272.

GRÜNAUER, F. 2005. Design, optimization, and implementation of the new neutron radiography facility at FRM-II. Doctoral Thesis. Technical University of Munich: Physics Department.

GUPTA, J.S. AND BHATIA, S.K. 2000. A modified discrete random pore model allowing for different initial surface reactivity. *Carbon* 38:47.

GUPTA, S. 2006. Global Energy Trends: Changing energy requirements of the developing world. https://netfiles.uiuc.edu/.../EnergyClubattheUniversityofIllinoisatUrbana.../GlobalEnergyTrends.pdf Date of access: 27 July 2009.

HALLIDAY, D., RESNICK, R. & WALKER, J. 2005. Fundamentals of Physics. 7th Ed. USA: John Wiley & Sons Inc. 1248p.

HANSON, S., PATRICK, J.W. & WALKER, A. 2002. The effect of coal particle size on pyrolysis and steam gasification *Fuel* 81:531.

HERZ, R.H. 1969. The photographic action of ionizing radiations in Dosimetry and Medical, Industrial, Neutron, Auto- and Microradiography. USA: Wiley-Interscience. 629p.

HOLLOWAY, S. 2005. Underground sequestration of carbon dioxide-a viable greenhouse gas mitigation option. *Energy* 30:2318-2333.

HURT, R.H., SAROFIM, A.F. AND LONGWELL, J.P. 1991. The role of microporous surface area in the gasification of chars from a sub-bituminous coal. *Fuel* 74:471.

HUTTINGER, K.J. & NATTERMANN, C. 1994. Correlation between coal reactivity and inorganic matter content for pressure gasification with steam and carbon dioxide. *Fuel* 73:1682.

JOHNSON, J.L. 1979. Kinetics of bituminous coal char gasification with gases containing steam and hydrogen. *Advances in Chemistry* 137:145.

JONES, K.W., FENG, H., LINDQUIST, W.B., ADLER, P.M., THOVERT, J.F., VEKEMANS, B., VINCZE, L., SZALOKI, I., VAN GRIEKEN, R., ADAMS, F. & RIEKEL, C. 2003. Study of the microgeometry of porous materials using synchrotron computed microtomography. *In*: MEES, F., SWENNEN, R., VAN GEET, M. & JACOBS, P. *Applications of X-ray Computed Tomography in the Geosciences.* Geological Society, London, Special Publications. 215:39-49.

JONES, R.B., McCOURT C.B. MORLEY, C. & KING, K. 1985. Macerals and rank influence on the morphology of coal char. *Fuel* 64:460.

JUBERT,K. AND MASUDI, H. 2009. Coal reserves in the United States and around the world. www.osti.gov/bridge/servlets/purl/32537-U88ALg/.../32537.pdf Date of access: 27 July 2009.

KANG, J., OSOSKOV, Y., EMBURY, J.D. & WILKINSON, D.S. 2007. Digital image correlation studies for microscopic strain distribution and damage in dual phase steels. *Scripta Materialia* 56:999-1002.

KARACAN, C.O. & OKANDAN, E. 2000. Assessment of energetic heterogeneity of coals for gas adsorption and its effect on mixture predictions for coalbed methane studies. *Fuel* 79:1963-1974.

KARACAN, C.O. & OKANDAN, E. 2000a. Fracture/cleat analysis of coals from Zongdulak Basin (northwestern Turkey) relative to the potential of coalbed methane production. *International Journal of Coal Geology* 44:109-125.

KARACAN, C.O. & OKANDAN, E. 2001. Adsorption and gas transport in coal microstructure: investigation and evaluation by quantitative X-ray CT imaging. *Fuel* 80:509-520.

KETCHAM, R.A. & CARLSON, W.D. 2001. Acquisition, optimization and interpretation of X-ray computed tomographic imagery: applications to the geosciences. *Computers & Geosciences* 27:381-400.

KOOPAL, L.K. 2001. Manual of symbols and terminology for physicochemical quantities and units, Appendix 2. http://www.iupac.org Date of access: 17 November 2011.

KÜHL, H., KASHANI-MOTLAGH, M.M., MÜHLEN H.J AND VAN HEEK, K.H. 1992. Controlled gasification of different carbon materials and development of pore structure. *Fuel* 71:879.

KUMAR, H., LESTER, E., KINGMAN, S., BOURNE, R., AVILA, C., JONES, A., ROBINSON, J., HALLECK, P.M. & MATHEWS, J.P. 2011. Inducing fractures and increasing cleat apertures in a bituminous coal under isotropic stress via application of microwave energy. *International Journal of Coal Geology* 88:75-82.

KUPER, K.E., ZEDGENIZOV, D.A., RAGOZIN, A.L., SHATSKY, V.S., POROSEV, V.V., ZOLOTAREV, K.V., BABICHEV, E.A. & IVANOV, S.A. 2007. Three-dimensional distribution of minerals in diamondiferous eclogites, obtained by the method of high-resolution X-ray computed tomography. *Nuclear Instruments and Methods in Physics Research A* 575:255-258.

KWON, T.W., KIM, J.R., KIM, S.D & PARK, W.H. 1989. Catalytic steam gasification of lignite char. *Fuel* 68:416.

LAINE, N. R., VASTOLA, F.J AND WALKER, P. L. 1963. The importance of active surface area in the carbon-oxygen reaction. *Journal of Physical Chemistry* 67:2030.

LAUBACH, S.E., MARRETT, R.A., OLSON, J.E. & SCOTT, A.R. 1998. Characteristics and origins of coal cleats: A review. *International Journal of Coal Geology* 35:175-207.

LEE, T.J. & KOON, O.W. 2009. Modified shrinking unreacted-core model for the reaction between sulphur dioxide and coal fly ash/CaO/$CaSO_4$ sorbent. *Chemical Engineering Journal* 46:57-62.

LEVENSPIEL, O. 1999. Chemical Reaction Engineering. 3rd ed. USA: John Wiley & Sons Inc. 582p.

LIN, C.L., MILLER, J.D., LUTTRELL, G.H. & ADEL, G.T. 2000. Development of an on-line coal washability analysis system using X-ray computed tomography. *Coal Preparation* 21:383-409.

LIU, H., LUO, C., TOYOTA, M., UEMIYA, S. & KOJIMA, T. 2006. Kinetics of CO_2/char gasification at elevated temperatures. Part 2: Clarification of mechanism through modeling and char characterization. *Fuel Processing Technology.* 87:769-774.

LONG, H., SWENNEN, R., FOUBERT, A., DIERICK, M. & JACOBS, P. 2009. 3D quantification of mineral components and porosity distribution in Westphalian C sandstone by microfocus X-ray computed tomography. *Sedimentary Geology* 220:116-125.

LU. G.Q. & DO. D.D. 1992. A kinetic study of coal reject-derived char activation with CO_2, H_2O and air. *Carbon* 30:21.

MAYLOTTE, D.H., KOSKY, P.G., LAMBY, E.J., SPIRO, C.L., DAVIS, A. & BENSLEY, D.F. Applications of X-ray computed tomography to coal studies. http://www.anl.gov/PCS/acsfuel/preprint%20archive/Files/29_1_ST.%20LOUIS_04-84_0044.pdf.pdf Date of access: 7 September 2010.

MAZUMDER, S., WOLF, K.-H.A.A., ELEWAUT, K. & EPHRAIM, R. 2006. Application of X-ray computed tomography for analyzing cleat spacing and cleat aperture in coal samples. *International Journal of Coal Geology* 68:205-222.

MILLER, J.D., LIN, C.L., GARCIA, C. & ARIAS, H. 2003. Ultimate recovery in heap leaching operations as established from mineral exposure analysis by X-ray microtomography. *International Journal of Mineral Processing* 72:331-340.

MILLER, J.D., LIN, C.L., HUPKA, L. & AL-WAKEEL, M.I. 2009. Liberation-limited grade/recovery curves from X-ray micro CT analysis of feed material for the evaluation of separation efficiency. *International Journal of Mineral Processing* 93:48-53.

MILLER, J.D. & LIN, C.L. 2009. High resolution X-ray Micro CT (HRXMCT) – Advances in 3D particle characterization for mineral processing operations. *Recent Advances in Mineral Processing Plant Design* 48-59.

NIKON METROLOGY. XTH 225 Micro-focus X-ray System. http://www.nikonmetrology.com Date of access: 20 October 2011.

PONE, J.D.N., HALLECK, P.M. & MATHEWS, J.P. 2009. 3D characterization of coal strains induced by compression, carbon dioxide sorption, and desorption at in-situ stress conditions. *International Journal of Coal Geology* (2009).

PONE, J.D.N., HILE, M., HALLECK, P.M. & MATHEWS, J.P. 2009a. Three-dimensional carbon dioxide-induced strain distribution within a confined bituminous coal. *International Journal of Coal Geology* 77:103-108.

REMEYSEN, K. & SWENNEN, R. 2006. Beam hardening artifact reduction in microfocus computed tomography for improved quantitative coal characterization. *International Journal of Coal Geology* 67:101-111.

SCHENA, G., SANTORO, L. & FAVRETTO, S. 2007. Conceiving a high resolution and fast X-ray CT system for imaging fine multi-phase mineral particles and retrieving mineral liberation spectra. *International Journal of Mineral Processing* 84:327-336.

SENNECA, O., SALATINO, P. AND MASI, S. 1998. Microstructural changes and loss of gasification reactivity of chars upon heat treatment. *Fuel* 77:1483.

SLEUTEL, S., CNUDDE, V., MASSCHAELE, B., VLASSENBROEK, J., DIERICK, M., VAN HOOREBREKE, L., JACOBS, P. & DE NEVE, S. 2008. Comparison of different nano- and micro-focus X-ray computed tomography set-ups for the visualization of the soil microstructure and soil organic matter. *Computers and Geosciences* 34:931-938.

SOWERBY, B.D., MILLEN, M.J. & RAFTER, P.T. 1988. Fast-neutron and Gamma-ray Transmission Technique for the On-line Determination of Moisture in Coal and Coke. *Nuclear Geophysics* 2:55-68.

STACH, E., MACKOWSKY, M.T., TEICHMULLER, M., TAYLOR, G.H., CHANDRA, D. & TEICHMULLER, R. 1982. Stach's Textbook of Coal Petrology. Berlin: Gebruder Borntraeger. 535p.

STUTZER, O. & NOE, A.C. 1940. Geology of Coal. Illinois: The University of Chicago Press. 461p.

VAN DYK, J.C., KEYSER, M.J. & COERTZEN, M. 2005. Syngas production from South African Coal sources using Sasol-Lurgi gasifiers. *International Journal of Coal Geology.* 65:243-253.

VAN GEET, M., LAGROU, D. & SWENNEN, R. 2003. Applications of X-ray Computed Tomography in the Geosciences. London: The Geological Society. 215p.

VAN GEET, M., SWENNEN, R. & DAVID, P. 2001. Quantitative coal characterization by means of microfocus X-ray computer tomography, colour image analysis and back-scattered scanning electron microscopy. *International Journal of Coal Geology* 46:11-25.

VANDERSTEEN, K., BUSSELEN, B., VAN DEN ABEELE, K. & CARMELIET, J. 2003. Quantitative characterization of fracture apertures using microfocus computed tomography. *In*: MEES, F., SWENNEN, R., VAN GEET, M. & JACOBS, P. *Applications of X-ray Computed Tomography in the Geosciences.* Geological Society, London, Special Publications. 215:61-68.

VERHELST, F., DAVID, P., FERMONT, W., JEGERS, L. & VERVOORT, A. 1996 Correlation of 3D-computerized tomographic scans and 2D-colour image analysis of Westphalian coal by means of multivariable statistics. *International Journal of Coal Geology* 29:1-21.

VIDELA, A.R., LIN, C.L. & MILLER, J.D. 2007. 3D characterization of individual multiphase particles in packed particle beds by X-ray microtomography (XMT). *International Journal of Mineral Processing* 84:321-326.

WALKER, P.L., RUSINKO, F. & AUSTIN, L.G. 1959. Gas reactions of carbon. Advances in catalysis and related subjects. New York: Academic Press. 133p.

WALL, T.F., LIU, G., WU, H., ROBERTS, D.G., BENFELL, K.G., GUPTA, S., LUCAS, J.A. & HARRIS, D.J. 2001. The effects of pressure on coal reactions during pulverised coal combustion and gasification. *Progress in Energy and Combustion Science* 28:405-433.

WANG, F.Y., ZHU, Z.H., MASSAROTTO, P. & RUDOLPH, V. 2007. A simplified dynamic model for accelerated methane residual recovery from coals. *Chemical Engineering Science* 62:3268-3275.

WCI. 2009. World Coal Institute. http://www.worldcoal.org Date of access: 31 August 2010.

WEEDA, M., ABCOUWER, H.H., KAPTEIJN, F. & MOULIJN, J.A. 1993. Steam gasification kinetics and burn-off behaviour for a bituminous coal derived char in the presence of H_2. *Fuel Processing Technology* 36:235.

WELLS, W.F. & SMOOT, L.D. 1985. Particle size dependence of coal reactivity. *Combustion and Flame 68*:481.

WIGLEY, F., WILLIAMSON, J. & GIBB, W.H. 1997. The Distribution of Mineral Matter in Pulverized Coal Particles in Relation to Burnout Behaviour. *Fuel.* 76:1283-1288.

WINKLER, B., KNORR, K., KAHLE, A., VONTOBEL, P., LEHMANN, E., HENNION, B. & BAYON, G. 2002. Neutron imaging and neutron tomography as non-destructive tools to study bulk-rock samples. *European Journal of Minerals* 14:349-354.

XRADIA. 2010. Basic Technology. http://www.xradia.com/technology/basic-technology/sources.php Date of access: 1 September 2010.

YAO, Y., LIU, D., CHE, Y., TANG, D., TANG, S. & HUANG, W. 2009. Non-destructive characterization of coal samples from China using microfocus X-ray computed tomography. *International Journal of Coal Geology* 80:113-123.

YE, D.P. AGNEW, J.B. AND ZHANG, D.K. 1998. Gasification of a South Australian low-rank coal with carbon dioxide and steam: kinetics and reactivity studies. *Fuel* 77:1209.

ZABLER, S., RACK, A., MANKE, I., THERMANN, K., TIEDEMANN, J., HARTHILL, N. & RIESEMEIER, H. 2008. High-resolution tomography of cracks, voids and micro-structure in greywacke and limestone. *Journal of Structural Geology* 2008:1-12.

ZHANG, L., HUANG, J., FANG, Y. & WANG, Y. 2006. Gasification reactivity and kinetics of typical anthracite chars with steam and CO_2. *Energy & Fuels* 20:1201.

ZHANG, Y., HARA, S., KAJITANI, S. & ASHIZAWA, M. 2008. Modelling of catalytic gasification kinetics of coal char and carbon. *Fuel* 2009.

Appendix A – Pyrolysis and gasification calculations

A calibration experiment was conducted, as a primary step, to determine the appropriate temperature at which a desired level of pyrolysis could be achieved. These experiments were performed on very similar samples, to accurately determine the stopping temperatures. The samples were loaded into the furnace assembly, whilst maintaining the appropriate nitrogen flow. A heating rate of 5 ℃/min was maintained wh ilst carefully monitoring the temperature of the furnace. One raised the temperature until no more mass was lost and this corresponded to the 100% pyrolysis level.

This mass value was used as a base to calculate the mass of volatiles lost at a 50% pyrolysis level. The corresponding temperature was then determined from the spreadsheet, in which the mass and temperature were automatically logged (section 8.1.3). The corresponding equations are as follow.

$$m_{100\%} = m_{initial} - m_{final} \qquad \textbf{Equation A.1}$$

$$m_{50\%} = m_{initial} - \frac{m_{100\%}}{2} \qquad \textbf{Equation A.2}$$

The gasification experiments commenced in a similar fashion, but with carbon dioxide as the reaction gas. It was more difficult to control the stopping points during the reaction, so time was used instead of temperature to determine the level of gasification. The furnace was operated isothermally with times associated to a 30% mass loss during gasification deemed appropriate for stopping points. Figure A.1 illustrates the mass profile, whilst figure A.2 illustrates the temperature profile that was obtained for coal particle W1. The mass and temperature profiles for the rest of the coal particles were similar and will not be presented here.

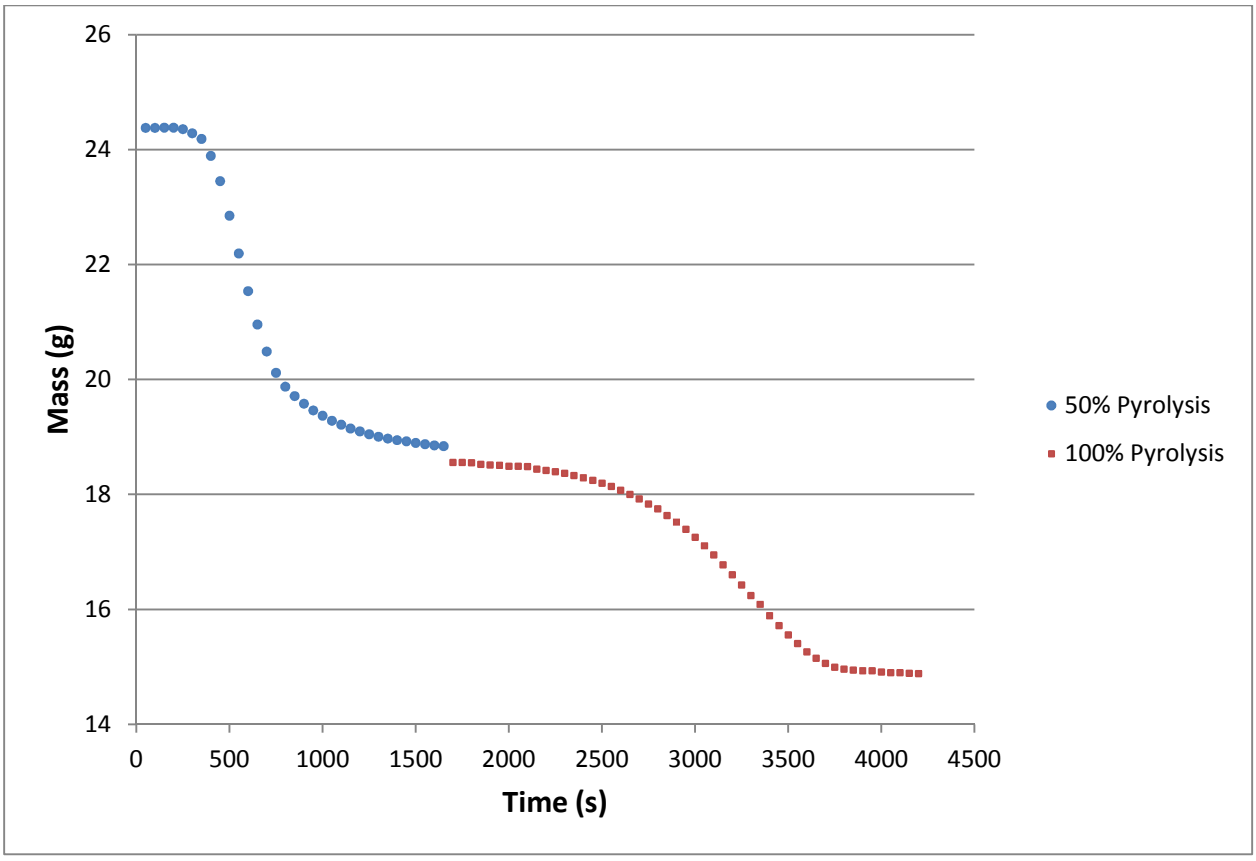

Figure A.0.1 Mass profile of particle W1

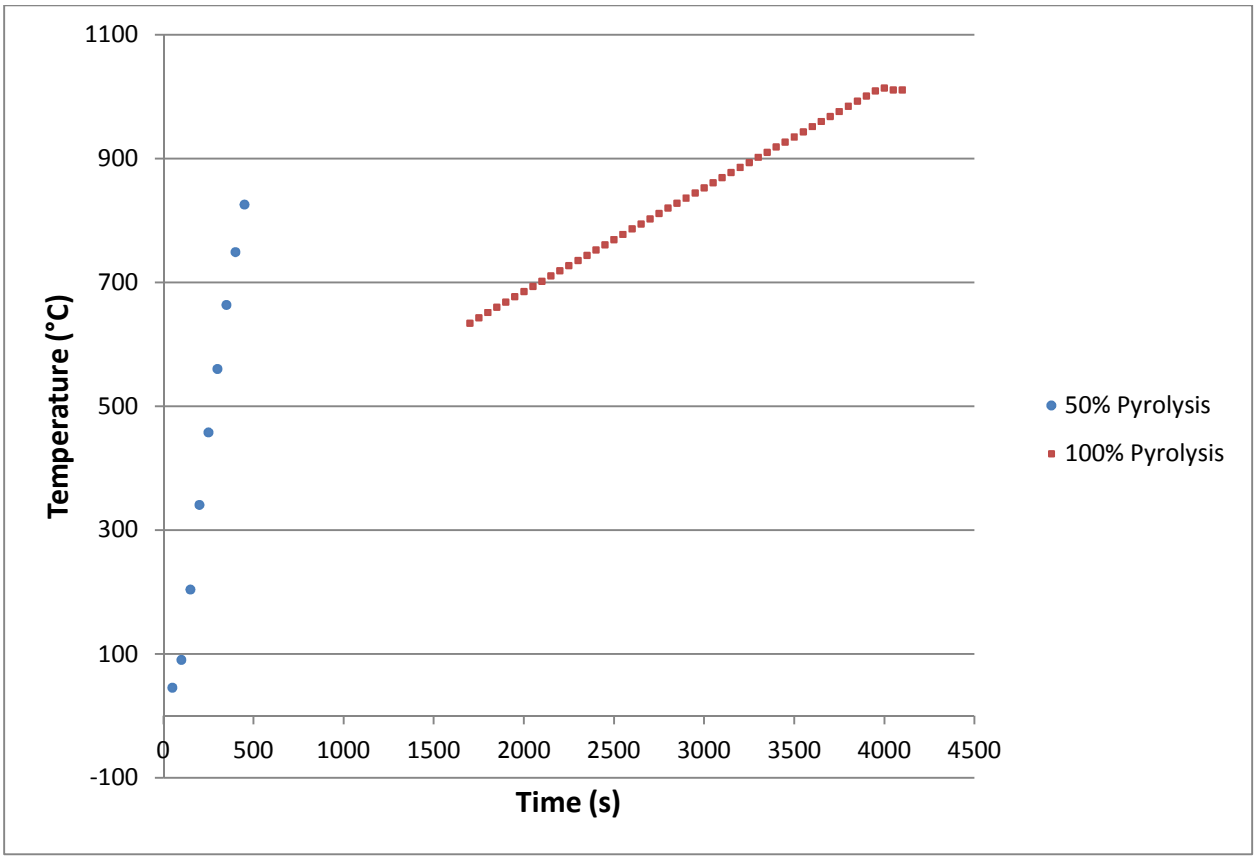

Figure A.0.2 Temperature profile of particle W1